In: Horizons in World Physics, Volume 278
Editor: Albert Reimer
ISBN: 978-1-61942-537-8

Chapter 1

COMPLEX RADIO ZEBRA PATTERNS ESCAPING FROM THE SOLAR CORONA AND NEW GENERATION MECHANISMS

G.P. Chernov*
IZMIRAN, Troitsk, Moscow region, Russia

Abstract

Sources of solar radio bursts in meter/decimeter/microwave ranges are located in the solar corona. The study of the radio fine structure is a key to understanding of plasma processes in the solar corona. The most intriguing fine structure is the zebra pattern (ZP) in continuous type-IV radio bursts (the regular harmonics in emission and absorption). A disputable discussion about nature of the ZP in the type IV radio bursts continues more than 40 years. Only in the last 5 years about 10 works devoted to an improvement of the mechanism based on the double plasma resonance (DPR, when upper hybrid frequency is equal to an integer of the cyclotron frequency,) were published, and 5 new models were proposed. The explanation to this is connected with the new observations of the uncommon forms of ZP, which it is difficult to interpret as the regular harmonics within the framework of known models. According to all works, which analyze mechanism based on the DPR, we must observe ZP in all continuous bursts. But observations suggest otherwise: ZP appears in the pulsation regime, and in not all bursts. Nevertheless, it is sometimes asserted that mechanism on DPR explains all basic properties of ZP, and it is indicated on the error of many authors in the calculations of the growth rates of plasma waves at the upper hybrid frequency: it is not possible to enlarge calculations for the regions adjacent with the hybrid band, since the dispersion relation - is correct only inside the hybrid band. However, the calculations, which show the significance of this erroneous approach should be conducted for the loss-cone distribution of fast particles in the relativistic approximation. Moreover, in a whole series of works it is noted that the contribution of the term, connected with the harmonic in the hybrid band, considerably exceeds contribution from those harmonics adjacent from above, especially for the slightly non-perpendicular propagation in the relativistic examination. New observations and incompleteness of many known mechanisms stimulate for the new developments. We show some properties of the ZP which cannot explained in the framework of the DPR model: the frequency drift of ZP stripes which changes synchronously with the space drift of the radio

* E-mail address: gchernov@izmiran.rssi.ru

sources, the frequency splitting of the ZP stripes, the superfine structure of the stripes in the form of millisecond spike-bursts etc. It is shown that simultaneous excitation of waves at ~30 DPR- levels in the corona is impossible for any realistic profile of the plasma density and magnetic field. All new properties of ZP are considered in the light of both old and new theoretical models. The main properties of the emission and absorption stripes can be explained in a model involving interactions between electrostatic plasma waves and whistlers, taking into account the quasi-linear diffusion of fast particles with the loss-cone distribution on whistlers. We also propose a new advanced model of the ZP. It is shown that in the system the weakly-relativistic mono-velocity beam of protons - the strongly nonisothermic plasma the slow beam mode can possess negative energy and the explosive instability with interaction of slow and rapid beam modes and ionic sound is developed. As a result of the weak spatial dispersion the generation of ionic sound is accompanied by the cascade process of coalescence, and the stabilization of explosive instability occurs. ZP is formed by scattering of fast protons on the ion-acoustic harmonics. The effectiveness of new mechanism in comparison with the previously discussed hypotheses is explained.

1. Introduction

The nature of the zebra pattern (ZP) has been a subject of wide discussion for more than 40 years. The ZP in the solar radio emission is the simultaneous excitation of waves at many (up to a few tens) of closely spaced, nearly equidistant frequencies. The basic parameters of ZP in the meter wave band are represented in the atlas by Slottje (1981). Now it is authentically known that in a regular ZP the frequency separation between the stripes grows with frequency: from 4 – 5 MHz at 200 MHz to ~ 80 MHz at 3000 MHz and to ~150 – 200 MHz at 5700 MHz. It is important to note that the relative frequency bandwidth of a separate stripe in emission remains almost stably constant with frequency, $\Delta f_e/f \approx 0.005$.

More than ten different models have been proposed for ZPs; most of them include some emission of electrostatic plasma waves at the upper hybrid frequency (ω_{UH}) (Kuijpers, 1975a; Zheleznykov and Zlotnik, 1975a,b; Mollwo, 1983; 1988; Winglee and Dulk, 1986). The most comprehensively developed ZP models involve mechanisms based on the double plasma resonance (DPR), which assumes that the upper hybrid frequency in the solar corona becomes a multiple of the electron-cyclotron frequency:

$$\omega_{UH} = (\omega^2_{Pe} + \omega^2_{Be})^{1/2} = s\omega_{Be} \quad (1)$$

where ω_{Pe} is the electron plasma frequency, ω_{Be} is the electron cyclotron frequency, and s is the integer harmonic number.

In order to explain the ZP dynamics in the framework of this mechanism, it is necessary that the magnetic field in the radio source varied sufficiently rapidly, which, however, contradicts the fairly low field values determined from the frequency separation between the stripes. Over the past five years, there appeared dozens of papers concerning the refinement of this mechanism, because, in its initial formulation, it failed to describe many features of the ZP. Kuznetsov and Tsap (2007) assumed that the velocity distribution function of hot electrons within the loss cone can be described by a power law with an exponent of 8–10. In this case, a fairly deep modulation can be achieved, but the excitation of waves at multiple double plasma resonance (DPR) levels is still impossible.

Fiber bursts differ from ZP stripes only by a constant negative frequency drift, and one of the first models explained the radio emission (*t*) of fiber bursts by the coalescence of plasma waves (*l*) with whistlers (*w*), $l + w \rightarrow t$ (Kuijpers, 1975a). In spite of the fact that then some more models were proposed (Alfvénic solitons, whistler solitons, MHD oscillations), this first model remains now most accepted. After the brief review by Kuijpers (1980) the situation in this sphere of activity was cleared up only in the review of Chernov (2006).

In Chernov (1976a; 1990), the mechanism $l + w \rightarrow t$ was proposed as an unified model in which the formation of ZPs in the emission and absorption spectra was attributed to the oblique propagation of whistlers, while the formation of stripes with a stable negative frequency drift (the fiber bursts) was explained by the ducted propagation of waves along a magnetic trap. This model explains occasionally observed transformation of the ZP stripes into fibers and vice versa.

The discovery of the superfine structure of the ZP, in the form of millisecond spikes was the most significant new effect in the microwave range (Chernov et al., 2003). The reliability of such a study strongly grew over the past few years in connection with numerous observations of fast radio bursts (millisecond spikes) during the stellar flares (Abada-Simon et al., 1995). It is amazing that the period of star spikes in the radio burst of the classical red dwarf AD Leo coincides with the period of spikes in the superfine structure of solar zebra stripes (~30 ms) (Osten and Bastian, 2006).

To overcome difficulties arising in different models, a new ZP theory based on the emission of auroral choruses (magnetospheric bursts) via the escape of the Z mode captured by regular plasma density inhomogeneities was recently proposed (LaBelle et al. 2003). This theory, however, fails to explain the high intensity of radiation emitted by separate incoherent sources. In addition, the theory imposes some stringent conditions, such as the presence of a large–amplitude ion–acoustic wave.

The existence of a ZP in the solar radio emission can be attributed to the existence of discrete eigenmodes in the nonuniform solar atmosphere. Several aspects of this mechanism were considered in Laptukhov and Chernov (2006); Barta and Karlicky (2006); Ledenev, Yan, and Fu (2006). In Laptukhov and Chernov (2006), dispersion relations were derived for a discrete spectrum of eigenmodes of a spatially periodic medium in the form of nonlinear structures formed due to the onset of thermal instability. The spectrum of eigenfrequencies of a system of spatially periodic cavities is calculated, and it is shown that such a system is capable of generating a few tens of ZP stripes, the number of which is independent of the ratio of the plasma frequency to the gyrofrequency in the source.

In practically all models the discussion deals with regular ZP. Problems appear with the interpretation of the frequently observed uncommon stripes of a ZP. For example, for explaining the so-called “tadpoles” (submerged in a developed ZP) special mechanisms were elaborated (Zheleznykov and Zlotnik, 1975a; Chernov, 2006). Rare attempts were made to explain other uncommon forms of ZPs (in the form of zigzags, complex splittings of stripes into the superfine structure). They cause big problems for the known models.

It is important to note that the model with the whistlers successfully explains the zigzags of stripes and their splitting, and also the variations in the frequency drift of stripes synchronously with the spatial drift of the sources of radio emission (Chernov, 2006). Since each new phenomenon provides its uncommon parameters of fine structure, and the entire variety of the parameters does not succeed in the statistical systematizing, below primary

attention is given to the analysis of separate phenomena. Just such a situation stimulates many authors to elaborate on new mechanisms.

In the present chapter, an attempt is made to evaluate what model most adequately describes the new observational data and to find out where the ZP stripes form (during the excitation of waves in the source or in the course of their further propagation). Calculations show that the DPR-based mechanism fails to describe the generation of a large number of ZP stripes in any coronal plasma model. Some other unsolved problems or difficulties in the DPR model are also examined in detail.

Here, it is shown that the new varieties of ZP succeed in explaining these phenomena within the framework of known mechanisms by taking into account the special features of plasma parameters and fast particles in the source. On the other hand, the formation of ZP stripes due to radio wave propagation through the coronal heterogeneities can be recognized as the most natural mechanism of ZP. The mechanism related to the excitation of discrete eigenmodes of the periodically nonuniform plasma (Laptukhov and Chernov, 2006, 2009) can yield the observed number of harmonics. However, in this case, only the possibility of generating harmonics in a one-dimensional stationary problem is considered, i.e., the frequency dynamics of stripes is not analyzed.

During the last several years some new varieties of ZP have been recorded. Now, it is necessary to estimate the possibility of their interpretation by taking into account all known models of ZPs.

2. Some Fragments of Old Original Observation

2.1. Zebra Pattern

Typical ZP in the meter range is shown in Figure 1 presenting two fragments in the event February 17, 1995. In the event February 17, 1992 the zebra patterns were observed in a complex type IV event during about four hours in the time interval 08 – 12 UT, and the radio source was also connected with an active dark filament without a big $H\alpha$ flare and microwave activity. For the first time we can see an entire frequency range occupied by ZP in a oscillating regime in the interval 180 – 350 MHz. The analysis of this event see in more detail in Chernov et al. (1998); Chernov (2006).

In this event, we could compare the frequency drift with the spatial source shifts during one of unusual frequency splitting of zebra stripes. For the larger persuasiveness we added to Figure 1 the one-dimensional SN distribution of zebra-stripe sources.

We had time resolution of Nançay Radio Heliograph (NRH) only 1 s, but the zebra stripes changed the sign of frequency drift at 10:58:22 UT from positive into negative with enough low frequency drift (remaining almost parallel to the time axis). Therefore this time resolution make it possible to recognize the spatial drift of sources as significant.

So, we see the spatial drift at 236.6 MHz in the beginning of this interval (about 10:58:08 UT) towards South and in the end (about 10:58:35 UT) towards North. In Figure 1 the direction of the spatial drift are marked by arrows in the centers of sources at the corresponding moments of SN distribution. Looking at Fig. 3 in Chernov et al. (1998) and being based on several Yohkoh/SXT images, it is tempting to locate the radio source of zebra

patterns in this event within a large trans-equatorial closed loop connecting AR 7056 and 7058. The source displacements in the direction S – N are quite anticipated therefore.

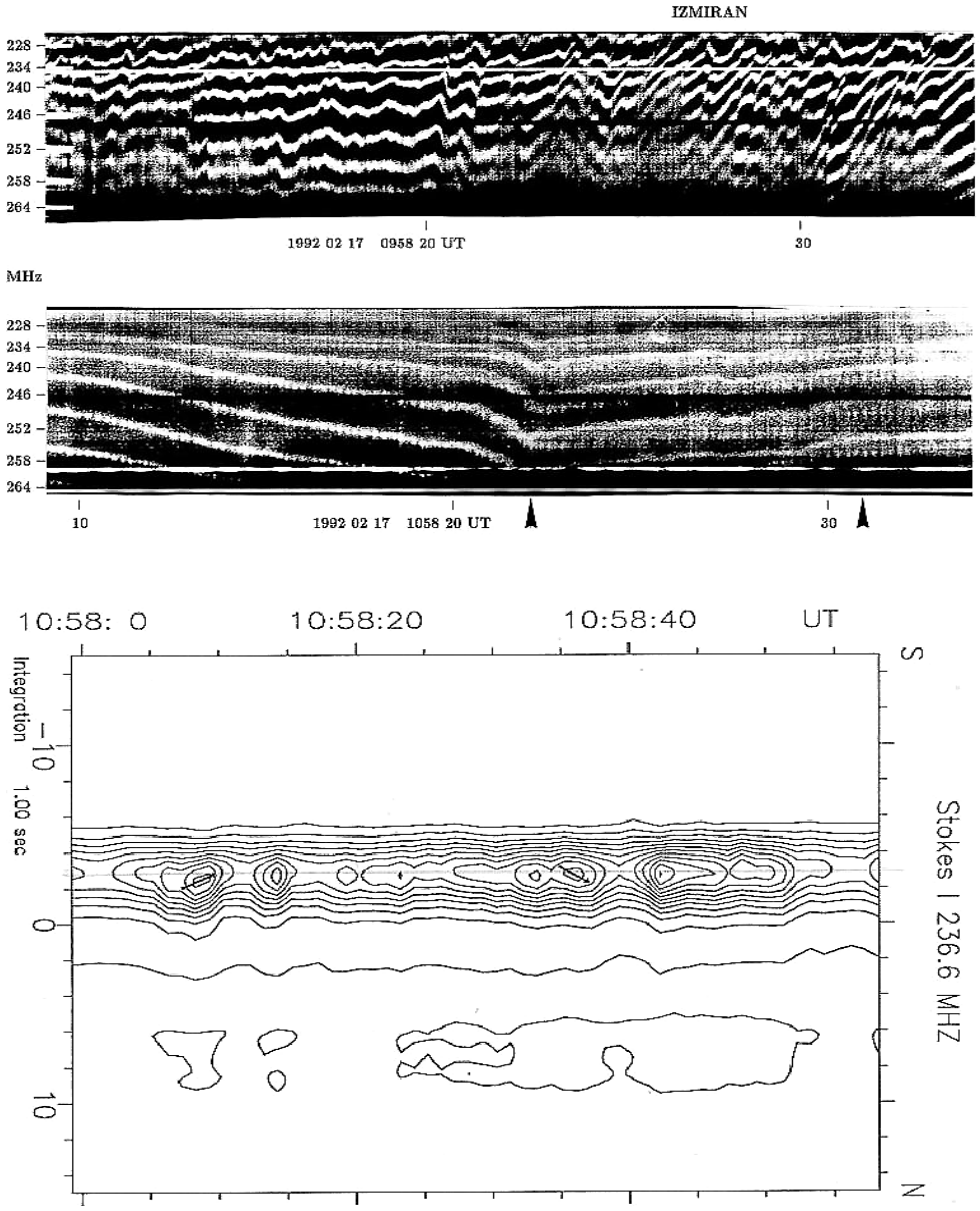

Figure 1. Top: Two fragments of zebra patterns recorded with the IZMIRAN spectrograph, (before and after the change of polarization sign) illustrating two kinds of sub-structures discovered. The top spectrum shows numerous sudden frequency shifts of zebra stripes. The bottom spectrum shows a case of stripe splitting (first arrow is the beginning) and dot-like structure of the upper frequency component (second arrow). Bottom: Contour plots of the one-dimensional SN brightness distribution measured by NRH at 236.6 MHz in intensity. The 0 channel gives the center of the solar disk. The arrows in the centers of sources at 10:58:07-10 UT and 10:58:34 – 37 UT show the direction of the spatial drift of sources (from Chernov et al., 1998).

Another example of the analysis of ZP with NRH is shown in Figure 2 in the event October 25, 1995. For the analysis of this event we used the data from simultaneous observations with several radiospectrographs (ARTEMIS, 100 – 500 MHz (Nançay), IZMIRAN, 25 – 270 MHz, Tremsdorf (Potsdam), 40 – 800 MHz), as well as the data from the radio-heliograph of Nançay (NRH) and the polarimeter in Trieste AO at frequencies 237, 327 and 408 MHz. (Chernov, 2005).

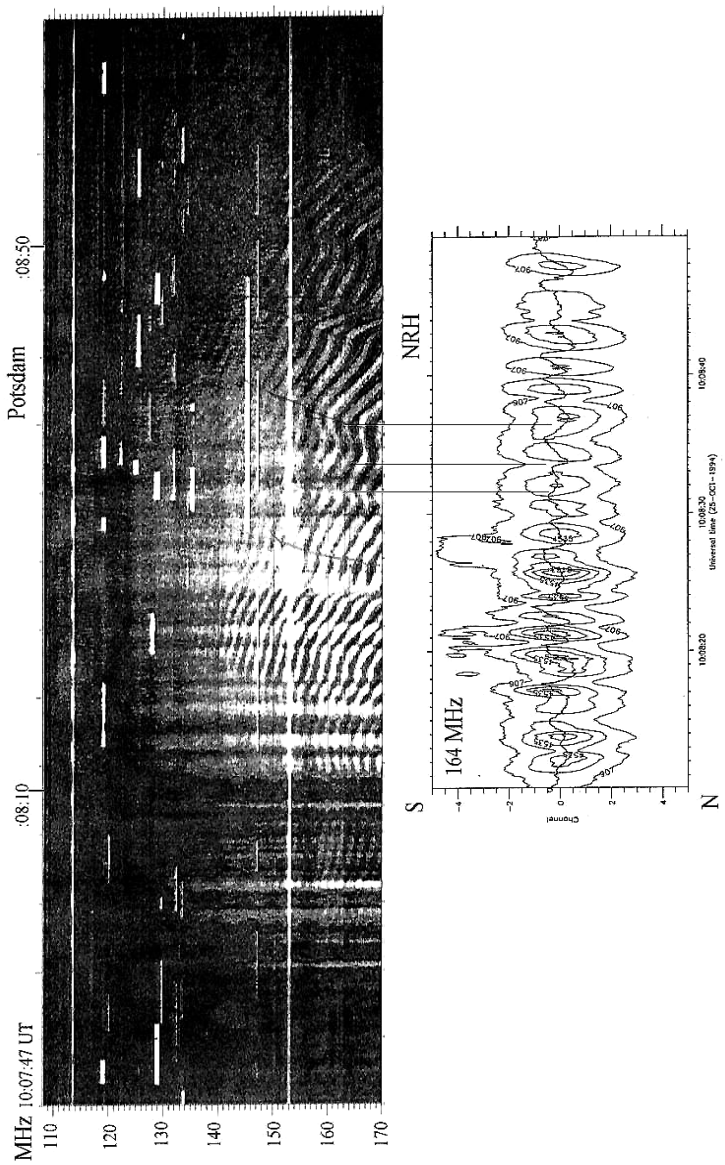

Figure 2. (Top): Dynamic spectrum of ZP against the background of periodic type III bursts in a part of the frequency range 110 – 170 MHz of the Potsdam spectrograph. (Bottom): One-dimensional (S – N) contour plots of the relative brightness distribution at 164 MHz (Nançay RH). The solid line passing through the maxima of the sources shows their spatial drift (from Chernov, 2005).

A part of the ZP dynamic spectrum recorded with the Potsdam spectrograph is shown in Figure 2. It is almost identical to the spectrum recorded at IZMIRAN. The lower part of Figure 2 shows the contour lines of the south-north (SN) distribution of the radio emission intensity at a frequency of 164 MHz (NRH).

The maximal intensity corresponds to the center of the ZP source after 10:08:33 UT or to a type III burst before this instant. The solid line that passes through the source centers shows the spatial drift of the sources at a fixed frequency. We note that the centers of the sources of the ZP and type III bursts coincide not only in the NS direction but also in the east-west (EW) direction (i.e., on the Sun disk).

The III type sources (at the beginning of spectrum) drift from south to north, whereas the ZP sources (at the end of spectrum) drift from north to south. In all the ZP absorption stripes, the source drifts is the same way as in the type III bursts (one such instant corresponding to 10:08:33.4 UT is shown in Figure 2 by the heavy vertical line). The labels on the vertical axis correspond to the numbers of the spatial channels of the Nançay radio interferometer. At a frequency of 164 MHz, one channel in the SN direction provides resolution of about 3.2'. Therefore, the average full width at half-maximum of the radio source (about 4.8') corresponds to one-and-a-half channel for both the ZP and type III bursts, whereas the maximal velocity of the spatial drift turns out to be > 90000 km s^{-1} (about 170 000 km s^{-1} for the last source). Taking into account the projection onto the disk, the actual velocities of the source are always > 10^{10} cm s^{-1} (i.e. close to the speed of light). Thus, the measured source size is actually the AR size and the observed drift velocities can only be attributed to fast (relativistic) particles. Approximately the same drift velocities of the ZP sources were observed earlier during the June 5, 1990 event (Chernov et al., 1994).

We also note the following important feature of the dynamic spectra: there are several humps in the ZP where the frequency drift changes its sign. The change in the sign of the frequency drift correlates with the change in the direction of the spatial drift of the ZP source. The negative frequency drift corresponds to the same source drift as for type III bursts.

The change in the direction of the source drift is accompanied by the change in the sign of the frequency drift (see, e.g., the instants 10:08:32 and 10:08:36.5 UT in Figure 2, which are marked by thin vertical lines). These results allow one to choose model of the ZP generation and to explain the width of the frequency band occupied by the ZP in the dynamic spectrum.

So, a correlation is noticed between the directions of frequency drift of stripes on the spectrum and the spatial drift of sources at the fixed frequency. The speeds of motion in the projection on the solar disk prove to be very large, ≥ 10^{10} cm s^{-1}.

2.2. Fiber Bursts

Young et al.(1961) the first reported observations of 'intermediate drift bursts' (fiber bursts) in the range 500 – 950 MHz in five events of 1959.The authors noticed almost all basic properties of IDB: the presence of absorption ('shadow'), moreover as from the high-frequency edge, so from the low-frequency one; the wide spread of frequency drift to low frequencies and even the reverse drift; the bursts occur usually in regular groups with almost constant frequency spacing, but on some occasions as isolated bursts.

The basic properties of FB are successfully represented by Kuijpers (1975a) (Figure 3), from the event March 6, 1972.

The large contribution to the statistics of observations of FB in the broad frequency range 150 – 1000 MHz was made by Elgarøy (1982). He has found a linear dependence between frequency drift velocity and observed bandwidth, the duration at one frequency t_f is determined by the length of exciter rather, but not by electron collision time. He proposed to define the magnetic field strength B in different ways: the values obtained with frequency separation between emission and absorption $\Delta f_{ea} \approx b_t = f_w \approx 0.25 f_{Be}$, (where f_w - whistler frequency, f_{Be} - electron cyclotron frequency) are compared with values defined using df/dt in the form:

$$B = 6.4(\ln f - 1.3)^{-2} |df/dt|, \tag{2}$$

if to identify the exciter velocity, defined by df/dt in the double Newkirk model with the group velocity of whistlers. He got a magnetic field of 1.4-1.8 G at 150 MHz, and about 13.5 G at 1000 MHz. These values give the plasma $\beta = nk_BT/(B^2/8\pi)$ nearest to 1 ($n = n_e + n_i$; $T = 1.5 \cdot 10^6 K$; k_B - Boltzman's constant, e, i - designate electrons and ions).

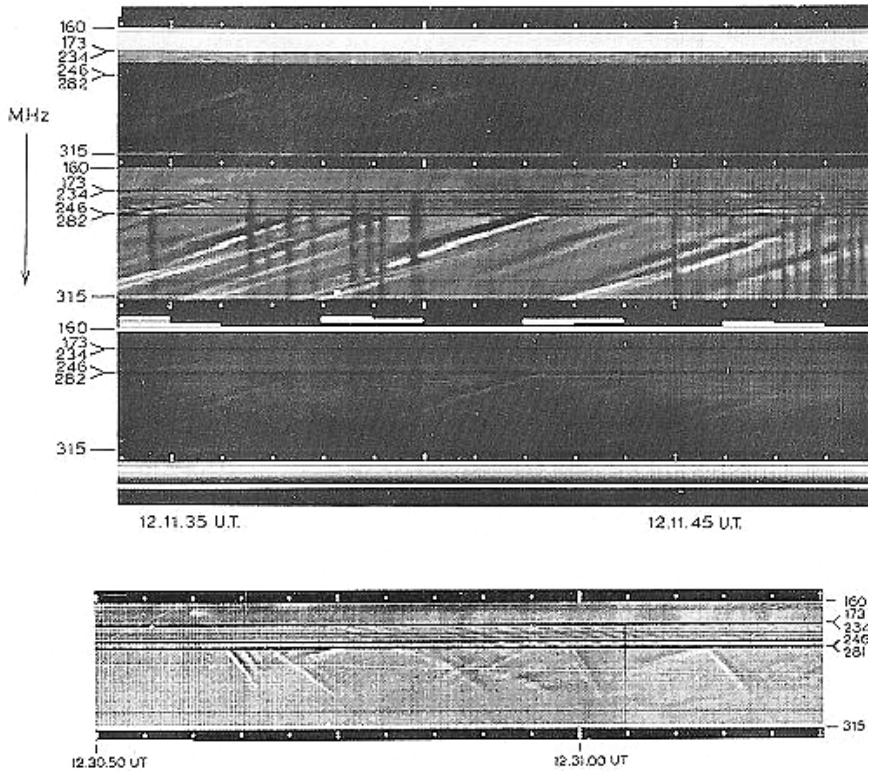

Figure 3. Two examples of intermediate drift bursts observed with 60-channel Utrecht spectrograph on March 6, 1972. Each channel has a width of 0.9 MHz. In the top panel fibers are clearly visible on the sensitive channels in the middle. Lower part - normal channel, upper part - circular polarization (from Kuijpers, 1975a).

The analysis of many cases of ZP near 3GHz in some events shows the full variety of fine structure similar to that seen in the meter range. In the event of October 29 2000, for about 20 minutes ZP and fiber bursts (FB) were followed by intermittent pulses of some

seconds (Chernov et al., 2001b). The FB and ZP have about the same spectral parameters, e.g. the frequency bandwidth of emission stripes $\Delta f_e \approx 20 \div 30$ MHz and the frequency separation between emission lines is 50 – 80 MHz in the range 2.6 – 2.8 GHz.

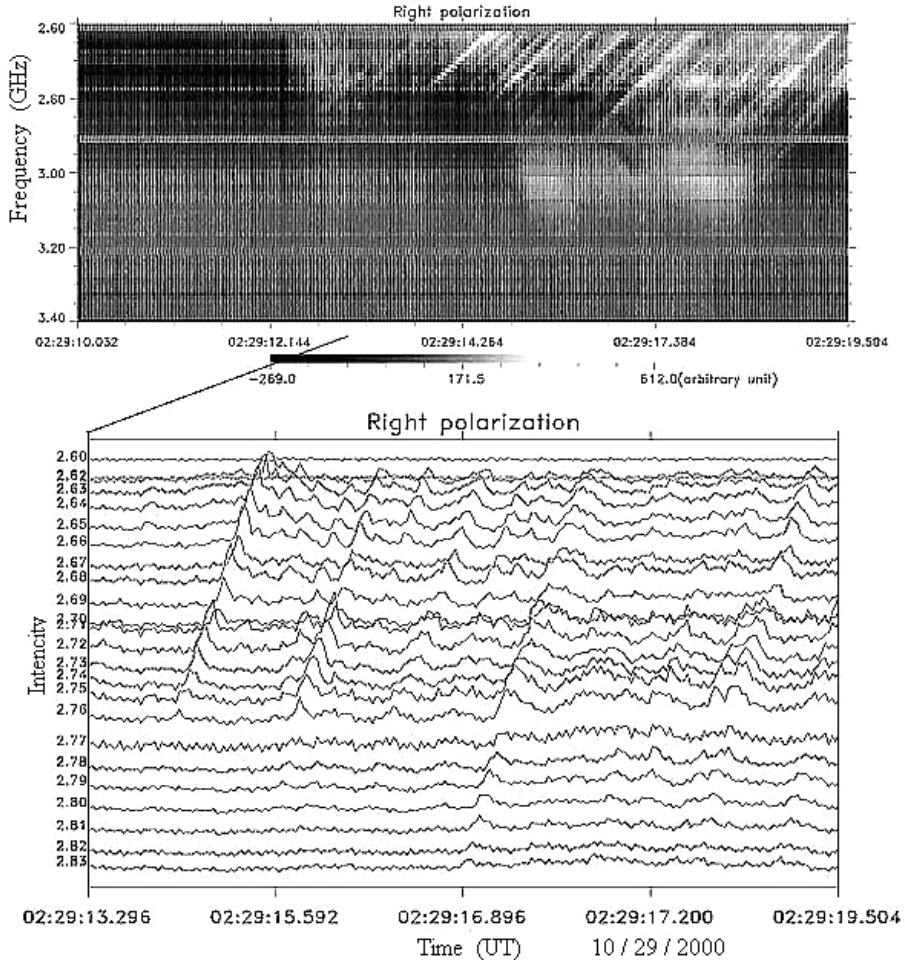

Figure 4. Radio spectrograms of fiber bursts in the event of 29 October 2000. The multi-channel profiles (bottom panel) show irregular character of fibers in time and almost constant frequency drift. (from Chernov et al., 2001b).

In Figure 4 after some ZP wiggles we can see a series of strong fibers with different periodicities and almost constant frequency drift rate ~ -240 MHz s^{-1}. However, the multi-channel profiles in the bottom panel show the small retarding of the drift rate of some fibers, drifting from 2.83 to 2.60 GHz, which seems completely natural, in accordance with formula (1) (frequency drift is proportional to magnetic field strength). We see that the high frequency IDB are found to be identical in their relative characteristics with FB in the metric range.

A detailed analysis of the multi-channel time profiles (see Fig. 3 in Chernov et al. (2001b) shows that the intensity level in the black stripes (between emission stripes) could be lower than the emission level of the main continuum (without ZP). Thus, the black zebra-stripes are visible not due to the absence of bright stripes, but due to an absorption of the main

continuum emission (a modulation effect). In this connection the main parameter of ZP and FB is not frequency separation between emission stripes ($\Delta f_s \approx 60 - 70$ MHz on an average), but the frequency separation between the emission and the adjacent low frequency absorption with a mean value $\Delta f_{ea} \approx 30 - 40$ MHz. Therefore we can assume that both of the fine structures have the same origin.

Sometimes, it is difficult to distinguish ZP stripes from FB. Figure 5 shows stripes in emission and absorption intersecting in the dynamical spectrum in the event June 5, 1990. In Chernov et al. (1994) an attempt is undertaken to analyze polarization time profiles of Trieste AO together with the positions of the radio sources of the separate zebra stripes by means of Nançay Radio Heliograph (NRH) at 164 and 236.6 MHz.. This long lasting type IV event is related possibly with a filament activation and eventual eruption, but is not initiated by a conspicuous flare. In such a case it was very simply to show that the radio source positions were connected to a region of southern magnetic polarity near the active region (AR) 6086. The radio emission was fully R-handed polarized and is thus likely to be in the ordinary mode.

In this case ZP was more pronounced in absorption (see in Figure 5, below spectra, the flux density time profiles in left-hand and righthand polarization of Trieste AO at 237 MHz), and the stripes with the negative frequency drift are similar to fiber bursts with low-frequency absorption. When an emission stripe from one set intersects an absorption stripe from another set, the emission stripe is strongly reduced. The process by which the continuum is extinguished therefore also reduces the emission stripe. This can only occur if the emission and absorption stripes are generated in the same volume. The absorption may be very pronounced: at 10:45:21 UT the modulation depth m_d at 237 MHz is about 90%. It is defined as $m_d = (I_{max} - I_{min})/(I_{max} + I_{min})$, where I, denoting the whole Sun flux density. It varies with time, e.g. after 6 s m_d decreases gradually from 66 to 27%. However near the end of the event a series of zebra stripes only in emission is observed.

Due to the limited time resolution of the NRH north-south array (the integration time of 0.25 s) we cannot describe the time history of displacements of all rapid variations seen e.g. in Figure 5 in the spectra and Trieste polarization profiles with the integration time of 0.02 s. The centroid of the continuum source, plotted by the dashed line through the center of the strongest contour (3rd row in Figure 5) was stable during the 13-s interval. However, during the zebra stripe the centroid undergoes an oscillating drift (the bottom panel): northward at the onset of the stripe, then southward near the brightest emission. The monotonic southward displacements were also observed in other series of zebra stripes in emission with the positive frequency drift (see Fig. 6 in Chernov et al.(1994)).

The maximum shift covered 0.56 channels (about 47'') that corresponds to the velocity component along the terrestrial north-south baseline of about $7 \cdot 10^4$ km s^{-1}. The measured r.m.s. variation around the mean value was of 0.025 channels (2''), therefore the position changes detected during zebra stripes are significant. Similar shifts of emission throughout isolated zebra stripes are also visible at 164 MHz with the east-west array (50 ms resolution). For example, during the interval of zebra stripes shown in Figure 6 the centroid of the source starts at a position east of the preceding continuum and drifts westward throughout the maximum brightness of the three emission stripes between 10:36:55 – 57 UT with the negative frequency drift. The total distance covered by the space drift is of the order of $2 \cdot 10^4$ km and the projected velocity $\approx 10^5$ km s^{-1}.

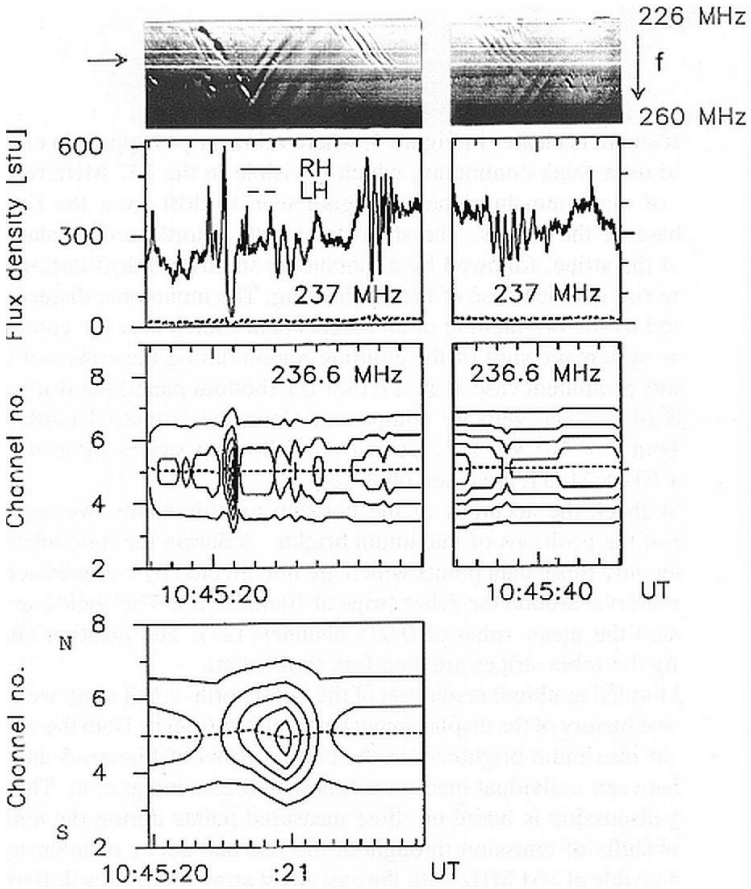

Figure 5. Oppositely drifting zebra stripes in the event June 5, 1990. The two top panels give the dynamic spectrum (IZMIRAN, the arrow points to 237 MHz) and the 237 MHZ records of the flux density in RH and LH polarization (Trieste AO). The abscissa is graded in steps of 1 s. The third panels from the top give the evolution of radio brightness and source position at 236.6 MHz (Nançay Radio Heliograph (NRH)), north-south array) with contours from 9 to 89% of the biggest intensity, in steps of 20%. The dashed line through the centre of highest contour gives the position of peak brightness. The vertical axis is graded in 1.4', channel numbers of NRH from terrestrial south to north. The projected position of the centre of the solar disk is in channel 0. The fourth panel shows a zoom of the zebra source around 10:45:21 UT (from Chernov et al., 1994).

The zebra stripes undergo several wiggles with a spasmodic (sawtooth) sign change of the frequency drift. We can note two such moments, 10:36:58 and 10:37:01 UT, and in both cases the space drift changes direction, to eastward. Furthermore, during one second into 10:36:59 – 10:37:00 UT the frequency drift was almost zero, and the spatial drift in this source was also retarded.

Thus, we observe specific relation between the directions of the frequency drift on the spectrum and the spatial drift of sources. In absorption stripes we see the whole continuum source. For this reason we always notice the shift of the center of source upon transfer from the emission stripe into the absorption stripe, since the position of the maximum brightness of continuum, as a rule, is considerably displaced from the maximum in the emission stripe.

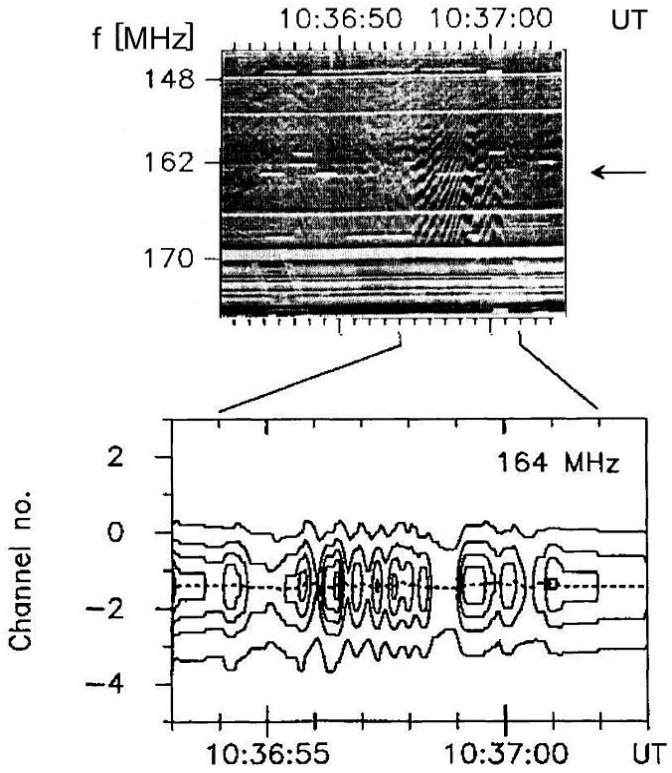

Figure 6. Temporal evolution of the dynamic spectrum (IZMIRAN) and source position (NRH) during an interval of zebra pattern in the event June 5 1990 near 164 MHz (the horizontal arrow on the right indicates 164 MHz). Below - the one-dimensional map at 164 MHz with east-west array; the position of maximum brightness is noted by the dotted line; 1 channel≈1.0', time resolution 0.05 s (from Chernov et al., 1994).

2.3. Manifestation of Quasi-Linear Diffusion on Whistlers in ZP and FB

We showed several fragments of ZP which it is difficult to explain within the framework of DPR mechanism (in its any version). At least, no one even attempted this to make. All the main properties of the emission and absorption stripes can be explained in a model involving interactions between electrostatic plasma waves and whistlers, taking into account the quasi-linear diffusion of fast particles with the loss-cone distribution on whistlers. Within the framework of this mechanism alone not simply the stripes in the emission and the absorption are explained, but also the entire dynamics of the stripes on the spectrum and of their radio sources (splitting of stripes, movements of the sources, superfine spiky structure).

The basic aspects of this model are in detail presented in Chernov (2006). Here, we will show only how it is possible to explain the observed correlation of frequency drift and spatial drift of sources.

The complete solution of the quasi-linear problem for the three resonances with particle sources and losses is very difficult, and has not yet been obtained either analytically or numerically. Usually, a simplified problem is posed, and quasi-linear equations are solved numerically for one resonance and one oscillation mode with a loss-cone distribution

function (Ossakov et al., 1972; Ashour-Abdalla, 1972; Sazhin, 1987; Bespalov and Trakthenherz, 1986; Stepanov and Tsap, 2002).

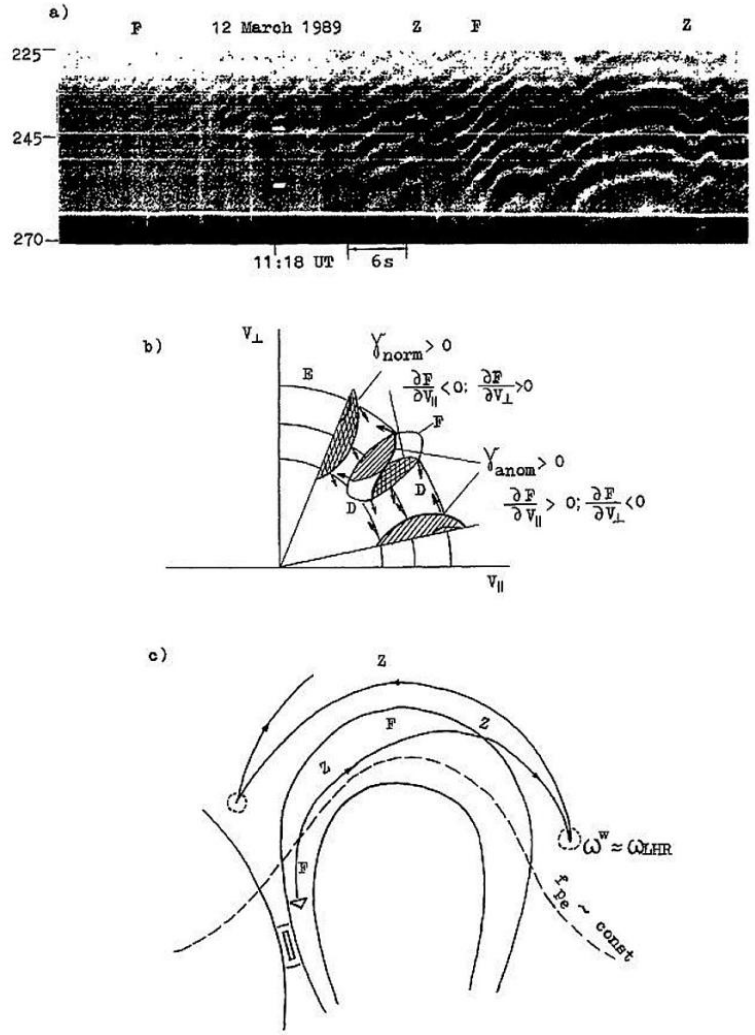

Figure 7. a): Dynamical spectrum of ZP with wave-like frequency drift in the type IV burst of March 12, 1989. The Z, F labels above the spectrum refer to the times when zebra stripes (Z) with a constant drift toward low frequencies become similar to fibers (F). b): Schematic presentation of the fan instability switching of whistler instability from normal Doppler cyclotron resonance (cross-hatched F regions) to anomalous resonance (single-hatched regions) due to the shift of the maximum (bump) of the distribution function F during diffusion along the diffusion curves D (arrows) from large values of $\upsilon\perp$ (where the operator $\hat{\Lambda} < 0$) to large $\upsilon\|$ (where $\hat{\Lambda} > 0$). c): qualitative scheme of a whistler trajectory explaining the possibility of ZP conversion into FB and inversely (from Chernov, 1990).

Figure 7b schematically shows the shapes of the distribution function of type anisotrpic beam at small, moderate and large pitch angles for three improvised moments of time in the course of the diffusion: with large $\upsilon_\|$ at small pitch angles, and large $\upsilon_\perp$ at large angles; in an intermediate position the equal contribution of $\upsilon_\|$ and $\upsilon_\perp$ is possible. If fast particles interact

with whistlers at the cyclotron resonance they move on the ($\upsilon_\perp$, $\upsilon_\parallel$) plane along the diffusion curves (D):

$$\upsilon_\perp^2 + \left(\upsilon_\parallel - \omega/k_\parallel\right)^2 = const \tag{3}$$

in the direction of decrease of the distribution function $F(\upsilon_\perp, \upsilon_\parallel)$ (Gendrin, 1981; Chernov, 1996).

Particles with the small pitch angles give their energy to the waves and they approach the loss-cone, and particles with large pitch angles increase their energy ($\upsilon_\perp$) due to the waves. However, only the part of the particles is poured out quickly into the loss-cone, directly it adjoining, and the loss-cone remains for a long time empty. Estimations of the time of life of the fast electrons with the scattering on the whistlers in the regimes of the moderate and strong diffusion give times 10 – 20 s (Bespalov and Trakhtenherz, 1986).

If the resulting flux of particles in velocity space is directed toward increasing particle energy, energy in the given range of velocities will be transferred from resonant waves to particles, and the wave will weaken. This physical process finds its theoretical reflection in the identity operator $\hat{\Lambda}$ (which has the meaning of a derivative along the curve D) in formulas for the whistler instability increment and the distribution function diffusion equation (Gendrin, 1981; Bespalov and Trakhtenherts, 1986):

$$\hat{\Lambda} = \frac{s\omega_{Be}}{\omega\upsilon_\perp}\frac{\partial}{\partial\upsilon_\perp} + \frac{k_\parallel}{\omega}\frac{\partial}{\partial\upsilon_\parallel} \tag{4}$$

For positive values of the increment the operator $\hat{\Lambda}$ should be negative. In Figure 7b we show that at the normal Doppler effect the increment γ_{norm} will be positive with the derivatives $\partial F/\partial\upsilon_\parallel < 0; \partial F/\partial\upsilon_\perp > 0$, and at the anomalous Doppler effect γ_{anom} will be positive with $\partial F/\partial\upsilon_\parallel > 0; \partial F/\partial\upsilon_\perp < 0$. In the intermediate position the beam contributes in the instability at both resonances, and the parts with positive γ_{norm} are cross-hatched, and the parts with positive γ_{anom} are single-hatched.

The smooth switching of the predominant contribution from the anomalous to normal Doppler resonances (and inversely) occurs in accordance with the sign of an operator $\hat{\Lambda}$. Thus, if the entire trap is filled up with the fast particles (prolonged injection), that the continuous quasi-linear diffusion on the whistlers begins to work in a self-oscillatory regime, when it is possible a switching of the instability from the predominance of the normal Doppler resonance to the anomalous one and back (an analogy with the fan instability (Shapiro and Shevchenko, 1987) and with the spike regime in the TOKAMAK (Parail and Pogutse, 1981). Such switchings of the instability indicate smooth (or sharp) changes in the direction of the whistler group velocity, which explain the frequently observed smooth (undulating) changes in the frequency drift of the stripes or sharper jumps in the form of sawtooth stripes, if the distribution function is deformed by a new impulse particle injection (Chernov, 1996).

Thus, smooth changes in the frequency drift of zebra stripes and the gradual conversion of ZP into FB and vice versa, shown in Figure 7a, it is possible to explain by the precisely

quasi-linear effects of scattering of fast particles on whistlers. Changes in direction of V_{gr}^{w} to the opposite one during the switching of resonances it is confirmed by the observations of the positions of sources. In Chernov (2006) in Figure 13 it is shown that the change of the sign of the frequency drift of stripes correlates with the change of the sign of the space drift of sources at the fixed frequency.

Figure 7c shows the qualitative scheme of the possible prolonged propagation of whistlers in the corona for the cases, when FB and ZP can appear alternatively during ~ 1 minute, and quasi-linear effects act in the shorter time intervals. Longitudinal whistlers excited in the base of the magnetic trap by particles accelerated in the region of magnetic reconnection at the normal resonance propagate upward along the trap and give fibers (F). The excitation on the anomalous Doppler resonance at large angle to the magnetic field can predominate at the apex of trap, and whistlers propagate downward (sometimes almost parallel to the level of constant f_{Pe}) to the possible mirror points (where $\omega \approx \omega_{LHR}$) (in ZP the positive frequency drift predominates).

2.3.1. Explanation of LF Absorption

The dark stripes of the ZP indicate not the simple absence of the increased emission, but the real absorption of background continuous emission, which is modulated by the ZP. One of the very obvious cases of real absorption in the ZP is given in Figure 5, where the absorption of the continuum exceeded 90% according to the data of NRH at the frequency 237 MHz.

The most reliable explanation of the absorption at the low-frequency edge from the stripe in the emission is obtained, if we take into account, that in the quasi-linear diffusion time the intensity of the plasma waves (critical for the continuous emission) is reduced in the volume of the whistler wave packet due to the electron diffusion on the whistlers.

So, with the whistler excitation on the normal resonance ($\upsilon_{\perp} > \upsilon_{\parallel}$) the maximum of the distribution function is displaced almost instantly to the high longitudinal velocities (to smaller pitch angles) due to the diffusion of fast particles on the whistlers, and the instability of the plasma waves on the double plasma resonance sharply weakens, that also is exhibited in the form of the dark stripe of the zebra-structure. But if the initial diffusion on the whistlers occurs on the anomalous resonance ($\upsilon_{\perp} < \upsilon_{\parallel}$), and the plasma Langmuir waves along the field are emitted, that in this case their level will be reduced because of the turn of the beam to the high transverse velocities. Unusual fibers (without the noticeable absorption) in the type II bursts are sometimes observed. Such fibers structure can be naturally connected with the propagation of the whistlers through the clusters of the plasma waves before the shock wave front. But before the wave front there is no trap, particles and waves disperse in the space, and diffusion on the whistlers does not work. Therefore the instability of plasma waves is not reduced in the volume of whistler wave packets and the absorption is absent. Thus, the natural and necessary consideration of the quasi-linear effects of the diffusion of fast electrons with the loss-cone anisotropy on the whistlers allows to explain a number of the important properties of fibers and ZP.

2.4. A Superfine Spiky Structure of ZP in Microwave Bursts

The discovery of the superfine structure of ZP, in the form of millisecond spikes was the most significant effect in cm range. According to Chernov et al. (2003), in 7 microwave bursts with ZP and FB a new effect was discovered by solar broadband radio spectrometer in Huairou station (Beijing, NAOC) (Fu et al., 1995) in the frequency range 2.6 – 3.8 GHz: zebra-stripes had own superfine structure, they were consisted of numerous fast spikes with duration at a limit of the time resolution of spectrometer ≈ 8 ms. The same superfine structure was observed in the event of April 21, 2002.

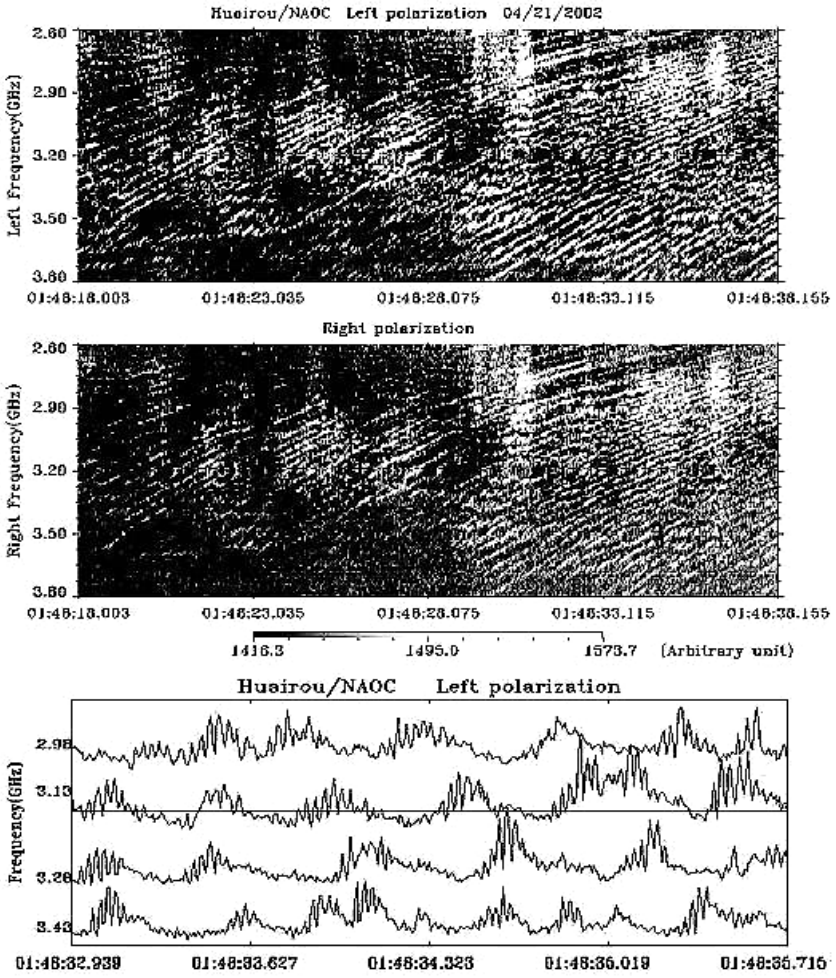

Figure 8. Zebra structure in the event of April 21, 2002. The two upper panels show the Huairou radio spectrograms in the 2.6 – 3.8 GHz range in the left and right polarization components with a zebra pattern at 01:48:18 – 01:48:38 UT, in which 34 stripes can be distinguished and whose frequency separation grows smoothly with frequency. The lower panel shows profiles of the intensities at four fixed frequencies. The profiles confirm the spike-like structure of each zebra stripe in emission. The dark stripes do not contain a spike-like structure, and the radiation level proves to be lower than the average level of continuum, shown by the straight line at a frequency of 3.13 GHz (from Chernov et al., 2005).

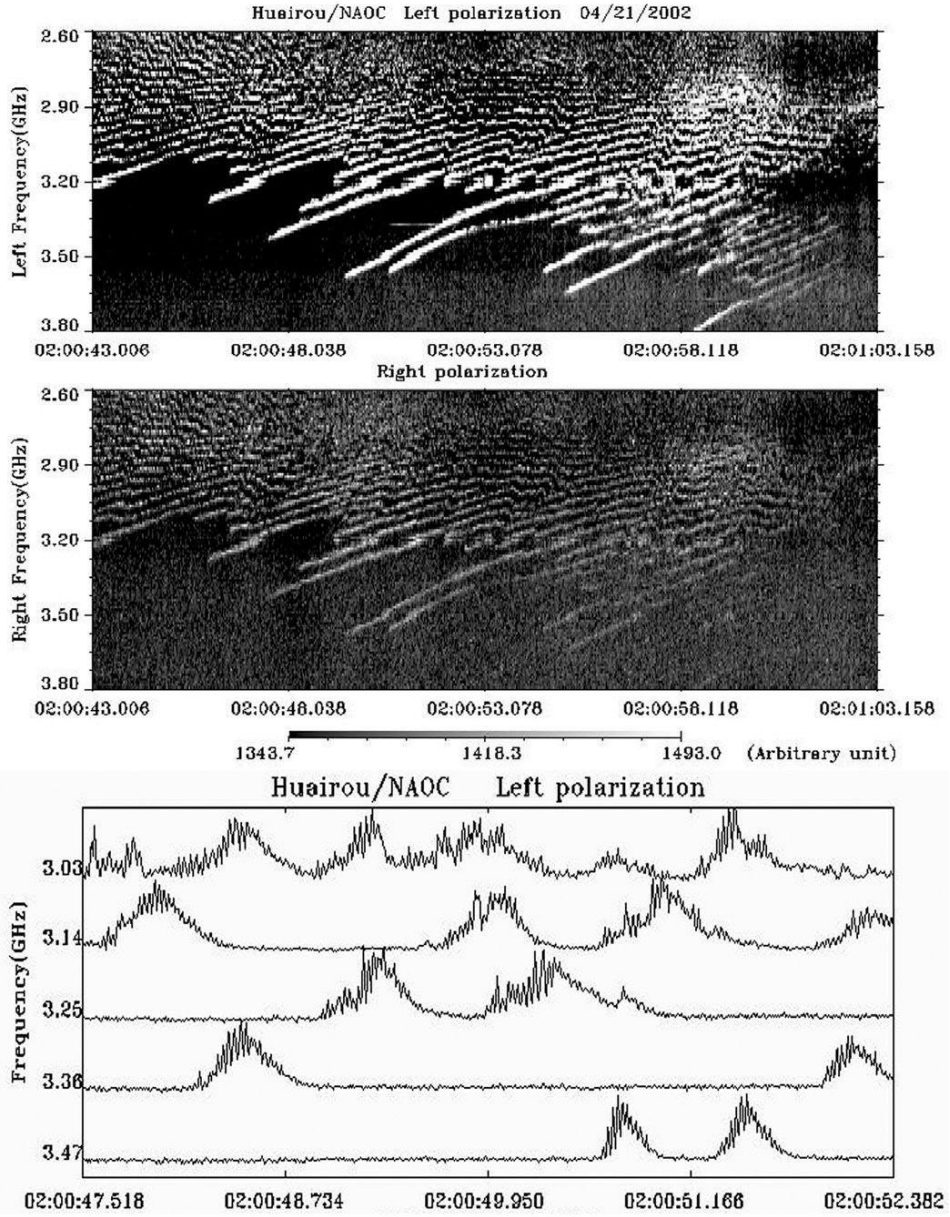

Figure 9. Zebra structure in the event of April 21, 2002 at 02:00:43 – 02:01:03 UT. The zebra stripes on the high-frequency edge of the spectrum are more similar to isolated fibers without any strict periodicity. The multichannel time profiles (in the bottom panel) show stripes in emission consisting of spikes as before. However, in the dark stripes the residual emission remains at a fixed level (from Chernov et al., 2005).

All series of the ZP in this event represented zebra stripes with negative frequency drift, which is more inherent to fibers. In Figure 8 and 9 two intervals with the most pronounced ZP are shown, taken with the NAOC spectrometer at 2.6 – 3.8 GHz. In the first fragment of 20 second duration from 01:48:18 UT 34 zebra stripes are counted in the range 2.6 – 3.8 GHz with a barely noticeable increase in frequency separation between stripes from 27 MHz at

2.8 GHz to 43 MHz at 3.7 GHz. It is remarkable that the relative value of the frequency separation proves to be about the same as in the meter range $\Delta f/f \approx 0.012$. The frequency drift of zebra stripes was negative and almost constant ≈ -120 MHz s^{-1} between 3.8 – 3.4 GHz, which is more characteristic of fibers. At the low frequency part of the spectrum a small deceleration of the frequency drift is observed. However, each 1 – 2 s, stripes undergo failures and jumps of frequency drift, covering several adjacent stripes with a small time delay. Sometimes shifts in the frequency lead to merging or splitting of stripes. Such effects are well known in the meter wave band. In the bottom of Figure 8 a short fragment of intensity time profiles of about 3 s duration is shown at four frequencies.

A detailed analysis of multichannel time profiles shows that each zebra stripe in emission has a spike-like structure. In the dark stripes (between the bright zebra stripes) the emission level can be lower than the level of burst background (lower than the average level of continuum, shown by a straight line at 3.13 GHz). Thus the presence of dark stripes is connected not with the absence of bright stripes (in emission), but with an absorption of background microwave emission. The polarization degree was weakly left-handed.

The fragment in Figure 9 shows some changes of ZP properties: the polarization degree becomes stronger and it grows with time and frequency; the frequency drift almost stops in the low-frequency part of the spectrum (sometimes the stripes are almost parallel to the time axis); however, in the high-frequency part of the band they are more similar to isolated fibers with a negative frequency drift (there is no strict periodicity). The multichannel time profiles (in the bottom panel of Figure 9) show that stripes in emission consist as before of spikes, however, in the dark stripes, deep dips in emission are not observed; the residual emission remains at a fixed level.

ZP was also observed in the pulsating regime, but almost all series of ZP were prolonged; in the examples in Figure 8 and 9 the duration exceeded 1 minute. The evolution of zebra stripes in several series began from a cloud of millisecond spikes with the gradual shaping of zebra stripes.

Identical spectra of zebra stripes with superfine structure (within the limits of instrument resolutions) obtained simultaneously at two observatories, confirm a solar origin of the ZP superfine structure (Chernov et al., 2006).

3. Recent Results of Zebra Patterns in Solar Radio Bursts

3.1. 2004 July 24 Event

Chernov et al. (2008) analyzed strange fiber structures in four events in decimeter range when small-scale fibers are organized into large-scale ZPs. They used spectral observations from the new Chinese spectrometer (Huairou station of NAOC, Beijing) in the range of 1.1 – 2.0 GHz with extremely high resolution of 5 MHz and 1.25 ms (Fu *et al*., 2004).

Figure 10 demonstrates a new variety of stripes in emission in the event on 2004 July 24. At the beginning of the event, separate narrow-band stripes (small fibers) were located along the frequencies, forming almost instantaneous pulsations (around 06:04:20 UT); then they were decomposed and aligned along the inclined straight lines that are parallel to the individual small fibers. At the end of this time interval the small fibers formed an almost

braided ZP (around 06:04:26 UT). The circular polarization of the fibers was dominantly of right-hand sign.

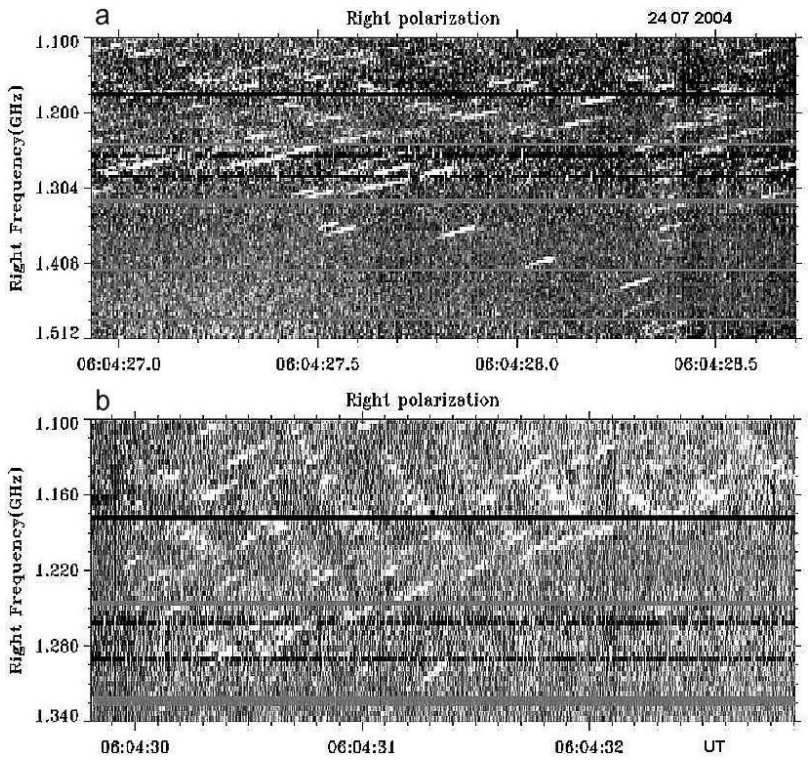

Figure 10. (a) Dynamic spectrum in the range 1.100 – 1.512 GHz in left and right circular polarizations recorded by the spectrometer of NAOC on 24 July 2004. (b) The continuation of the 24 July 2004 event in the range 1.100 – 1.340 GHz in the right- circular polarization (the radio emission is fully polarized) (from Chernov et al., 2008).

One second later (Fig. 10a), they were located once more along the inclined straight lines (06:04:27.0 – 06:04:28.5 UT), and a new special feature was seen two seconds later (06:04:30 UT): they were localized along the straight lines, but with the reverse (positive) drift. In one more second (06:04:31 – 06:04:33 UT), this special feature was already clearly the basic prevailing structure (Figure 1b) which is basically regarded as large-scale ZP stripes drifting to higher frequencies with the speed of about 270 MHz s^{-1}. These structures were terminated at a certain high-frequency boundary which drifted to lower frequencies with the speed of approximately – 67 MHz s^{-1}.

In Figure 10 only right polarization channels are presented because the polarization degree was 100%. The fiber structure appeared as a forerunner of the rise of continuum which continued for more than three minutes, but no more fine structure was observed.

The flare of M1.0 1F class occurred at 06:01 – 06:04 – 06:10 UT in the active region (AR) 10652 (N07W20). The analyzed fiber structure was observed after several strong pulsations at the very beginning of the smooth rise of a flare continuum in the unpolarized emission whose duration was about 5 minutes.

According to the spectral data of IZMIRAN in the frequency range of 270 – 25 MHz, the pulsations had a continuation in the meter-wave range in the form of type III bursts, where they stopped at frequencies near 200 MHz in the form of J- bursts. Later the flare continuum lost any fine structure, and the event ended, without type II bursts or any coronal mass ejection (CME).

In the absence of spatially-resolved radio observations, the position of the radio source can be inferred from the image of the flare in the chromosphere of TRACE 1700 Å data (Strong *et al*. 1994). At the moment 04:07 it was superimposed on the magnetogram (Solar Flare Telescope, NAOJ/Mitaka). Three bright flare kernels were located to the west of the preceding sunspot of this AR, above the quadrupole-like structure of the magnetic field with a peculiar X- point at the center of the flare region.

The two flare kernels were located above the S- magnetic polarity; therefore the radio emission of right circular polarization should correspond to the ordinary wave mode. The flare kernels in the 195Å images were also located exactly above the bright regions seen in the 1700 Å images, and the radio source in right circular polarization at 17 GHz (Nobeyama Radio Heliograph) was also located in this place. The largest radio flux was recorded in decimeter and meter ranges, indicating the magnetic reconnection occurred high in the corona. As a matter of fact, in the 1700 Å images we see bright tops of the flare loops. The decimeter radio source is expected to be found below the flare current sheet (where the acceleration of fast particles would take place). The positive frequency drift of the large scale ZP stripes may be caused by the downward motion of a plasma ejection from the reconnection region with the Alfvén velocity. On its way this ejection would meet a flare loop arcade that was expected to be rising. The high-frequency boundary of the termination of emission can be the consequence of this collision.

3.2. 2004 November 3 Event

This event was most powerful and most prolonged, with diverse fine structures and duration of about 2 hours, over the course of repetitive brightenings of the flare. For the analysis we selected only its first part (with a duration of about 25 minutes), at the beginning of which small-scale fibers were observed (Figure 11), and, as in the previous events, it was also a forerunner of the entire event.

The first glance at Figure 11 reveals certain similarity to the event of 2004 July 24: at first, the small-scale fibers occurred chaotically scattered along the frequencies, then they were localized at some frequencies and formed large-scale ZP stripes, and at the end they broke up again to separate into chaotic fibers, which gradually (during ≈ 1.5 min) broke up into a cloud of chaotic spikes. The essential difference lies only in different polarization. Here, it was of moderate right-hand sign.

Figure 12 helps to better estimate the parameters of the small fibers that composed the large-scale ZP. The time profiles at the fixed frequency of 1.216 GHz show that all profiles are symmetrical, and have an almost Gaussian shape. The frequency drift of fibers was stable and constant, ≈ – 270 MHz s^{-1}, and for the large-scale ZP, it was ≈ 630 MHz s^{-1}.

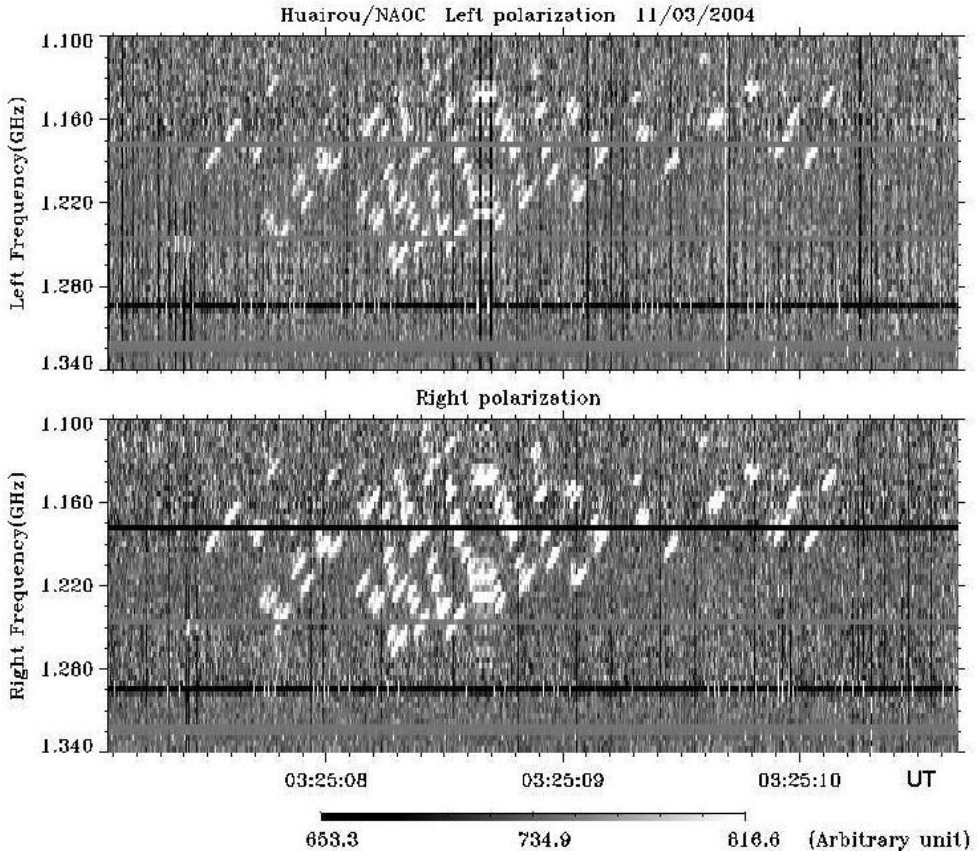

Figure 11. The beginning of the 2004 November 3 event in the frequency range 1.100 – 1.340 GHz, showing moderate right-hand polarization: the small-scale fibers are re-grouped into large-scale ZP stripes (from Chernov et al., 2008).

The flare of M1.6 1N class has occurred at 03:23 – 03:35 – 03:57 UT in AR 10696 (N09E45). The analyzed fiber structure was observed at 03:25:07 UT at the very beginning of the smooth rise of a flare continuum in the non-polarized emission whose duration was about 25 minutes. According to Culgoora spectral data, strong type II bursts began at 03:33 UT at frequencies near 120 MHz (estimated shock speed 750 km s^{-1}), accompanied by a powerful CME (SOHO/LASCO C2) after 03:54 UT (whose estimated speed was 918 km s^{-1}).

After about 03:30 UT the polarization of the fine structure changed sign, and the left-handed polarization became predominant. The dynamics of flare processes can be tracked according to RHESSI hard X-ray data in the 6.0 – 7.0 keV energy band, the Nobeyama radio map at 17 GHz (Chernov *et al.* 2008). At 03:26 UT the radio source had a triple structure (in accordance with the distribution of sunspots in the AR) with a big source of predominantly right-hand circular polarization above the following spot of the S-polarity. A single HXR-source was located above this radio source. At 03:30 UT a new HXR source appeared in the south-western portion of the AR. Thus, the strengthening of the radio source at this moment was connected with the development of the flare above the small leading spot of N-polarity. In the higher energy band 14.0 – 16.0 keV, even two new sources have appeared in the same

location. So, it is possible to conclude that the radio emission corresponded to the ordinary wave mode both at the beginning and in the maximum of the event.

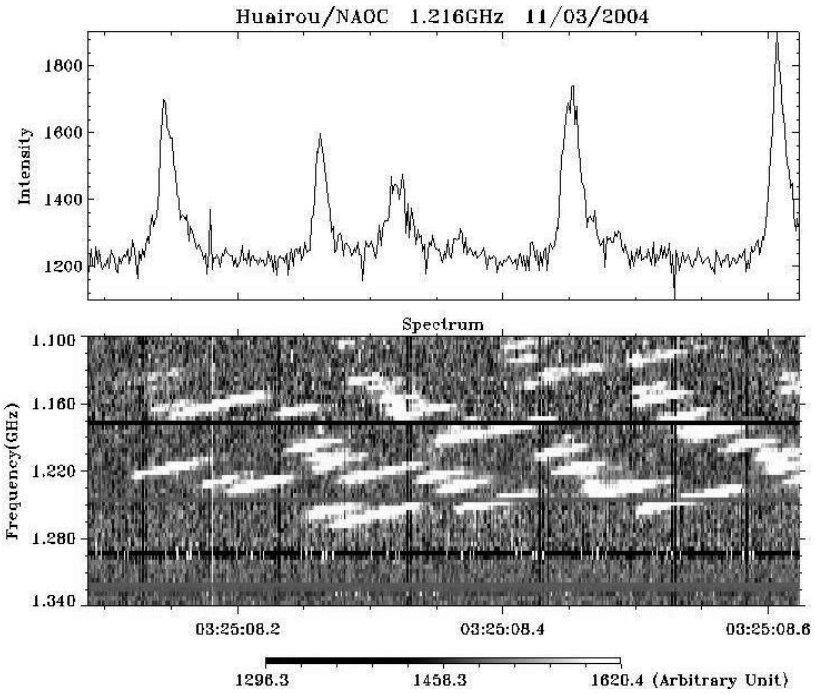

Figure 12. The magnified dynamic spectrum (bottom) and the time profile at 1.216 GHz (top) of the fiber structure on 2004 November 3 (from Chernov et al., 2008).

We can derive the following conclusions from the observations of two events with small-scale fiber bursts as a substructure of large-scale ZPs:

- Narrowband fibers almost always drift to lower frequencies with the speed that is typical in usual fiber bursts, and sometimes they are similar to the ropes of fibers in the meter range.
- In two events the fibers evolved from chaotic features in the dynamic spectrum to a regular structure (in the form of large-scale ZP stripes) and again to disorder, being gradually converted into the spike-bursts.
- Large-scale ZPs were limited at high frequencies by a boundary drifting to lower frequencies with the speed of – 70 to – 90 MHz s^{-1}.
- The radio emission was moderately or strongly polarized and corresponded to the ordinary wave mode.
- The fiber structure appeared as a forerunner of the entire event.
- The fibers, as well as large-scale ZP, do not reveal absorptions at the low frequency edge.
- A superfine structure in small-scale fibers was not detected with a time resolution of 1.25 ms.

In two other events (2004 December 22 and 2004 October 31) small-scale fibers can be regarded as the fine structure in type III bursts and broadband pulsations (Chernov *et al.* 2008).

3.3. December 13, 2006 Event

3.3.1. Introduction

The most recent large flare of the 23rd cycle was observed on 2006 December 13 (02:10 – 05:10 UT) in the active region NOAA 10930 (S05W24–27). This was an unusual event by its importance (X3.4/4B) and fast coronal mass ejection (CME). The flare also provided the richest material for the analysis of fine structures of radio emission in the microwave range. Numerous spikes in absorption of millisecond duration are the main feature of radio emission observed during the decay phase of the flare. The Solar Broadband Radiospectrometer (SBRS) in the range of 2.6–3.8 and 5.2–7.6 GHz (Huairou Station, NAOC) carried out the radio observations (Fu *et al*. 2004). The frequency resolution of the SBRS is 10 MHz, and the cadence is 8.0 ms.

During this long-lasting event, different types of common fine structures were observed (e.g. spikes in emission, usual zebra-patterns and fast pulsations). However, during the decay phase together with the spikes in emission, spikes in absorption began to appear. The latter were first randomly distributed in the frequency range 2.6–3.8 GHz, then they exhibited fast pulsations and trajectories of type III-like bursts in the dynamic spectrum. Furthermore, numerous type III bursts in absorption were observed for about one hour.

The impulsive phase of this event with some fragments of zebra patterns has already been described by Yan, *et al.*(2007). Fast radio pulsations were examined in Tan *et al.* (2007). They assumed that a resistive tearing-mode oscillation in the current-carrying flare loops modulated the microwave emissions and formed the pulsating structures. The positions of X-points is between two magnetic islands. There are many X-points in each flare loop.

The spikes in emission and fiber bursts were studied by Wang *et al.* (2008). Chen and Yan (2008) already reported the absorptive spikes in this event. The type III-like burst in absorption had been explained by Chen and Yan (2008) as a fragmentary injection of new particles in a loss-cone leading to quenching of the loss-cone instability of plasma waves at the upper-hybrid frequency. Parameters of the bursts in absorption (instantaneous frequency bandwidth and duration, frequency drift *etc*.) depend on parameters of new beams of particles.

A general description of absorptive spikes in this event was carried out by Chernov *et al*. (2010). The reason for the appearance of spikes in absorption at the decay phase of the event should be understood. It was necessary to estimate how the physical parameters vary in the event, and how the type III-like bursts are formed from the absorptive spikes (with elements of ZP stripes).

The first spikes in absorption appeared at 02:53:08 UT. Further, over more than one hour, different combinations of the spikes in absorption and the type III- like bursts in absorption and in emission were observed. The latter appeared simultaneously and both with positive and negative frequency drift. For the analysis, it is important to know what kind of specific features of the flare were associated with the appearance of bursts in absorption.

Figure 13 shows the timing and frequency range of fine structures in the dynamic spectrum of the whole event. It is evident that spikes in emission (yellow bars) were observed over the whole event while the spikes in absorption (red) were only observed in the decay phase.

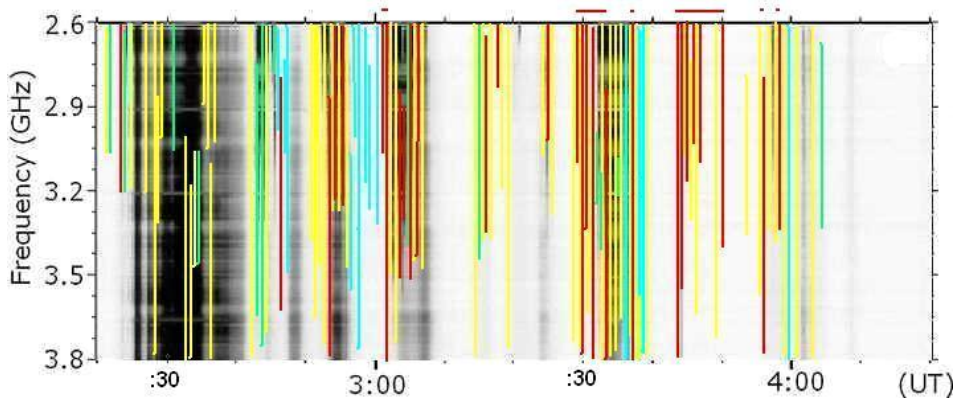

Figure 13. The dynamic spectrum of the whole event 13 December 2006 in the frequency range of 2.6 – 3.8 GHz. The emission is displayed in a negative picture (darker means stronger emission). The color bars indicate timing and frequency range of fine structures: yellow – spikes in emission, red – spikes in absorption, blue – fiber bursts, green – zebra pattern. The red horizontal bars at the top show the time intervals when spikes in absorption formed type III-like bursts (from Chernov et al., 2010).

3.3.2. New Flare Brightening in TRACE- Images

The further dynamics of the flare was outlined in more detail with the TRACE- images in the 195 Å passband. They show flare loops with temperature of $1.8 \cdot 10^6$ K. Six images taken from TRACE catalog data (http://trace.lmsal.com/trace _cat.html) are shown in Figure 14.

According to the TRACE images of the 195 Å passband at the impulsive phase, the flare consisted of many bright kernels distributed over the entire active region and bright large-scale loops, which extended predominantly from the north-west to the south-east, connecting to distant spots. During the impulsive phase in the eastern part of the active region, five consecutive flare brightenings were observed. After approximately 02:40 UT the TRACE images show thin loops (arcades) along the large-scale X-ray loop which began to be formed westwards. After approximately 02:47 UT, the new loops started to appear successively towards the west.

On the first TRACE 195 Å image in Figure 14 (02:48 UT) new bent loops appeared in the western part of the region and began to ascend. The three images (03:02, 03:20 and 03:23 UT) illustrate the subsequent rising of these bent loops and some changes above them which suggest rapid flows. At 03:20 UT the bent loop did look like a cusp for the first time.

After approximately 03:36 UT, the restoration of the magnetic structure began, and the bent loops (with a possible apex) began to descend. At 04:23 UT, the bent loops finally descended, and the burst activity completely ceased after that. During this time, about ten peaks of radio emission occurred at 2.84 MHz (Figure 1 in Yan, *et al*. (2007)). Diverse bursts in absorption were observed during practically each peak.

Typical fragments of bursts in absorption are shown in Figures 15 and 16. It should be noted that the usual fine structures in emission, zebra pattern (green bars in Figure 13) and fiber bursts (blue bars) were observed over the whole event as well (see also Figures 17 and 18).

According to the Nobeyama Radio Heliograph (NRH) data at 17 GHz (see Figure 2 in Chen and Yan (2008) the peak of the radio continuum burst was located above the northern flare ribbon in the negative magnetic polarity. During the new flare brightening at 03:28 UT, the radio source revealed asymmetry with a second maximum above the western part of the northern flare ribbon. This location coincides with the new helmet-shaped loop in the western part of the loop arcade after 03:23 UT (Figure 14).

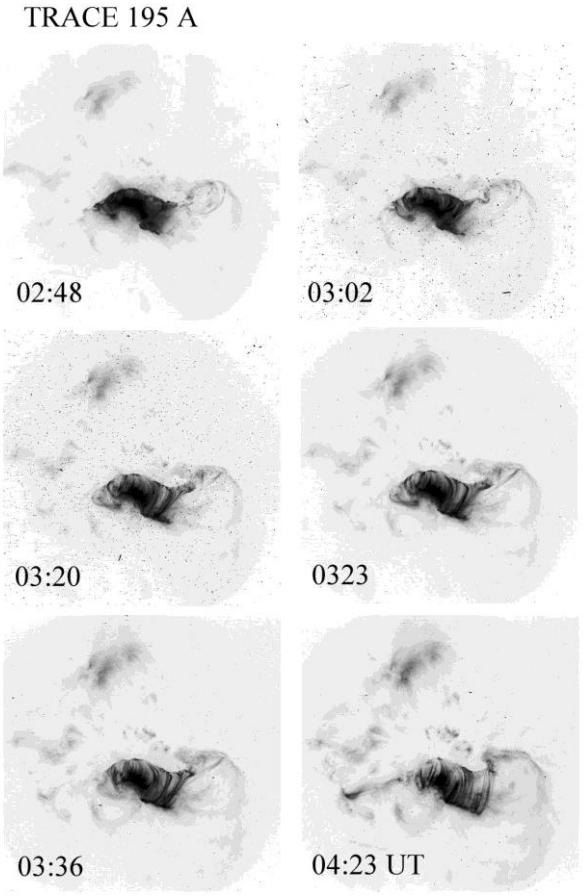

Figure 14. The development of the flare in the western part of the post-flare arcade in the TRACE EUV passband 195 Å (from Chernov et al., 2010).

3.3.3. Features of Bursts in Absorption

Figures 15 and 16 show the appearance and the detailed development in time of spikes in absorption according to the data of SBRS (in the frequency range 2.8–3.6 GHz). Only the right-handed circular polarization (RHCP) components of SBRS are shown because, during the decay phase of the event, the emission was fully right-handed polarized.

The first spikes in absorption appeared at 02:53:08 UT (Figure 15a). All spikes had different frequency bandwidths, from point-like (in one pixel with the size of 10 MHz, 8 ms) to 400 MHz, but no bursts showed frequency drift. Therefore, each spike represents an instantaneous frequency bandwidth. Most of them were scattered randomly in the frequency and time domains. During the time interval shown in Figure 15a, we did not notice specific patterns in appearance of spikes in absorption and in emission. The spikes in absorption and emission appear simultaneously at different frequencies and they are distributed randomly with respect to each other.

After 03:01:28 UT, the non-drifting spikes began to be built along the inclined trajectories and to form the absorptive bursts, similar to type III bursts, shown in Figure 15b. The analysis of such bursts in the interval 03:01:28 – 03:01:37 UT is very important. The first group of isolated spikes at 03:01:29.5 UT were built along two type III-like trajectories, with different frequency separations between spikes. Then, the large dark type III-like burst in absorption with a longer duration of 0.12 s appeared. The subsequent two trajectories consisted of isolated spikes again. In addition, several following type III trajectories were accompanied by spikes with diversified frequency bandwidths and frequency drift rates (see the continuation of possibly similar activity in Figure 15e).

It is important to note that the isolated spikes along the type III trajectories were shifted in frequency with separations approximately equal to the bandwidth of the spikes (≈ 80 MHz). However, in the following type III-like large bursts, they overlapped in frequency (they became more broad-banded, ≈ 160 MHz). The strongest spikes appeared one after another, *i.e.*, with the period equal to their duration (8 ms). Thus, it is not completely excluded that spikes actually have smaller bandwidths and shorter duration, due to the limited frequency and time resolution of the instrument (10 MHz and 8 ms). After 03:01:31 UT, clouds of spikes in emission began to appear, with approximately the same parameters, but they did not form type III bursts in emission.

In the interval 03:03:00 – 03:03:10 UT, fragments of the large-scale ZP in emission appeared in the HF edge of the powerful emission (the top panel in Figure 17). A large-scale ZP means that the frequency separation between stripes is around 170 MHz, the largest value found in this event (see Table 1 in Yan *et al.* 2007). Numerous spikes in emission and absorption were seen superimposed on ZP stripes. The spikes in absorption constituted the absorption stripes of the ZP. Previously, only spikes in emission were reported as substructures of ZP emission stripes (Chernov *et al*., 2003; Chernov *et al.*, 2005).

Such a complex combination of different structures continued up to 03:24:30 UT, when the reverse drifting bursts in absorption appeared as the prevailing structure. However, in contrast to type III-like bursts in absorption, they did not show clear spike substructures. To be more precise, maybe the spikes were not resolved by the instrument, or perhaps substructures do not exist at all. Over the next few seconds the reverse-drifting bursts in emission appeared, and alternated with the bursts in absorption almost over the entire frequency range of the spectrometer. Until 03:25:22 UT, the range of the intermittent reverse-drifting bursts was from 2600 to 3000 MHz.

After 03:29 UT a new powerful flare brightening began, and in the mean time bursts in absorption with new properties appeared (Figures 15c and 15d). The frequency of ≈3400 MHz became the “boundary” between the bursts of the opposite drifts.

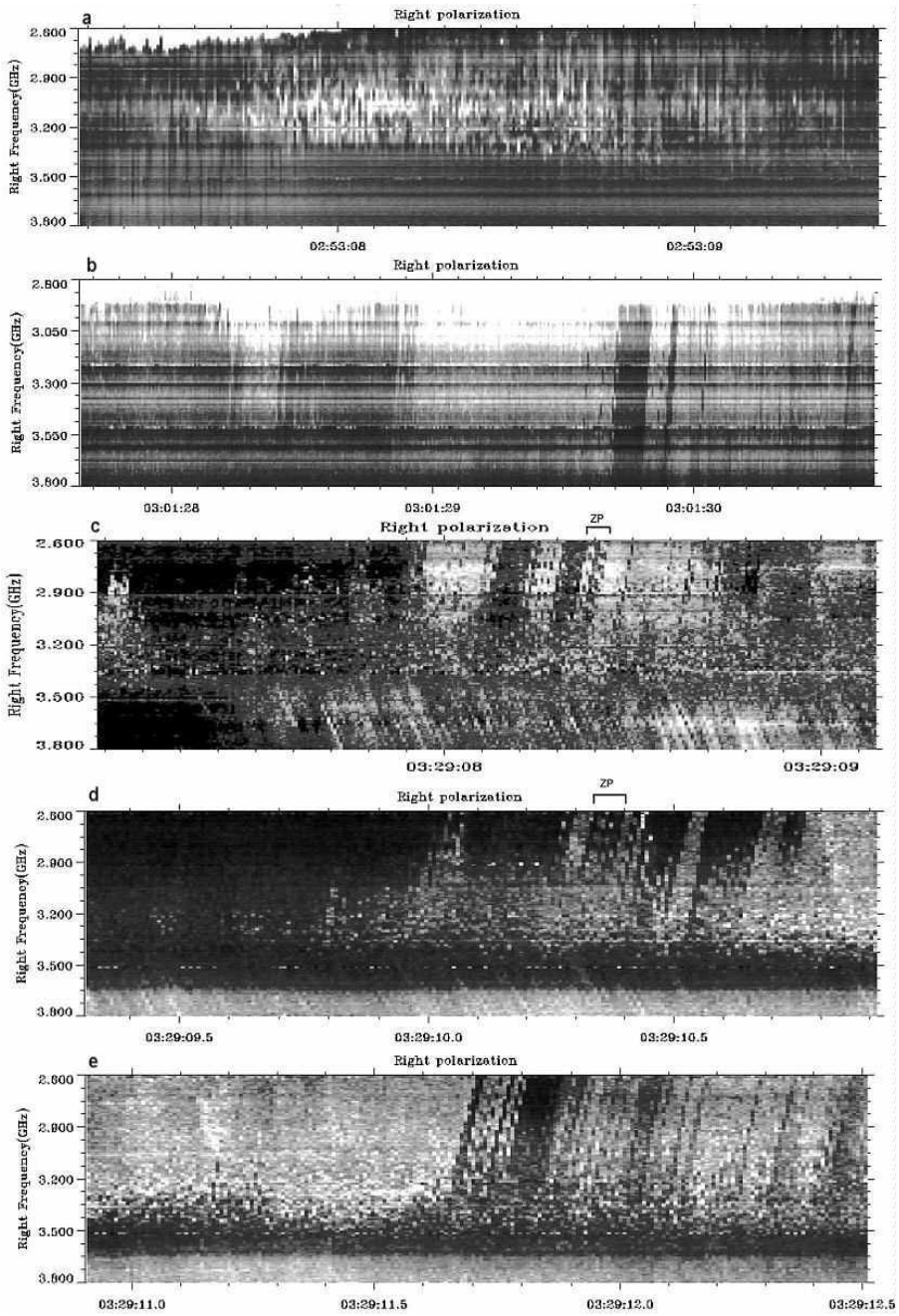

Figure 15. Dynamic spectra of the component of the right-handed circular polarization in 2.6 – 3.8 GHz showing the consecutive development of the absorptive spikes at 02:53 UT and of type III-like busts consisting of spikes in absorption at 03:01 and 03:29 UT. The frequency and time scales are different in different panels (from Chernov et al., 2010).

The bursts in absorption with the fast direct (negative) drift appeared at the higher frequencies, and the reverse-drifting bursts in emission and absorption appeared at the lower frequencies. We did not notice any correlation between bursts of different drift. Moreover, the

drift to higher frequencies of the latter bursts was approximately three times slower, around 3.6 GHz s^{-1}, and they actually looked like classical fiber bursts with typical absorption from their LF edge (Chernov, 2006) but with reverse drift. The low-frequency bursts in absorption were composed of spikes with almost no frequency separation (03:29:08.15 – 03:29:08.25 UT).

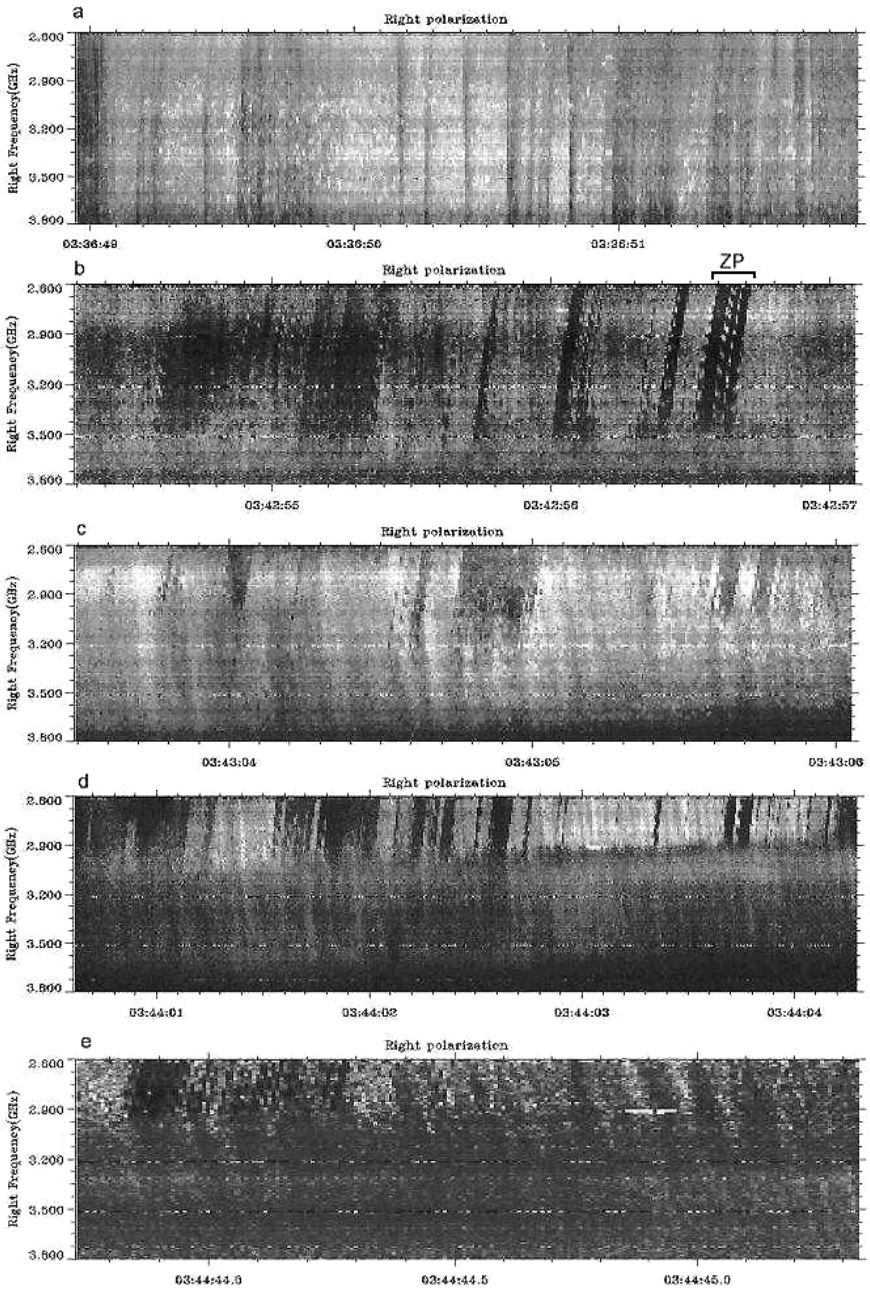

Figure 16. The continuation of the development of the right-hand circularly polarized component in 2.6 – 3.8 GHz in the time interval 03:36 – 03:44 UT showing the absorptive type III-like bursts accompanied by the reverse-drifting bursts in emission and absorption (from Chernov et al., 2010).

The spikes that formed the type III-like bursts had a wide range of parameters and showed no regularity in appearance. The spikes, as the substructures of type III-like bursts, are clearly visible in Figures 19 and 20 with enlarged spectra and time profiles at two fixed frequencies.

However, at 03:29:08.4 – 03:29:08.5 UT in Figure 15c in the type III-like bursts (in the frequency range 2.60 – 3.05 GHz) it is possible to distinguish absorptive ZP-like stripes (noted on top by symbols ZP), which drifted to higher frequencies and consisted of spikes. A similar but short fragment of ZP-like stripes repeated at 03:29:10.3 in the frequency range of 2.60 – 2.90 GHz (Figure 15d).

In the subsequent two minutes (03:30 – 03:32 UT) the powerful pulsations in emission (partially interrupted with broadband pulsations in absorption) and clouds of narrow-band spikes in emission were observed. At 03:32:16 UT, several stripes with a usual ZP appeared (the second panel in Figure 17) with the narrow frequency separation (of ≈40 MHz). Numerous spikes in emission and absorption accompanied these several ZP stripes.

In Figure 16, further development of bursts in absorption is represented, when the helmet-shaped flare loop on the western edge of the arcade began to descend (the image at 03:36 UT in Figure 14). In Figure 16a, pulsations in absorption (or type III-like bursts), are seen against the background of a large cloud of spikes in emission. The pulsations did not reveal a strict periodicity, but the spikes in absorption are visible as the substructures of pulsations.

Against the background of such pulsations during 03:36:57 – 03:36:58 and 03:37:04 – 03:37:05.5 UT, the type III-like trajectories containing isolated almost point-like spikes in emission appeared. Again, the classical fiber bursts at 03:37:12 – 03:37:25 UT against the background of pulsations in emission and absorption were observed (a part of these fibers is shown in the middle panel of Figure 18), when the flare brightening was decaying. These fiber bursts were gradually transformed into broadband stripes predominantly in absorption with the decreasing frequency drift. Then the reverse-drifting (almost through the entire range) fiber bursts appeared again during 03:37:34 – 03:37:38 UT. Further, the fibers against the background of powerful pulsations and the clouds of spikes in emission (03:37:49 – 03:38:10 UT) appeared again.

This entire dynamics is very important for understanding the appearance and development of the uncommon bursts in absorption. During three more minutes, the clouds of strong spikes in emission were observed. At the end of this interval, broadband pulsations in emission and absorption with the reverse drift accompanied these clouds. The pulsations were followed by the type III-like bursts in absorption which consisted of non-drifting spikes in absorption. During the time interval 03:42:56.5 – 03:42:56.7 UT (Figure 16b), spikes in absorption formed the absorptive ZP-like stripes. In this time interval, all features of the type III-like bursts in absorption noted above (during the different moments) were seen.

The initial HF boundary of the absorptive bursts was slightly displaced downwards, up to ≈3500 MHz. In the middle part of this spectrum, weak non-drifting pulsations with the same HF boundary remained noticeable. The main structure here – the non-drifting spikes in absorption – is the building blocks of all other forms of bursts (see also Figure 16c).

Let us note the basic properties of type III-like bursts in absorption we observed.

- The type III-like trajectories consisted of isolated spikes which overlap both in frequency (from the HF part) and frequency separation (from the LF part of the

spectrum). These single (broken) trajectories appeared prior to the larger dark type III-like bursts, as well as after them.

- In the large absorptive bursts we were able to count 4-5 sequential trajectories of spikes, which did not show a noticeable frequency-time correlation between them. The drift velocity of type III-like bursts was ≈ -12 GHz s^{-1}.
- In several moments, the spikes in absorption in sequential trajectories displaced smoothly to HF, and formed the ZP-like stripes; the maximum duration of stripes was about of 0.12 s in the last burst in Figure 16b. The frequency drift of the stripes was ≈1700 MHz s^{-1}, almost the same as that in the first absorptive ZP-like stripes during 03:29:08 – 03:29:14 UT.

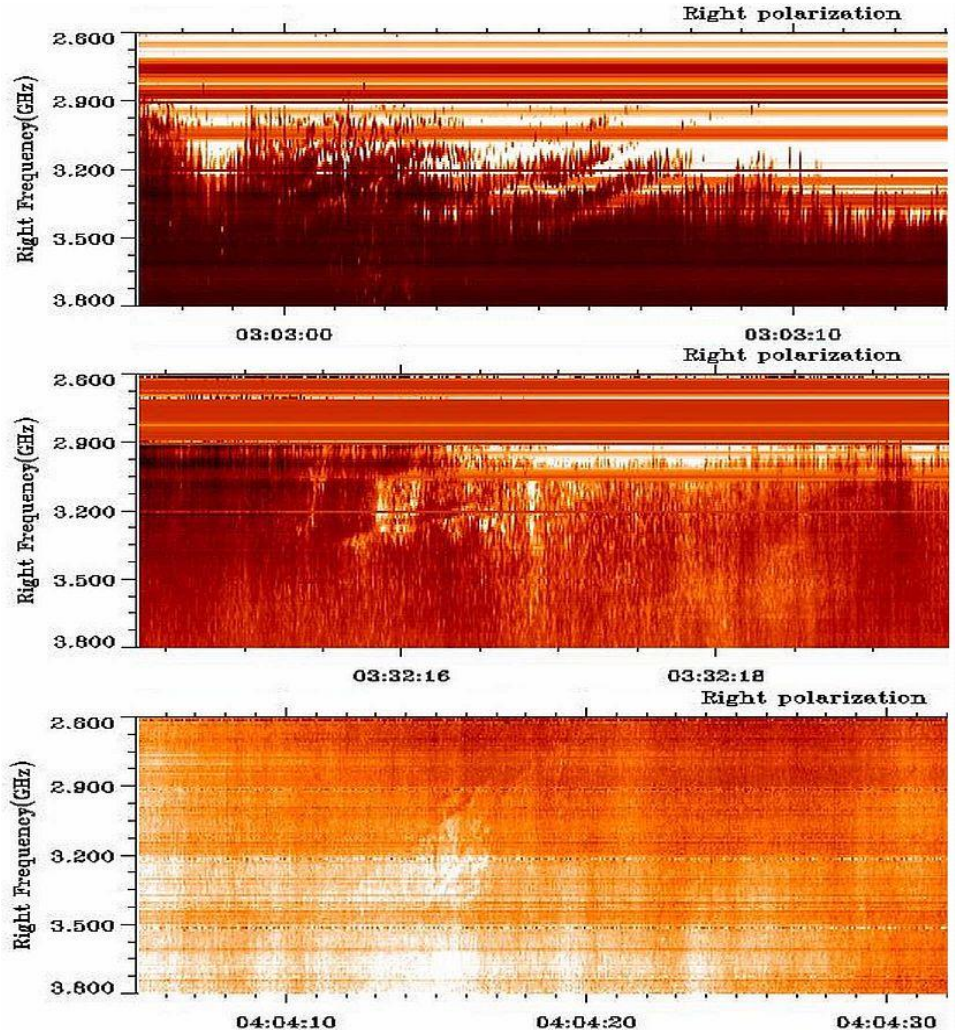

Figure 17. Enlarged spectra showing the ZP at the post-maximum phase of the event. The top panel shows spikes in emission and absorption superimposed on ZP stripes. The spikes in absorption constituted the absorption stripes of the ZP. Numerous spikes in emission and absorption were accompanied several ZP stripes in the middle panel. Note the unusual (braided) ZP in emission and absorption - in the bottom panel (from Chernov et al., 2010).

All these details are more easily visible in enlarged spectra in Figures 19 and 20. Similar short ZP elements drifting like type III bursts (or almost vertical columns) are known in the meter range. For example, Slottje (1972, in his fig. 6C) showed numerous almost vertical columns of the ZP. In this case, repeating columns of the ZP can be explained by fast pulsations in absorptions (sudden reductions). Several examples of fast, almost vertical, columns of the ZP in emission (without sudden reductions) were presented in Chernov (1976b) (see also fig. 19 in Chernov (2006)). Here, we will examine similar fast elements of the ZP, but in absorption and with a much higher time resolution in the microwave range.

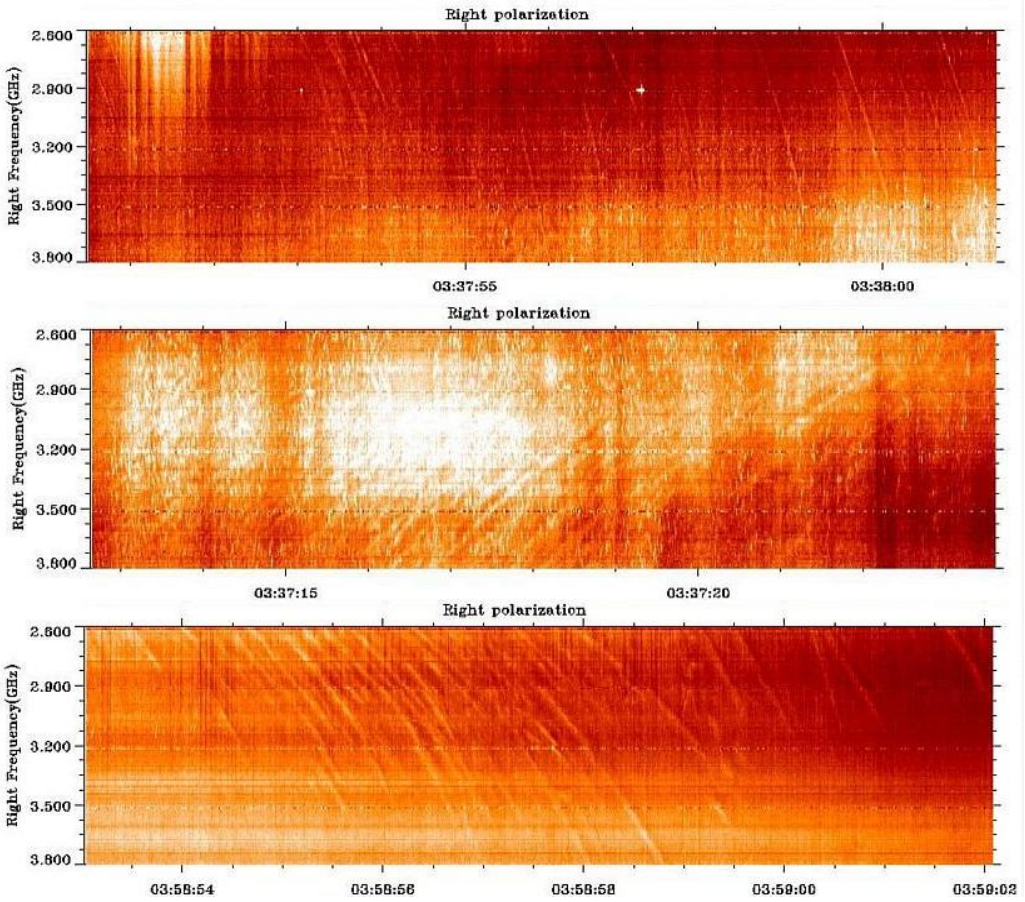

Figure 18. Fiber bursts at the decay phase of the event. In the three panels spikes in emission and absorption are superimposed on fibers or are simultaneously visible. The time scales are different in different panels (from Chernov et al., 2010).

Parameters characterizing the observed spikes in emission and absorption are summarized in Table 1. Let us note that the spikes of type 3 have more strictly fixed duration of 8 ms and smaller spread of the frequency bandwidth, and they are repeated strictly through 8 ms.

Five seconds after the absorptive type III bursts (at 03:43:03 UT), a new special feature appeared. The HF boundary of bursts in absorption shifted to lower frequencies, down to 3000 MHz (*i.e.* the radio source must have been displaced upward). Simultaneously, the bursts in emission drifting to HF (or the reverse-drifting type III bursts) with a fixed period ≈

0.1 s appeared (Figure 16c). Their drift velocity was approximately the same as that in the dark bursts, namely 12 GHz s^{-1}. Then, during almost one minute after 03:43:03 UT the clouds of spikes in emission began to be superimposed on such structures. From Figure 16d, it is evident that at 03:44:01 UT a new property appeared: the HF boundary of type III-like absorptive bursts smoothly displaced to lower frequencies; simultaneously the reverse-drifting bursts in emission stopped at the same frequency boundary; in this case they became less prolonged and more frequent (the period became ≈ 0.03 s).

Table 1. Parameters of spikes in emission and absorption

Type	Range (GHz) [1])	Duration (ms)	Bandwidth (BW) (MHz)	Relative BW (%)	Period (ms)	Frequency drift
1	0.3 - 1.2	8−16	10−220	0.3 – 7.4	8 → 50	| [2])
2	0.3 - 1.2	8−16	20−400	0.67 – 13.3	8 → 50	|
3	0.3 - 1.0	8	30−160	1.0 – 2.4	8	|
Average absolute error		8	10	0.3	8	

[1]) Frequency range inside 2.6 – 3.8 GHz.

[2]) | - means vertical spikes, the frequency drift approaches infinity.

Type 1 – spikes in emission; Type 2 – groups of spikes in absorption; Type 3 – spikes in absorption as substructures of type III-like bursts.

We note that at frequencies higher than the HF boundary, the reverse-drifting bursts continued in absorption and with the period that characterized the reverse-drifting bursts in the emission one minute ago (≈0.1 s). The general appearance of this fragment began to resemble a "herringbone structure" (well known in type II bursts in the meter wave band). The only difference is that it was related to the bursts in absorption. The type III-like burst in absorption and reverse-drifting bursts started at the same frequency, and the starting frequency slowly drifted to the low-frequency region with a drift rate of about –60 MHz s^{-1}. As indicated by Klassen (1996), this could be a signature of propagating bidirectional electron beams originating near the reconnection area. In our event, the reverse-drifting bursts in emission with their starting frequency below 2.6 GHz may indicate the existence of the second site of acceleration above in the corona. At this time (after 03:36 UT), the cusp-shaped flare loop continued to descend (Figure 14), and the activity rapidly changed.

After 03:44:05 UT, the bursts in absorption disappeared together with the HF boundary. The reverse-drifting bursts in emission which covered almost the whole frequency range became dominant bursts. During 03:44:41 – 03:44:44.5 UT the bursts in absorption reappeared, partially with the fragments of the "herringbone structure". This is shown in Figure 16e, where it is also possible to note that at the end of this interval, the reverse-drifting bursts (almost over the entire range) in absorption followed. In the course of the subsequent several minutes after 03:44:45 UT, the bursts in emission and absorption in different combinations with the spikes in emission and absorption still existed. In the course of the last flare brightening (03:55 – 04:05 UT), the bursts in emission (pulsations and spikes) predominated, although the complex forms of bursts in absorption (without type III-like bursts) irregularly appeared.

During 03:58:54 – 03:58:59.2 UT the classical fiber bursts with the reverse drift appeared once more (see the bottom panel in Figure 18). It is remarkable that several stripes of the ZP (with the spiky structure) were observed at the higher frequencies (5.2 – 5.7 GHz) at this moment. Thus, in the course of the whole period discussed here, the conditions for the excitation of a usual ZP and fiber bursts irregularly appeared. During 04:04:12 – 04:04:20 UT the final series of peculiar slow-drifting stripes, exhibiting different absorption and emission characteristics (as elements of the ZP), were observed (the bottom panel in Figure 17).

After 04:05 UT, several small events appeared in the radio emission at 2.84 GHz (Fig. 1 in Yan *et al.* (2007)), but the continuum level gradually decreased to the pre-flare level.

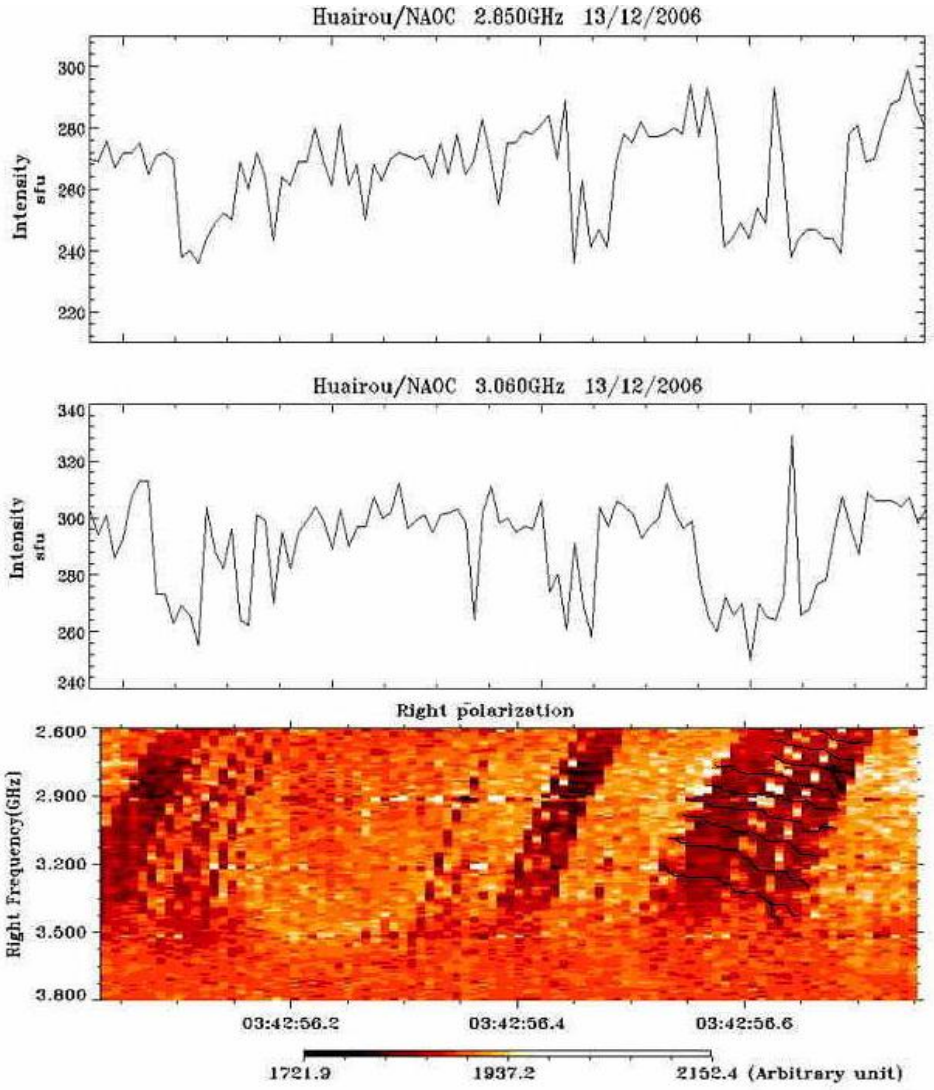

Figure 19. Enlarged spectrum and time profiles at two fixed frequencies (2.85 and 3.06 GHz) of ≈ 0.7 s duration showing the modulations during the type III-like bursts in absorption with a ZP. The absorptive ZP-like stripes are marked by thin black lines (from Chernov et al., 2010).

3.3.4. Time Profiles of Bursts in Absorption

Figure 19 shows the enlarged spectrum of the sharpest type III-like bursts in absorption at 03:42:56 UT whose duration was ≈ 0.7 s. The intensity profiles at two frequencies (2.85 and 3.06 GHz) clearly show the modulations due to the bursts in emission and absorption. In terms of the absolute scale in solar flux units (s.f.u.) the maximum flux in emission reached 330 s.f.u. and the minimum flux (in absorption) ≈ 240 s.f.u. with the average level of the continuum of ≈ 280 s.f.u.

The maximum of modulation depth at frequency 3.060 GHz was observed between the spike in absorption at ~ 03:42:56.60 UT and the spike in emission 03:42:56.68 (about 80 s.f.u.).

Between the three type III-like bursts in absorption, the ZP looks like the classical one (Chernov, 2006): the increased emission in the bright stripes (two high picks on the profiles) and the moderate absorption in the dark ones (here the absorption is even with respect to the average level of flux in the type III-like bursts in absorption). In the spectrum of Figure 19 another property of the usual ZP is clearly seen: the smooth increase with frequency of the frequency separation between the stripes. It increased from ≈ 80 MHz at the frequency of 2700 MHz to ≈ 150 MHz at 3400 MHz.

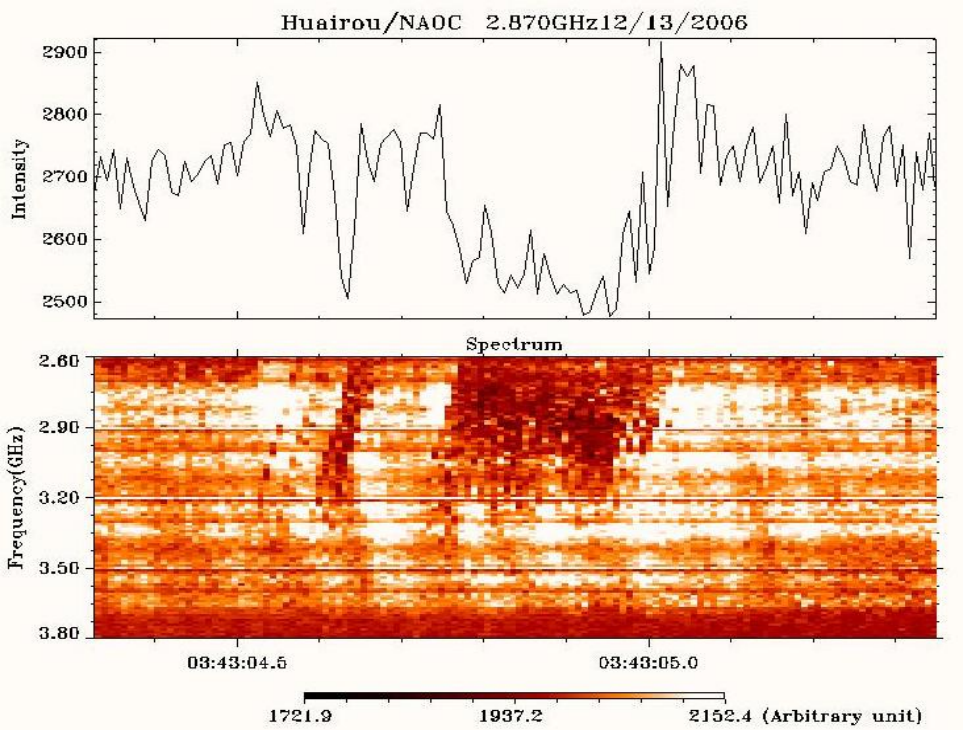

Figure 20. Enlarged spectrum and time profile of ~ 1 s duration at a fixed frequency of 2.87 GHz, showing the modulations during the type III-like bursts in absorption. The intensity scale is in arbitrary units. The spikes, as the substructures of type III-like bursts, are clearly visible (from Chernov et al., 2010).

In the type III-like bursts consisting of isolated spikes in absorption (for example, a trajectory at 03:42:56.3 UT), the instantaneous frequency bandwidth of the spikes also increased with frequency from of 30 to 100 MHz. The decreasing frequency separation

between them, disappeared at the frequency of ≈ 3400 MHz. The latter was not coordinated with the frequency separation of the absorptive stripes of the ZP. However, at other onsets noted above for similar bursts this property was not observed.

The ZP-like stripes appear to be parallel. We can distinguish six stripes against the background of type III-like bursts in absorption (they are marked by thin black lines in the spectrum) and three stripes from the LF edge remained diffuse. However, this conclusion depends on many factors: on the conditions in the radio source and on the rate of particle acceleration in different parts of the radio source. The precise measurements of the frequency drift showed that its speed also increased with the frequency: from 1000 MHz s^{-1} to 1700 MHz s^{-1}. Thus, it is possible to say that this was a usual ZP, but it was observed against the background of type III-like bursts in absorption. The ZP-like absorptive stripes remained noticeable even against the background of the type III-like absorptive bursts.

Figure 20 shows the distribution of the spikes in absorption in the background of another type III-like burst in absorption. The spikes were distributed randomly, but they tended to form several short stripes. Such structures of the spikes were called 'braided ZP' by Slottje (1981) (see the event 1970-07-27) and 'lace bursts' by Karlicky *et al.* (2001) because of the variety of the ZP.

Brief Conclusion from Observation

In spite of the complexity of the analyzed phenomenon, let us isolate the basic properties of the bursts in absorption.

The basic structural element (a building block) of all bursts in absorption was the spikes whose duration was close to the limit of the instrument resolution (8 ms) and the instantaneous frequency bandwidth was on average ≈ 70- 80 MHz.

The dynamics of appearance and development of spikes is very rapid. It changed every several seconds.

The type III-like bursts in absorption were basic structures of the absorptive spikes. In three brief moments, the absorptive spikes created ZP-like stripes which lasted for δ 0.1 s.

The complex combinations of the drifting bursts in emission and absorption sometimes exhibited the form of a `herringbone structure.

The activity of absorptive bursts alternated (or were simultaneously observed) with the usual fine structure in emission: spikes, broadband pulsations, ZPs and fiber bursts.

This entire interval of the peculiar fine structure was observed during several flare brightenings in the western part of the flare arcade above the south magnetic polarity. We believe that during this time the magnetic reconnection probably took place. The right sign of polarization corresponded to the ordinary wave mode.

The bursts in absorption were sometimes observed in the meter-wave range (Chernov *et al.*, 1998), but the event discussed here for the first time revealed a wide variety of absorptive bursts in the microwave range.

3.4. Other Events

Small fibers similar to ones shown in Figure 10 were observed by Dabrowski *et al.* (2005) (Figure 21). However, the authors discuss them as drifting spikes. Dynamical

radiospectrograms of the spikes were recorded in the 1352−1490 MHz frequency band which was split into 46 channels each 3 MHz wide. The time resolution of the collected data is equal to 80 μs, the highest ever obtained. The observations of the radio spikes have been collected with the 15 m radio telescope of Torun Centre for Astronomy, Nicolaus Copernicus University in Torun, Poland. The observed radio spikes have internal structure and form chains (rope-like fibers and braided ZPs). They occurred during the bulk motion of the plasma along the long loops, observed with the TRACE telescope in the 171 Å band.

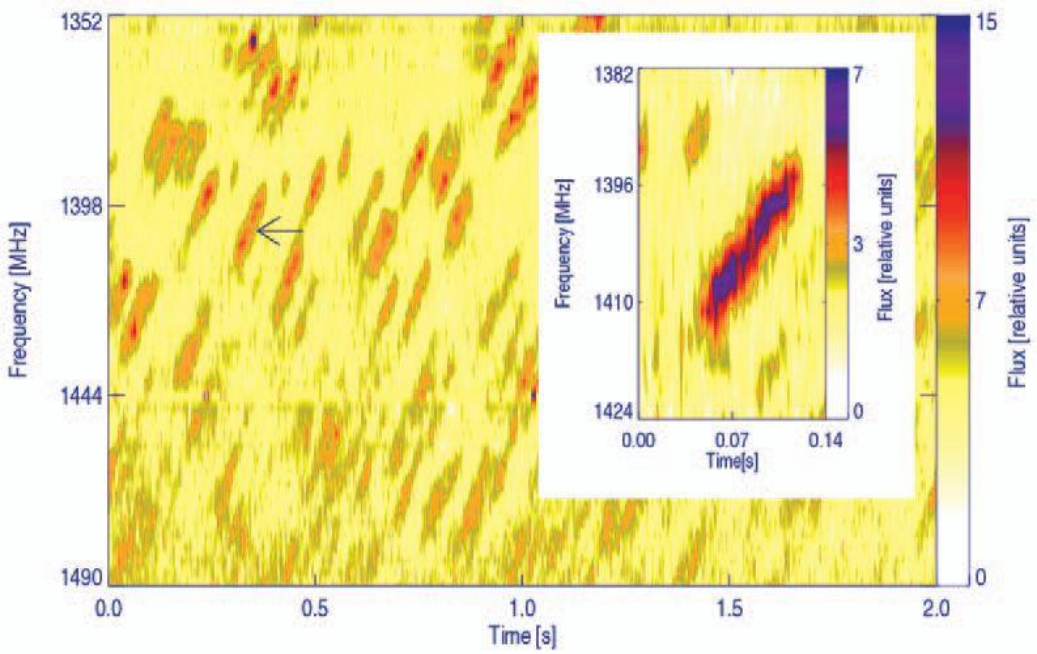

Figure 21. Dynamic radio spectrogram of the dm radio spikes recorded on 2001 October30, beginning at 12:20:27 UT (from Dabrowski et al., 2005).

Another kind of spike (called dot emissions) was observed with the Brazilian Solar Spectroscope (Meszarosova *et al.,* 2008) in the dm range of 950−2640 MHz with variable time and frequency resolution between 10−1000 ms and 1−10 MHz, respectively. An example of a group of dot emissions arranged as zebra-like chains observed on 1999 March 19 is shown in Figure 22 (as a part of fig. 1 from Meszarosova *et al.* (2008)). Figure 22b presents a global view of the dot emissions. The time and frequency resolution is 100 ms and 5 MHz, respectively. Figure 22c reveals a detailed view showing the dot emissions with undulating chains resembling the zebra pattern. Figure 22d shows the radio flux in time at 1400 MHz where peaks with an intensity of ~ 130 SFU correspond to individual dot emissions (horizontal line in panel *c*).

Figure 23 shows an example of the structural evolution of the group of dot emissions observed on 1999 October 19. This group starts with some irregular dot emissions (panel a) but later they evolve into almost regular fiber-like (panel b) and zebra-like (panel c) chains. At the end, the group of dot emissions again becomes irregular (panel d). During times of dot emission, no background burst emission was detected.

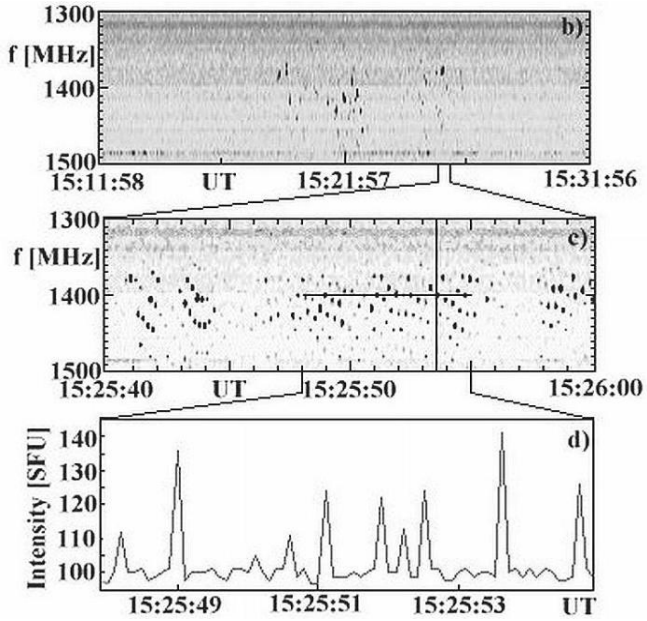

Figure 22. Dot-emissions (in black) arranged as zebra-like chains observed on 1999 March 19: b) global view of dot emissions, c) zebra-like chains, d) radio flux in time at 1400 MHz (horizontal line in c) (from Meszarosova et al., 2008).

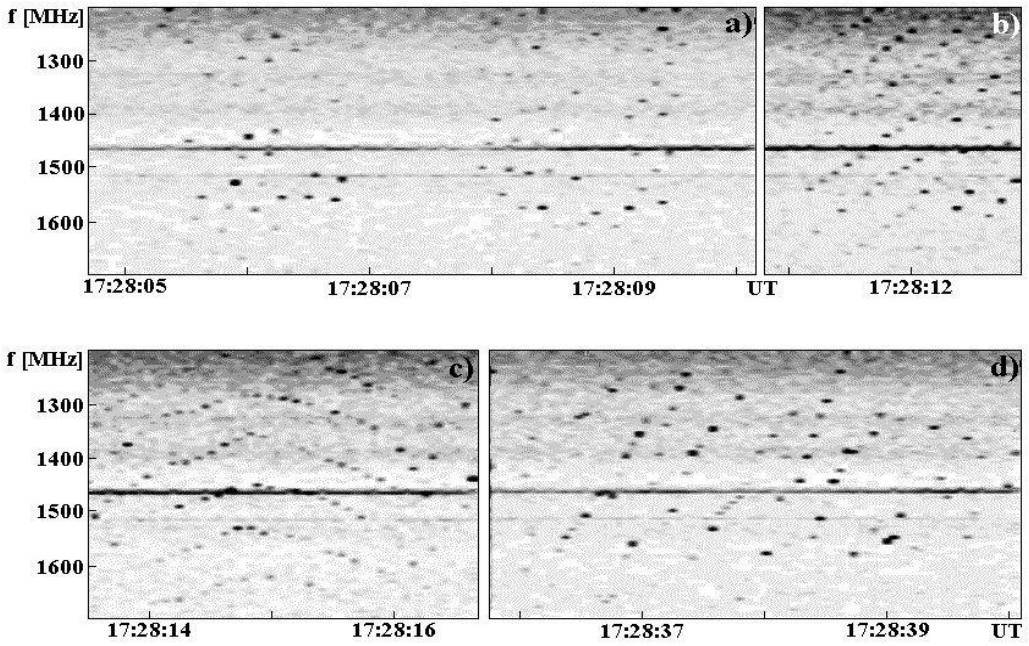

Figure 23. Example of the arrangement of the series of the dot emissions (in black) observed on, 1999 October 19: irregular dot emissions (panel a)), fiber-like chains (panel b)), zebra-like chains (panel c)), and irregular dot emissions (panel d)) (from Meszarosova et al., 2008).

Sych *et al.* (2006) and Zlobec and Karlicky (2007) studied the characteristics of the zebra-associated spike-like bursts during 2003 August 5 event that were recorded by the Ondřejov radio spectrograph in the range 1 – 2 GHz with time resolution 100 ms (upper panel in Figure 24). Simultaneously, the spiky structure was examined using the 1420-MHz polarization profiles of the Trieste Astronomical Observatory with a very high time resolution of 1 ms (bottom panel in Figure 24). The selected spike-like bursts show a duration (with a mean value of about 7.4 ms at half power) and it is not influenced by the polarization. For the selected bursts there was just a "tendency" that the weaker component (L- polarization channel) should be delayed. Zlobec and Karlicky (2007) realized that the L continuum was generally low with respect to the R continuum; however, the polarization of the spikes does not always match the contemporaneous polarization of the continuum.

The observed superfine structure (spikes) of zebras can be interpreted as proposed by Chernov, Yan, and Fu (2003). Nevertheless, Zlobec and Karlicky (2007) think that the model based on the double plasma resonance (DPR) as proposed by Bárta and Karlický (2001) and Karlický *et al.* (2001) is also possible. Namely, this model explains both the zebras and the spikes by the same double plasma resonance process; the spikes are generated by the interruption of the DPR process by assumed turbulence (density or magnetic field variations).

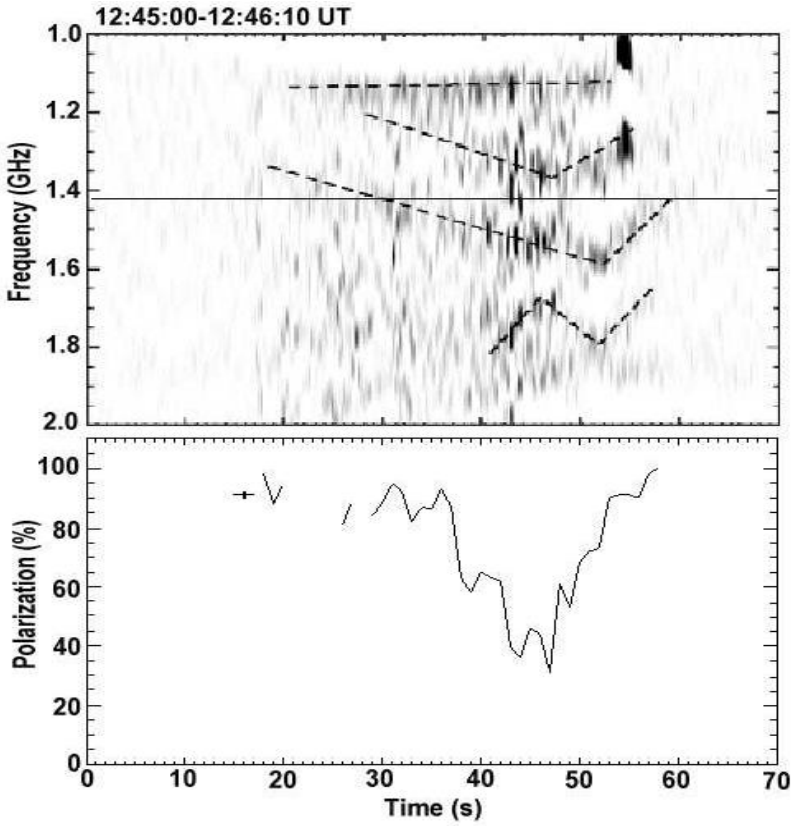

Figure 24. Upper panel: Part of Figure 5 from the paper by Sych et al. (2006) showing the time evolution of the spike-like bursts clustered into zebras forming "V" like structure (in the event August 5, 2003). Bottom panel: contemporaneous time evolution of the mean polarization (in R-sense) of the selected spike-like bursts at 1420 MHz (from Zlobec and Karlicky, 2007).

Magdalenic' *et al*. 2006 reported supershort structures SSSs (spikes), in particular as substructures of the ZP and as tadpoles in the range 265 – 350 MHz using the solar radiospectrograph Artemis IV (Greece) with a time resolution of 10 ms (Figure 25). The spikes in the ZP exhibit a duration of 11 – 13 ms, shorter than what was reported earlier in the meter range. Tadpoles are comprised of an emission "eye" with a duration of ≈50 ms at the high-frequency side of the burst and a stretched absorption "body" with a bandwidth of ≈40 MHz. In spite of distinctive differences (the emission tails of the tadpoles are not visible), the Slottje (1972) tadpoles and these tadpole-like SSSs belong to a class of physically equivalent bursts.

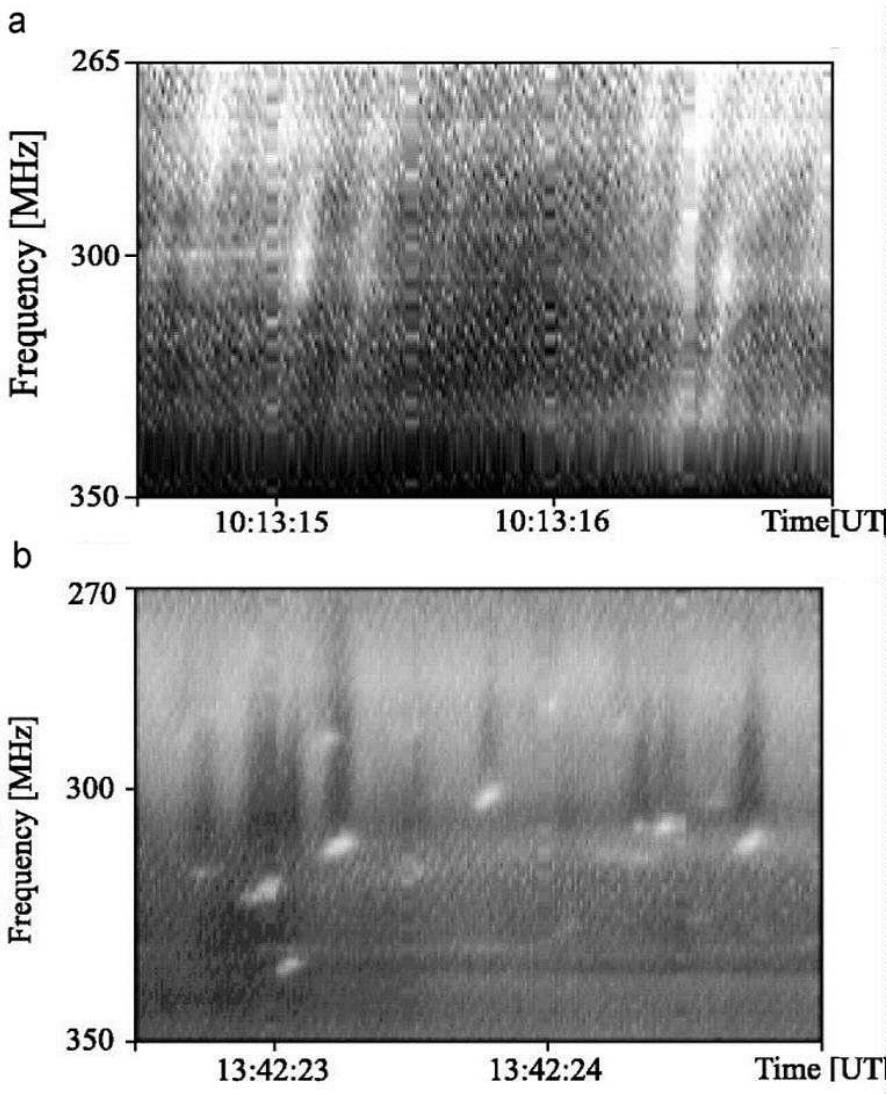

Figure 25. Artemis IV dynamic spectra of negatively drifting supershort structures (SSS) in the background of the ZP with a superfine structure (a) and tadpole-like bursts (b) in the event 2000 April 15, (from Magdalenic' et al. 2006).

4. General Discussion of the Events

4.1. 2004 July 24 and November 3 Events

Small-scale fibers differ from usual fiber bursts only by narrow total frequency bandwidth and they are similar to ropes of fibers, therefore the usual (that is, most accepted) mechanism for fiber bursts should work, namely the coalescence of a plasma wave (l) with whistlers (w): $l + w \rightarrow t$ (Kuijpers, 1975b; Chernov, 1976a; 1990). However, the propagation of whistlers is limited by a small magnetic trap in the form of fast shock fronts escaping from a region where magnetic reconnection occurs (Chernov, 1997). In our case the periodicity of fibers was not so evident, and fibers were organized as large-scale stripes of a ZP. So, these ZP stripes become visible only when whistlers propagate through the ZP source.

In our events the radio sources cannot be point-like ones, since in such a case one whistler wave packet should produce all zebra stripes simultaneously, but we did not see such a feature. Since the small fibers were not connected by a unique straight line in the dynamic spectra, we cannot assume that one whistler wave packet passes through several DPR levels consecutively in an extensive source. So, the unique possibility remains that whistlers are excited at the same DPR level simultaneously with the plasma waves. Without whistlers, ZP stripes cannot be visible, at least in the DPR model with loss-cone distribution function, in accordance with numerical results of electrostatic instability in Kuznetsov and Tsap (2007). Whistlers without a plasma wave cannot be detected either, but a plasma wave of low energy will be sufficient (at places of DPR) to emit radio waves of sufficient intensity. Thus, whistlers "highlight" DPR levels.

In order to confirm this hypothesis, let us estimate the magnetic field strength B in two ways. One is from the observations of separate fibers using the model of the whistlers, and the other is from large-scale ZP in the DPR model. If the hypothesis is correct, these values of the field strengths should be equal.

From the whistler model for small fibers we have $\Delta f_e \approx f_w \approx 0.1\ f_{Be}$ (f_w is the whistler frequency), and a mean value Δf_e = 12.5 MHz (for the events of July 24 and November 3), and we obtain $B \approx 45$ G.

In the DPR model the frequency separation depends on the scale heights of density (N_e) and magnetic field ($L_{Ne} = 2N_e\ (dN_e/dr)^{-1}$ and $L_B = B\ (dB/dr)^{-1}$ (Zlotnik *et al.*, 2003):

$$\Delta f_s / f_B \approx L_B / |L_{Ne} - L_B| \qquad (5)$$

For Δf_s = 72 MHz (for the November 3 event) we could obtain about the same value B = 46 G for $L_{Ne} = 1.4 \cdot 10^9$ cm and $L_B = 5 \cdot 10^8$ cm. In the flare region the plasma is very inhomogeneous and such scale heights are realistic. In our events only 3 – 4 large-scale stripes of ZP (or DPR- levels) are simultaneously formed in the spectrum which demonstrates the small sizes of local L_{Ne} and L_B in flare inhomogeneities. Four DPR levels are simply produced at harmonic number s = 10 – 14 with such a ratio of scale heights.

The stable frequency drift of fibers implies that the magnetic field changes little during the lifetime of the structure (Chernov, 1990). The frequency drift of fibers is mainly determined by the group velocity (υ_{gr}) of whistlers, and we have $\upsilon_{gr} = 2c \times f_{Be}/f_{Pe} \times [x(1-x)^3]^{1/2}$, where $x = f_w/f_{Be}$ is the ratio of whistler frequency to cyclotron frequency (Kuijpers, 1975a). If

we assume the parameter x varies little during the lifetime of the structure, and f_{Be}/f_{Pe} has a consistent value due to the DPR condition, then υ_{gr} would vary little and consequently the whistlers would cause a stable frequency drift of fibers, at least within a certain DPR level. Therefore the positive frequency drift of large-scale ZP can be connected with the downward motion of the source. In the absence of a good analytical model of electron concentration in the upper chromosphere, we will use a graphical representation given, for example, in the model of Allen (in Figure IV.1 of Krüger (1979)). Utilizing the dependence of plasma frequency (f_{Pe}) on height (r), it is possible to roughly estimate the value of the gradient of f_{Pe} between 1000 and 2500 MHz to be on the order of 240 MHz/10^8 cm. Then, we can use the simplest expression for the definition of the velocity of propagation:

$$V \approx 2\frac{df/dt}{f}\frac{N_e}{dN_e/dr} = \frac{df/dt}{df_{Pe}/dr}. \qquad (6)$$

The frequency drift df/dt = 630 MHz s^{-1} will correspond to the velocity of about 2590 km s^{-1}. Such a value might be more than a typical Alfvén velocity. Therefore it is possible to assume that the plasma ejection that moves downward from the magnetic reconnection region has caused a shock wave.

In the July 24 event the drift of 220 MHz s^{-1} implies the velocity ≈ 900 km s^{-1}, which is somewhat more than the Alfvén velocity ($V_A \approx$ 700 km s^{-1} for the estimated value of B = 45 G).

The drifting boundary of the emission termination at the high frequency edge of a large-scale ZP may mean that a moving shock front meets a rising closed magnetic loop. So, the conditions for DPR are satisfied only in a narrow height interval, below the magnetic reconnection region, and only at the very beginning of events. After such a collision they will be destroyed, and large-scale zebra stripes will be transformed into a braided ZP (Figure 10b). Thus, the radio source showing such a fiber structure differs from the radio source of the rope of fibers only by the absence of a magnetic trap (only one shock front) where fast particles could make periodic bouncing motions, and by short lived conditions for the DPR. The absence of any absorption is simply explained by the absence of continuum emission at the very beginning of events. Only the pulsations in the October 31 event were observed against a weak continuum, and we could detect some fragments of absorption between fibers (fig. 6 in Chernov *et al.* (2008)).

Thus, we assume that the usual mechanisms can be applied for the interpretation of such a fiber structure: the coalescence of whistler waves with plasma waves producing fiber bursts and the DPR- model for large-scale ZPs. However, the following special features of the plasma wave excitation in the radio source must be present. Both whistler and plasma wave instabilities are too weak at the very beginning of the events (the continuum is almost absent), and the fine structure is almost invisible. Moreover, according to the recent simulations of Kuznetsov and Tsap (2007), the fast electrons with a loss-cone distribution cannot excite a high enough level of electrostatic waves in the DPR levels, so that the separate stripes would be visible. Then, whistlers generated directly at the DPR levels by the same fast electrons will "highlight" the radio emission only from these levels due to the interaction with plasma waves and we observe small-scale fibers as a substructure of a ZP. More precisely, the whistler packets may bring about sufficient plasma wave energy as well as a new composition of the particle distribution, therefore the DPR levels could be more pronounced and "highlighted".

Wu *et al.* (2007) interpreted the small-scale fibers in the November 3 event as drifting spikes emitted from "solitary kinetic Alfvén waves" (SKAWs) by fast electrons accelerated by the electric field and trapped in SKAWs. However, they did not discuss the reasons for the formation of fibers along the stripes of large-scale ZPs. Furthermore, the source of the strong Alfvén waves, which accelerates a large fraction (≈ 0.1) of the background electrons at the beginning of the event also was not examined.

We have not adopted the model of LaBelle *et al*. (2003), since it is supposed to be applied to the explanation of a large number of stripes with a narrow frequency separation. In the large-scale ZP in question, on the contrary, the frequency separation is considerably wider than in the usual ZP. Recent evaluation by Chen and Yan (2008) on the validity of the mechanism of LaBelle *et al.* (2003) indicated that, with the realistic values of the density contrast (with $\delta \leq 0.2$) the model cannot account for the large number of ZP stripes.

However, we cannot completely exclude the possibilities of application of the new models, based on the existence of the bands of transparency and opacity when the radio waves propagate through spatially periodic medium (for example, Laptuhov and Chernov, 2006). It is possible that the large-scale ZP is the result of this selectivity with the specific scale of thermal heterogeneities, which move downward from the flare region, and small-scale fibers are caused by additional quasi-periodic modulation of these heterogeneities, for example, by a fast magneto-sonic wave propagating from below. Or alternatively and more simply, the radio waves meet on their way the small- and large-scale heterogeneities which move in different directions, *i.e.* a radio wave is filtered by transparency bands twice. These possibilities require more detailed study.

4.1.1. Other Events

Considering all aspects of the observed dot emissions, Meszarosova *et al.* (2008) think that the dot emissions are generated in a similar way as zebras (Ledenev et al. 2001) or lace bursts (Karlický et al. 2001). Thus, they propose that the dot emissions are produced in the solar atmosphere at the locations where the so-called double plasma resonance condition (1) is fulfilled. The upper-hybrid waves at these locations can be generated e.g. by the anisotropic beam ($T_\perp > T_\parallel$, where $T_\perp$ and $T_\parallel$ are the temperatures of energetic electrons across and along the magnetic field, respectively) accelerated during the flare's primary energy processes. The beam anisotropy can be naturally formed along magnetic field lines by an escape of fast electrons from slower ones. Then these upper-hybrid waves are transformed to electromagnetic waves (with the frequency $\omega_{el} \approx \omega_{UH}$ or $\omega_{el} \approx 2\omega_{UH}$), which are observed by radiospectrographs on the Earth. This process is a resonant one which means that its intensity can be several orders of magnitude higher than those associated with non-resonant processes. This can explain the fact that, at times of dot emission, no background burst emission was detected.

Using this model, we can explain not only individual dot emissions, but also their chains. The beam along its trajectory generates dot emissions in several resonance locations (*s*-harmonics). The higher *s* means a higher height of the dot emission source in the solar atmosphere. Thus fiber-like chains of the dot emissions can be formed. On the other hand, zebra-like chains of the dot emissions can be explained by a sequence of anisotropic beams producing dot emissions nearly at the same position on the same *s*-harmonic. Even the whistler waves, which are considered in the model of fibers, can enhance emission at the

locations with double resonance conditions. Therefore both forms of zebra-like and fiber-like chains are possible.

Due to similarities in morphology and characteristic properties between the dot emissions and dots in the fine structures of zebras and fibers, Meszarosova *et al.* (2008) think that both have a similar physical origin. They found that fiber-like chains of the dot emissions evolve into zebra-like chains and vice versa. These changes are in agreement with the idea of Chernov *et al*. (1998) who proposed that both the zebras and fibers are generated by whistler packets. The propagating whistler packets may also generate dot emissions at the positions in the solar atmosphere where the double resonant conditions are fulfilled (see also, Sawant et al. 2002; Krishan et al. 2003). Furthermore, they propose that the chaotic character of some groups of dot emissions is due to rapidly varying plasma parameters (in the MHD turbulence) in the region of dot-emission sources.

4.2. December 13 2006 Event

From the observations discussed above in detail, we are able to understand the reason for the appearance of the spikes in absorption, as well as the variable nature of their parameters. The main task is to explain formation of the absorptive type III-like bursts and absorptive ZP-like stripes of the absorptive spikes, in combination with different bursts in emission.

Let us recall that the loss-cone instability is the most probable mechanism of the continuous radio emission of the type IV bursts (including microwave bursts). Plasma waves are excited at the upper hybrid frequency by the fast electrons, captured in a magnetic trap, where the particle-velocity distribution with the loss-cone is formed (Stepanov, 1974; Kuijpers, 1975a; Zhelezhyakov, 1995; Kuznetsov and Tsap, 2007). The maximum amplification of waves occurs under the conditions of double plasma resonance (DPR, when the upper hybrid frequency is close to integer harmonics of the electron cyclotron frequency). The appearance of a usual ZP and fiber bursts during the entire event attests to the fact that the loss-cone velocity distribution actually existed.

The dips in emission (corresponding to bursts in absorption) mean the quenching of the loss-cone instability. According to Zaitsev and Stepanov (1975), Benz and Kuijpers (1976), and Fleishman *et al.* (1994), this quenching can occur because of additional injection of fast particles, which fill the loss-cone. The process of the quenching of instability is examined in detail in a recent paper by Chen and Yan (2008). The authors showed (Fig. 26) that the beam with a linear dimensions of ≈ 220 km and a Maxwellian particle-velocity distribution inside the loss-cone causes absorption with a frequency bandwidth of ≈ 60 MHz (due to the cyclotron self-absorption of upper-hybrid waves). The calculated absorptive depth corresponds to the observed value: the modulation in the growth rate in Figure 26 corresponds exactly to the observed absorption depth of ≈17% in our Figure 19. Let us note that according to the calculations by Kuznetsov and Tsap (2007), the beams with the power-law spectrum with a large spectral index should give bursts in emission (the spiky superfine structure of the ZP stripes).

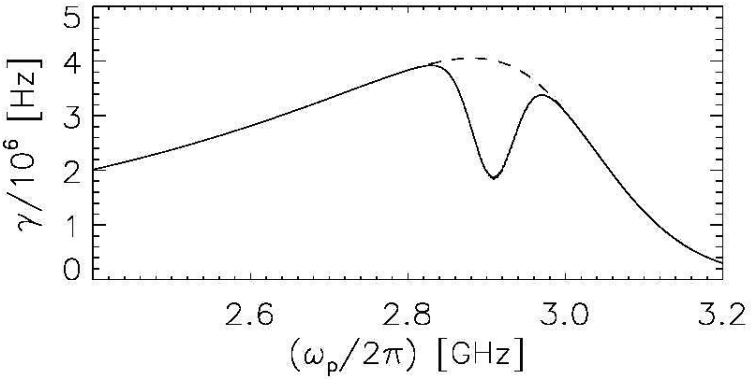

Figure 26. Dependence of the total growth rate γ of the upper hybrid waves on the plasma frequency. The initial growth rate result corresponds to a value of s = 15. Signs of an absorption feature with a frequency bandwidth of about 60 MHz can be clearly seen (from Chen and Yan, 2008).

Taking into account the fact that absorptive spikes do not always follow type III trajectories, and that they are often a random collection of instantaneous bursts, it is natural to assume a random acceleration of small-scale beams occurs. The dimensions of the beam would then determine the instantaneous frequency band. The quenching of instability occurs only when the instability develops in the location of the beam. Then the beam rapidly leaves the region, and the emission will be restored there. Most likely, the maximum effect is achieved in the DPR conditions. Therefore, when the moving beam reaches a neighboring DPR- level, a certain space between the spikes in absorption will be formed. By this method, it is possible to explain the discrete nature of absorptive spikes. Various parameters of the absorptive spikes can be associated with different local gradients of density and magnetic field. At the beginning of the interval of bursts in absorption, the spikes in absorption were still accompanied by spikes in emission with the similar parameters (Figure 15a). It means that at this moment not all beams were confined in the trap. This untrapped part of the beams would have given off bursts of emission, although the beams did not move ahead further, possibly, they were reflected.

In the mildly inhomogeneous corona, the DPR- levels are the surfaces whose size perpendicular to the line of sight is more than 10,000 km. Compared to this size, the magnetic loops are very narrow and inhomogeneous in density, so that the DPR- levels in the adjacent loops cannot coincide with each other. If the beams of particles were periodically injected along one loop, then we should always see ZPs. Therefore, most likely they are injected consecutively in time and simultaneously in several loops. In cases like this, we would often observe almost random distributions of spikes in the type III-like bursts (Figure 20). However, if the DPR- levels almost coincide among the adjacent loops, then a smooth displacement of dark spikes would be produced, and at these moments the ZP will appear. The frequency drift of the ZP-stripes (≈ 1700 MHz s^{-1}) can be explained by an appropriate displacement of the DPR- levels in the corona. Even a slow downward motion of a loop making a sharp angle with respect to the gradient of plasma frequency (which exactly occurred, according to the TRACE images in Figure 14) could lead to rapid lowering of DPR- levels in the corona, which will also explain the frequency drift of ZP stripes. During the resistive tearing-mode instability (see below), the

condition of frozen magnetic flux is disrupted, and magnetic field line can move independently of the plasma (Aschwanden, 2004, p. 414).

The beam traveling between the DPR- levels can give impulsive contributions to the emission on the Cerenkov resonance, so that the appearance of bright ZP stripes (spikes in emission) is entirely expected (the plasma mechanism of type III bursts). The frequency drift of type III-like absorptive bursts (≈ 12 GHz s^{-1}) would correspond to the speed of the electron beam not exceeding of 10^{10} cm s^{-1} in accordance with Allen's density model of the corona (see Fig. IV.1 in Krüger (1979)).

Wang *et al.* (2008) considered that the spikes in emission are generated by the electron cyclotron maser (ECM) mechanism. However, the majority of spikes with right circular polarization were observed during flare brightening in the northern flare ribbon in the south magnetic polarity. Thus, the radiation mode was ordinary. Two episodes with left circular polarization were connected with the brightening in the southern flare ribbon (see the black rectangle in fig. 3b of Wang *et al.* (2008)) where the north magnetic polarity could be dominant. This also means the ordinary wave mode dominates, while in the ECM radiation the extraordinary mode should dominate (Fleishman and Melnikov, 1998). For this very reason the estimations of the magnetic field strength obtained by Wang *et al.* (2008) in the ECM model almost exceed by an order of magnitude the ones obtained by Yan *et al.* (2007) using the frequency separation of ZP stripes.

The simultaneous presence of bursts in emission and absorption with different drift rates (Figure 16c and 16d) testifies that at least two places of particle acceleration exist at the different heights. In accordance with Figure 14 (the pictures at 03:23 and 03:36 UT) we can assume that above the cusp-loop, in the course of the post-flare restoration of the magnetic structure, a magnetic island was probably formed, and particle acceleration occurred in the two current layers located above the flare cusp-loop (upward) and above the magnetic island (downward). Such an assumed scheme coincides with the sketch of the magnetic configuration proposed for this flare in fig. 8 in Guo *et al*. (2008).

As Schwenn *et al*. (2006) diligently noted, despite many decades of indirect observations suggesting the presence of a current sheet, such as soft X-ray cusp structures (Tsuneta, 1996) and horizontal inflow, direct observations of the formation and evolution of a current sheet in the solar atmosphere have been missing. Strong observational evidence for reconnection comes from the post-eruption emission and dynamics. Our radio observations also testify to the probable case for reconnection in the erupting solar corona.

The rise of helmet-shaped loops in three TRACE images at 03:02, 03:20 and 03:23 UT in Figure 14 allows us to propose the existence of a single X- point above the helmet-shaped loop, and the initiation of flows due to the magnetic reconnection. The consecutive flows may be associated with the formation of magnetic islands above the helmet loop. The sketch of the magnetic configuration can be similar to fig. 8 of Pick *et al.* (2005) as a two-dimensional cut of the three-dimensional configuration across the twisted flux rope. Similar two-dimensional magnetic configurations were often discussed in many numerical simulations (Tsuneta, 1996, Lin and Forbes, 2000, Aschwanden, 2004, and references herein). The three-dimensional flux rope is in fact anchored (line-tied) to the photosphere. The theory of three-dimensional reconnection is presented in greater detail in the book of Priest and Forbes (2000). The two-dimensional representation is mostly done for convenience, but the magnetic structure is three-dimensional (see fig. 4 in Roussev *et al.* (2003) for a view of the very complicated magnetic field configuration). All special features of two-dimensional reconnection enumerated in Pick *et*

al. (2005), are also valid in our case. In the framework of an erupting flux rope, magnetic reconnection occurs behind the twisted rope. The accelerated particles form beams along the newly reconnected field lines and propagate both upward and downward.

Two places of acceleration, separated in height suggest the tearing-mode instability, in that two (or more) magnetic islands were formed and the entire activity at the post-eruptive phase is associated with the restoration of the magnetic structure.

The analysis of microwave pulsations by Tan *et al.* (2007) confirms such an evolution of the flare. They concluded that the flaring region consisted of many current-carrying compact loops. In each current-carrying flare loop, the resistive tearing-mode instability will trigger the formation of a series of multi-scale magnetic islands. The X-point is located between the two magnetic islands. The opposite frequency drifts of pulsations also suggest the particle acceleration occurs in the opposite directions.

The radio bursts drifting in the opposite directions in the frequency coverage of the spectrograph (Figures 16c and 16d) indicate the simultaneous existence of two places of particle acceleration in the current sheets between the magnetic islands. The fast particles moving from the higher to the lower corona are responsible for the type III burst in emission with the reverse drift. The fast particles moving from the lower to the higher corona are seized in the magnetic trap and give off the type III-like bursts in absorption with negative drift.

Karlicky and Barta (2007) found that electrons are accelerated most efficiently in the region near the X-point of the magnetic reconnection at the end of the tearing process and the beginning of the restoration of the magnetic configuration.

In this connection, all intervals of new peaks in the burst profile at the decay phase (Fig. 1 in Yan *et al*. (2007)) were very rich in spikes of absorption, type III–like bursts consisting of spikes in absorption and usual ZPs and fiber bursts with different frequency drifts (see Figures. 15–18). The appearance of ZP and fiber bursts means the loss-cone velocity distribution of fast particles inside the radio source (magnetic islands) exists.

The beams, accelerated above the flare loop would have propagated upward and fallen into the magnetic trap, where the loss-cone distribution of fast particles was already present, and would have caused bursts in absorption. The particles accelerated above the magnetic island would have probably propagated along the overlying magnetic loops downward (where the loss-cone distribution was absent). They might have simultaneously produced the reverse-drifting bursts in emission. The comparison of spectra in Figure 16b – 16d suggests a slow lift of the lower site of particle acceleration, which may have created a kind of `herringbone structure'. After ≈ 03:44:01 UT, the reverse-drifting bursts in emission were stopped by the drifting boundary (a hump of the `herringbone structure'). At higher frequencies, their continuation transformed to bursts in absorption (though their relationship is not very clear). The loss-cone distribution was probably formed there up to this moment and the quenching of instability by additional beams already became the main effect.

The difference in the parameters of these bursts in absorption (they were prolonged, broad-banded and diffuse) indicates that these beams were larger in scale and their velocity dispersion was wide (≈1). The velocity dispersion in the beams, critical for the spikes in absorption, was much less than 1. New beams with great longitudinal velocities stimulate the whistler generation at the anomalous Doppler resonance and as a consequence, the formation of ZP stripes in emission (in Figure 19 at 03:42:56 UT) could be explained in the whistler model (Chernov, 1996).

When the slowly drifting boundary became almost indistinguishable at 03:44:44 UT, the diffuse reverse-drifting bursts in absorption covered the whole frequency range (2.6 – 3.8 GHz), and the spikes in absorption almost disappeared. At this moment, the existence of the magnetic island must have ended.

5. New Theories of ZPs

5.1. What Is New in Improved Dpr-Based ZP Theories?

The mechanism proposed in LaBelle *et al.* (2003) can be regarded as an important step in attempts to improve the DPR-based model. The escape of the Z mode is considered at one DPR level (a point radio source), whereas the harmonics are assumed to be eigenmodes that propagate through regular inhomogeneities, such as an ion-acoustic wave. The number of harmonics is large only if density variations in the ion-acoustic wave reach ~20%. However, as was shown in Chen and Yan, (2008), it is hardly possible that such a strong ion-acoustic wave can be generated in the solar corona; in fact, the amplitude of density variations is no more than ~2%. In this case, only several ZP stripes can be generated by this mechanism, whereas up to a few tens of stripes are usually observed. In our opinion, a disadvantage of this theory is that it fails to explain the high intensity of radiation emitted by separate incoherent sources.

In the basic papers on the DPR theory (Zheleznyakov and Zlotnik, 1975a; Winglee and Dulk, 1986) the velocity distribution function of fast particles was assumed to be narrow, with an infinitely small spread in velocities; therefore, calculations of the growth rates of upper hybrid waves could hardly provide a realistic picture (Chernov, 2006). Besides, Winglee, and Dulk (1986) restricted themselves by consideration of the Maxwellian distribution of particles over momentum that could significantly affect the results obtained. This was clearly demonstrated in Kuznetsov and Tsap (2007), where the following electron distribution function of the loss-cone type was chosen (see Figure 27):

$$f_p(p,\theta)=\varphi(p)\begin{cases}0, & \theta \le \theta_c-\Delta\theta_c \\ \dfrac{\theta-\theta_c+\Delta\theta_c}{\Delta\theta_c}, & \theta_c-\Delta\theta_c<\theta<\theta_c, \\ 1, & \theta>\theta_c\end{cases} \tag{7}$$

where the function $\varphi(p)$ describes the electron distribution over momentum and θ_c is the loss-cone boundary with a width $\Delta\theta_c << 1$.

In old papers, the term associated with the velocity spread, to be more exact, the spread over particle momenta ($\Delta p/p$), was left in the expression for the anti-Hermitian part of the plasma permittivity. In the course of the new analysis Kuznetsov and Tsap (2007) conclude that the non-relativistic approximation cannot be used for investigation of the generation of upper-hybrid waves at the double plasma resonance when $s >> 1$.

The authors used the condition of the cyclotron resonance of waves and accelerated electrons in the form:

$$\dot{\psi}_s = \omega - \frac{s\omega_B}{\Gamma} - k_z \upsilon_z = 0 \tag{8}$$

where $\dot{\psi}_s$ is the time derivative of the phase difference between the waves and the gyrorotating particles, υ_z is the longitudinal component of electron velocity (υ), and $\Gamma = (1 - \upsilon^2/c^2)^{-1/2}$ is the relativistic factor.

Here, it is necessary to recall that Zlotnik *et al.* (2003) assume that the dispersion relation (A.6) is correct only inside the hybrid band. They obtained a very narrow maximum of the growth rate due to at the estimation of $\Delta k_\perp/k_\perp$, the velocity dispersion $\Delta\upsilon_\perp/\upsilon_\perp$ was missed as the infinitesimal quantity. This is already examined in detail in Chernov (2006). Zlotnik *et al.* (2003) assume also that many authors (Winglee and Dulk, 1986; Kuznetsov and Tsap, 2007) erroneously conclude that the kinetic instability of plasma waves described by the dispersion relation (A.6): $\omega^2 \cong \omega_p^2 + \omega_B^2 + 3k_\perp^2\upsilon_T^2$ - may contain several harmonics, while it is valid only inside the interval $\Delta\omega \leq \omega_B$. This assertion is correct, mainly, without taking into account relativistic correction and for the strictly perpendicular propagation. Zlotnik and Sher (2009) showed that in this case the harmonics, which adjoin the hybrid band on the top, give the overstated contribution to the value of increment, and this leads to the expansion of its maximum. To answer this question, new calculations with the precise dispersion relation will only help. At least, Kuznetsov and Tsap, 2007 assert that comparison with the exact solution of the dispersion relation shows that the equation of upper-hybrid waves (A.6) describes well the behavior of the oscillation branch with normal dispersion even at $\lambda \geq 1$, including the frequencies above the hybrid band. Moreover, Robinson (1988) has shown that weakly relativistic effects (especially in the case of *slightly non-transversal propagation*) cause the branches with normal dispersion corresponding to different harmonics to reconnect to one another at $\omega \approx s\omega_B$. As a result, a single continuous branch is formed. In addition, the condition of touching of the loss-cone boundary and the resonance curve can be satisfied only for one certain value of *s*. Since the contribution of the term associated with this harmonic will considerably exceed the contribution of other terms in the sum for the loss cone with a sharp boundary (when $\theta_c \rightarrow 0$; see the following), we can neglect the summation over harmonics and assume that the growth rate $\gamma \approx \gamma_s$, where γ_s is the growth rate at the *s*-th harmonic.

In the course of the analysis Kuznetsov and Tsap (2007) derived the final form of the imaginary part of the dielectric permeability (in the relation for γ):

$$\begin{aligned} \operatorname{Im}\varepsilon_{||}^{(s)} \approx & -2\pi^2 m^4 c^2 \frac{\omega_p^2}{k^2}\frac{n_b}{n_0}\Gamma^3 J_s^2\left(\frac{k_\perp p_\perp}{m\omega_B}\right)\times \\ & \left[\frac{\partial\varphi(p)}{\partial p} + \frac{\varphi(p)\tan\theta_c}{p\Delta\theta_c}\left(\frac{s\omega_B}{\Gamma\omega\sin^2\theta_c} - 1\right)\right]\frac{\Delta p_z}{p} \end{aligned}, \tag{9}$$

where the momentum p = $(p_z; p_\perp)$ and the parameter Γ correspond to the point of tangency $p_{\perp 0} = p_{z0} \tan \theta_c$ (see Figure 27); $J_s(\xi)$ is the first-order Bessel function.

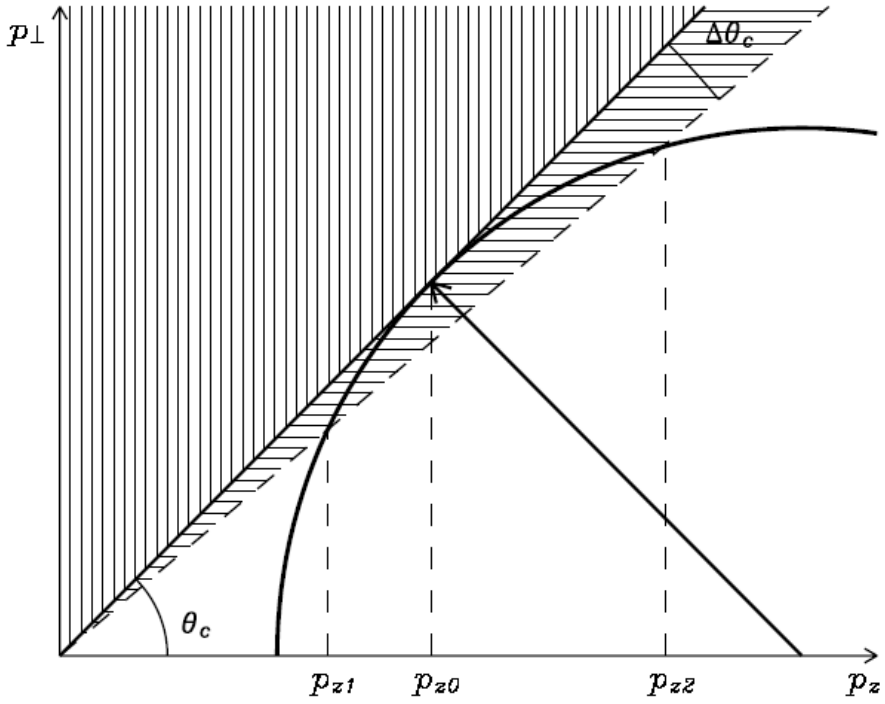

Figure 27. Schematic of the loss-cone distribution and the resonance curve in the space of electron momenta (from Kuznetsov and Tsap, 2007).

The derivation of Formula (9) somewhat differs from the corresponding procedure in the work of Zheleznyakov and Zlotnik (1975) because of another normalization condition for the function fp(p) and a misprint in the tensor of the dielectric permeability by the coefficient in front of the matrix (which contains the relativistic electron mass ($\tilde{m}$) rather than the rest one (see Appendix in Kuznetsov and Tsap (2007).

As a result of calculations, for the Maxwellian distribution of particles over momentum ($\varphi_1(p) = A_1 exp(-p^2/2p_h^2)$) of the loss-cone type (7) and real values of the velocity spread (~0.1), the modulation depth between the peaks of the growth rates turns out to be too small. However, calculations performed with a power-law velocity distribution function with an index of power of 8–10 yielded a modulation depth that was quite sufficient for the ZP formation at many harmonics (Figure 28).

A steep power-law spectrum of particles can be considered as an analog of a small velocity dispersion, although such spectra are sometime observed, especially in repeated bursts of hard X-ray emission (data from RHESSI).

Kuznetsov and Tsap (2007) and Kuznetsov (2007) applied their results to interpret 34 ZP stripes with a superfine structure in the form of millisecond spikes in the 2.6–3.8 GHz frequency range (Fig. 29) under the assumption that the electron beams were generated strictly periodically. It is important to note that the straight lines, which connect spikes in the

adjacent ZP stripes (in the right panel in Fig. 29) can be drawn at any inclination. Thus, the velocity of beams can be any value, and it is selected arbitrarily.

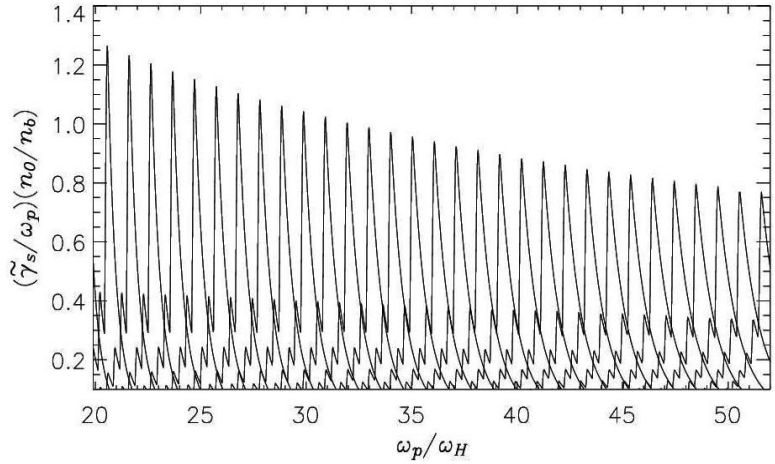

Figure 28. The dependence of the maximal growth rate of upper-hybrid waves on the plasma parameters for the power-law distribution of electrons over momentum (from Kuznetsov and Tsap, 2007).

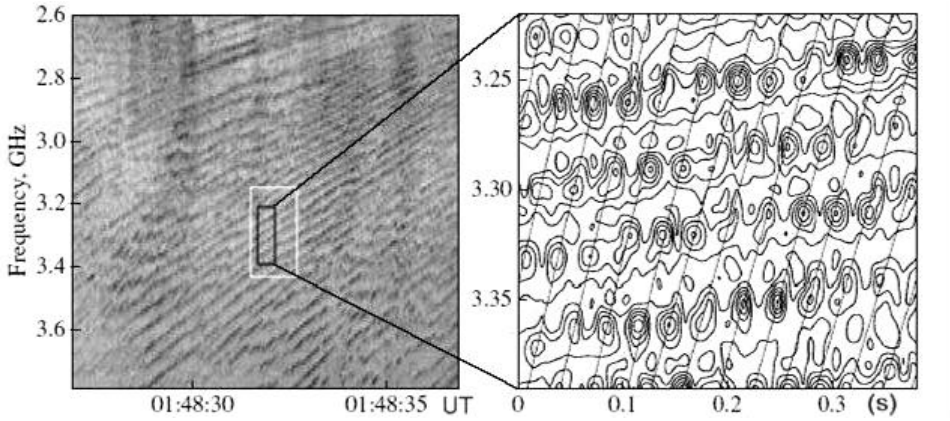

Figure 29. ZP in the frequency range 2.6–3.8 GHz in the event 2002 April 21. The magnified fragment of the spectrum (on the right) demonstrates the superfine structure of stripes in the form of periodic millisecond spikes, which, for better visualization, are shown by contour levels of the intensity (from Kuznetsov, 2007).

However, if we consider the possibility of simultaneous excitation of waves at 34 DPR levels in the corona, assuming that the plasma density depends on the altitude by the conventional barometric formula $f_P = f_{P0} \exp[-(h-h_{B0})/10^4 T]$ and the magnetic field, by the formula derived in Dulk and McLean (1978) from the radio data, $B = 0.5\ (h/R_s)^{-1.5}$ where R_s = is the Sun's radius, then we obtain that 34 DPR levels extend in the corona up to altitudes of ~65000 km, which, according to current knowledge, correspond to the plasma frequency ~250 MHz.

We calculated the DPR levels shown in Figure 30 by using a barometric formula with the commonly accepted coronal plasma parameters: the electron temperature T_e = 1.2 10^6 K and the initial plasma frequency f_{P0} = 3800 MHz at the altitude h_{B0} = 20000 km. If we use a dipole dependence of the magnetic field for cyclotron harmonics, then the DPR resonances at harmonics with $s \geq 50$ will occur at altitudes higher than 100000 km. Thus, the simultaneous excitation of waves at 34 levels in the corona is impossible for any realistic profile of the plasma density and magnetic field (if we do not assume it to be smaller, on the order of magnitude of the local density and magnetic field scale heights). For example, if we assume that the magnetic field decreases with altitude more slowly (see, e.g. fig. 55 in Zheleznyakov (1995)), then there will only be a few DPR levels at low harmonics. It should be noted that, as a rule, only the first several cyclotron harmonics are easy to excite, whereas the excitation of harmonics with $s > 50$ is hardly possible.

In this connection, let us note that in the following paper (Kuznetsov, 2008) the author proposed an alternative mechanism: a model in which the superfine temporal structure is formed due to modulation of the radiation by downward propagating MHD oscillations. The wavelet analysis showed a decrease of the period of spikes (from 40 ms at 2.6 GHz to 25 ms at 3.8 GHz). Variation of the observed period of oscillations is caused by a variation of the speed of the DPR levels (due to the Doppler effect). It was found that in the considered event on 2002 April 21 the MHD oscillations should have a period of about 160 ms and a speed of about 1500 km s^{-1}. This model allows us to explain the observed variation of the pulse period with the emission frequency.

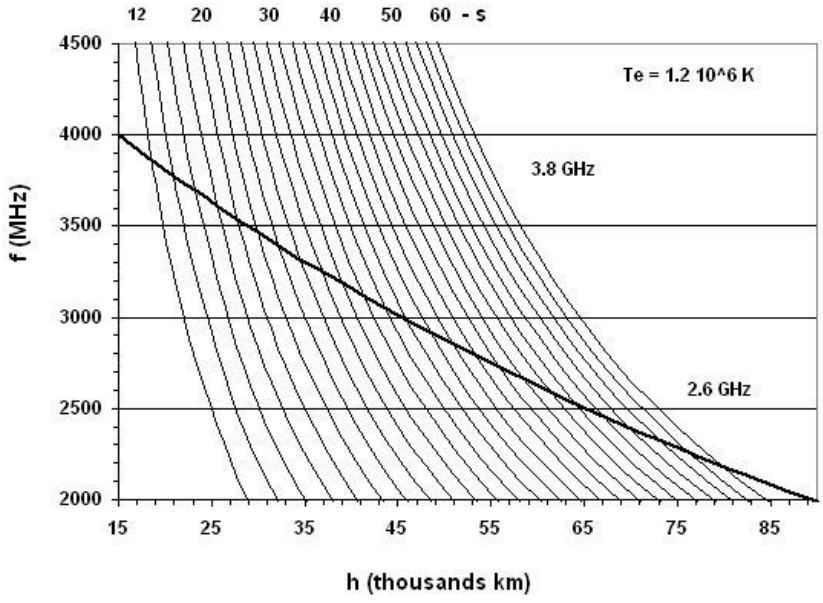

Figure 30. Altitude dependence of the plasma frequency in accordance with the barometric law (heavy line) and altitude profiles of the electron cyclotron harmonics s (light lines) in the solar corona. For the electron temperature Te = 1.2 · 106 K and initial frequency fP0 = 3800 MHz at an altitude of hB0 = 20 000 km, 34 DPR levels form between 2600 to 3800 MHz in the plasma layers (from Laptuhov and Chernov, 2010).

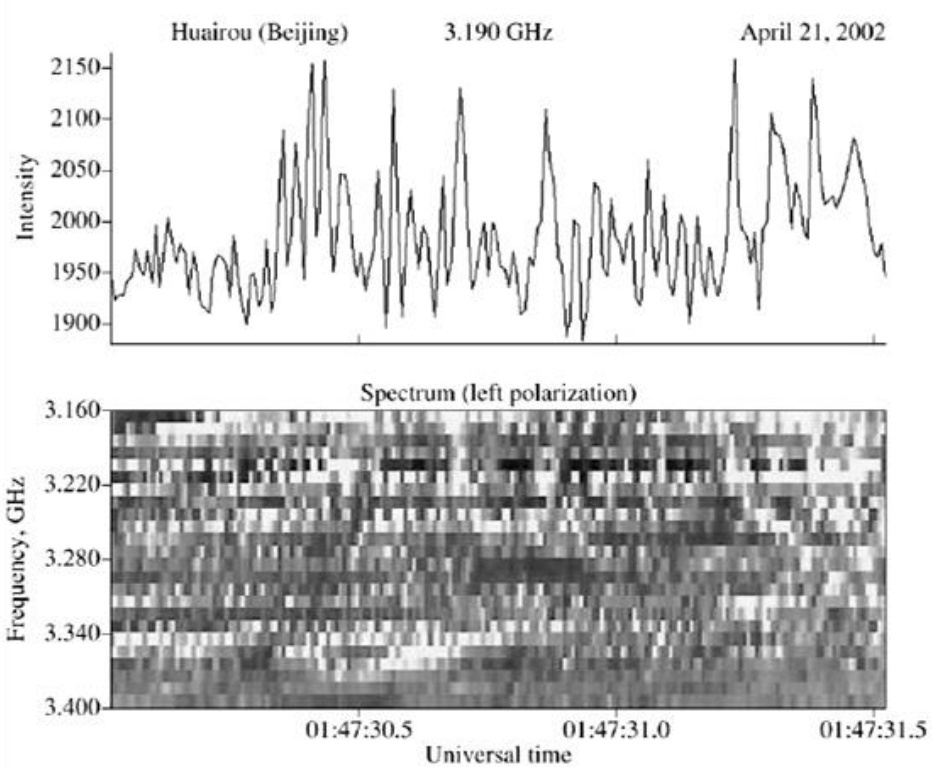

Figure 31. Superfine structure of the continuum in the form of spikes with a period of ~30 ms (from Laptuhov and Chernov, 2010).

At the same time, the frequency drift rate of the zebra stripes (increasing with an increase of the frequency from 60 to 160 MHz s^{-1}) was explained by the upward moving DPR levels. The observed polarization degree was connected with a partial depolarization when the emission propagates through a region with a transverse magnetic field. Both of these last effects were often used in many other papers (other events). However, there cannot be a universal interpretation because the frequency drift is often oscillating (like a saw-tooth) and the degree of polarization may be very different (sometimes with a change of sign during the event).

However, the superfine stripe structure in the form of millisecond spikes is apparently produced during the generation of the primary continuum radio emission, rather than arising in the course of ZP formation. This is confirmed by the detailed analysis of the time evolution of the spectral amplitudes of continuous radiation several seconds before the appearance of the ZP. It is seen from Figure 31 that, when there is not yet regular ZP stripes, the time dependence of the radiation intensity at the frequency 3.19 GHz clearly exhibits regular spikes with a period of ~30 ms. This period is then present in the ZP (see Figure 29). Thus, the superfine structure is not a consequence of wave excitation at DPR levels.

The superfine structure was also observed in the meter wavelength range. It was shown in Chernov *et al.* (1998) that such a spiky structure can arise due to periodic acceleration of fast particles provided that the simultaneous splitting of the ZP stripes is caused by the excitation of whistlers under the conditions of normal and anomalous Doppler effects (new beams).

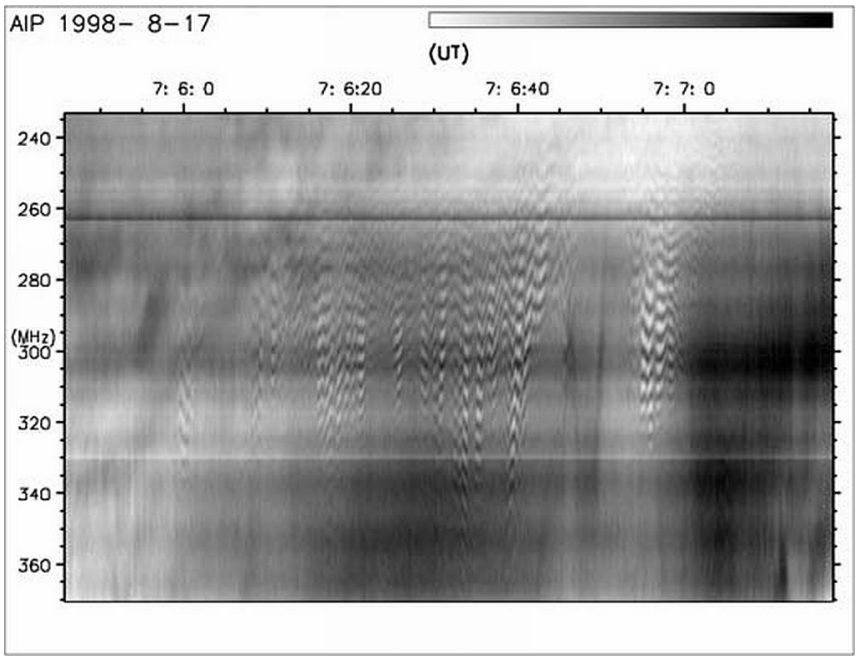

Figure 32. Dynamic radio spectrum with zebra patterns in fast drifting envelopes recorded on 1998 August 17 by the spectrograph of the Astrophysical Institute Potsdam (from Zlotnik et al. 2009).

Zlotnik *et al*. (2009) give an analysis of the occurrence of zebra patterns in fast drifting envelopes of continuum absorption, based on radio spectra of the Astrophysical Institute Potsdam shown in Figure 32. For the explanation of a ZP in fast drifting (type III burst-like) envelopes, it is proposed that we should consider complementary multinonequlibrium components of the coronal plasma in the DPR model. ZPs should be related to the emergence of fast particle beams. However, prior to the electron beam emergence, the nonequilibrium plasma consists of two components: one having a loss-cone distribution f_1 with velocity υ_1 and causing the background continuum and another one f_2 of DGH type (Dory, Guest, and Harris, 1965) with velocity υ_2 being able to provide the DPR effect and thus causing the ZP.

The loss-cone component is denser and cooler than the DGH component. Thus, for many reasons the stronger continuum can dominate the zebra pattern, making it invisible in the dynamic spectrum. If the electron beam emerges, it fills the loss cone, quenches the loss-cone instability (according to Zaitsev and Stepanov (1975)), and causes a type III-like burst in absorption. The switch-off of the continuum during the electron beam passage makes the zebra pattern visible against the absorption burst background. Some specific parameter conditions should be fulfilled:

- for the zebra structure excitation by the DGH component f_2 (υ_2 $\upsilon/_T \sim 15 - 30$) there exist reasonable intervals of velocity $\upsilon_1 \sim (1/6 - 1/2)$ υ_2 and electron number density $N_2 < N_1 < (10^2 - 10^7)N_2$ for the component f_1 where the proposed generation scheme is valid;
- $N_b >> N_1$ is a necessary condition for the absorption burst;

- the proposed scenario is only valid if the beam velocity ($\upsilon_b \approx c/3$) is much greater than the bulk velocity of electrons in the loss cone ($\upsilon_2 / \upsilon_1 \approx 3 - 6$) but the beam does not excite plasma waves.
- the beam electrons with great longitudinal and small transverse velocities fill the loss cone, while the electrons with great transverse and small longitudinal velocities enrich the DGH function f_2 with additional electrons, then an enhanced brightness of zebra stripes is observed.

If even one of these conditions is broken, the ZP can hardly appear. The authors conclude that the described scheme quite naturally explains the (at first glance enigmatic) appearance of a zebra pattern during the electron beam passage without a type III burst in emission. However, two distributions (DGH and loss-cone) can exist simultaneously but in rather different places of the radio source.

We should also observe several properties of ZP stripes in the spectrum that were not noted in Zlotnik *et al*. (2009). Not all the type III-like envelopes have negative frequency drift; it is possible to note almost instantaneous changes in the broadband (07:06:31 UT) or even cases showing positive drift (07:06:25 UT). A ZP is visible between the envelopes. It is possible to trace continuous ZP stripes lasting through five envelopes with the spasmodically changing drift. The ZP is only strengthened during the envelopes and it is experienced the sharp jumps in drift (by zigzags).

Such almost vertical pulsating envelopes of the ZP are not so rare phenomena. For instance, let us see an excellent sample in Fig. 6C in Slottje (1972). In the event from 1974 July 3 similar ZP envelopes were continuing during several hours (Slottje ,1981; Chernov, 1976b). Smooth or abrupt changes in the frequency drift of ZP stripes in the event on 1994 October 25 were discussed in Chernov (2005) on the basis of the natural mechanism of the formation of stripes in absorption due to the diffusion of fast particles in whistlers. The whistler waves are always generated simultaneously with the plasma waves at an upper hybrid frequency by fast particles with a loss-cone velocity distribution. This diffusion process is examined in Chernov (1990) and in more detail in Chernov (1996; 2005). The important feature was noted there: the changes in the sign of the frequency drift correlate with the change in the direction of the spatial drift of the ZP radio source (see Figures 2 and 7). The loss-cone distribution function changes due to the diffusion and the whistler generation switches from normal Doppler resonance to an anomalous one. In such a case, the whistler group velocity changes its direction to the opposite, which results in the change of the sign of the frequency drift of ZP stripes. Additional particle injection can only accelerate this process and strengthen the instability of whistlers, which can be related to the strengthening of the ZP in drifting envelopes in the event examined in Zlotnik *et al*. (2009).

Thus, in the model with the whistlers, the absorptive ZP stripes are not formed due to the quenching of the loss-cone instability, but due to only the scattering of fast particles on whistlers and only in the whistler wave packet volume. This mechanism explains the spasmodically changing frequency drift, and it does not require any strict specific complementary parameters.

The appearance of absorptive bursts depends strongly of parameters of new beams. Chen and Yan (2008) showed that the large scale beams with longtime injection (~ 1 s) are responsible for broadband type III- like absorptive bursts, and only the small scale beams

with very short injection times (~ 0.2 ms) could be responsible of absorptive spikes (see fig. 7 in Chen and Yan (2008)). New beams with great longitudinal velocities enrich the whistler generation in anomalous Doppler resonance (Chernov, 1996) and as a consequence, the formation of ZP stripes. This explains strengthening of ZP- stripes during drifting envelopes (Fig. 32). We could propose that the same effect is included in bright ZP stripes in absorptive type III-like bursts in the event on 2006 December 13 (Fig. 19). However, in such a case the whistler generation and, as a consequence, the formation of ZP stripes also depend strongly on the velocity distribution in the new beams.

In the recent small critical review of Zlotnik (2009), the advantages of the DPR model and the main failures of the model with whistlers are refined. The author asserts that the theory based on the DPR effect is the best-developed theory for ZP origin at meter-decimeter wavelengths at the present time. It explains in a natural way the fundamental ZP feature, namely, the harmonic structure (frequency spacing, numerous stripes, frequency drift, etc.) and gives a good fit for the observed radio spectrum peculiarities with quite reasonable parameters of the radiating electrons and coronal plasma. The statement that the theory based on whistlers is able to explain only a single stripe (e.g., a fiber burst) was made in Zlotnik (2009) without the correct ideas of whistler excitation and propagation in the solar corona.

Zlotnik uses the term "oscillation period" of whistlers connected with bounce motion of fast particles in the magnetic trap. Actually, the loss-cone particle distribution is formed as a result of several passages of the particles in the magnetic trap. Kuijpers (1975a) explain the periodicity of fiber burst using this bounce period (~1 s). And if we have one fast injection of fast particles, whistlers (excited at normal cyclotron resonance) are propagated towards the particles (they disperse in the space). Quasilinear effects thereby do not operate in normal resonance.

ZP is connected rather with whislers excited at anomalous resonance during long lasting injection. In such a case, waves and particles propagates in one direction, quasilinear effects begin operate and their role increases with increasing duration of injections. ZP is excited because the magnetic trap should be divided into zones of maximum amplification of whislers, separated by interval of whistler absorption (see in more details Chernov (1989; 1990)). The bounce period does not interfere with this process, but it can be superimposed on ZP.

However, the whistler amplification length is always small (on the order of $\leq 10^8$ cm in comparison with the length of the magnetic trap being $>10^9$ cm) for any energy of fast particles (Breizman, 1987, Stepanov and Tsap, 1999). According to Gladd (1983), the growth rate of whistlers for relativistic energies of fast particles decreases slightly if the full relativistic dispersion is used. In this case, the whistlers are excited by anisotropic electron distributions due to anomalous Doppler cyclotron resonance.

Later, Tsang (1984) specified calculations of relativistic growth rates of whistlers with the loss-cone distribution function. It was shown that relativistic effects reduce slightly growth rates. According to Fig. 8 in Tsang (1984), the relativistic growth rate is roughly five times smaller than the no relativistic growth rate. However, the relativistic growth rates increase with the perpendicular temperature of hot electrons $T_\perp$. According to Fig. 5 in Tsang (1984), the growth rate increases about two times with increasing of the electron energy from 100 to 350 keV, if to keep fixed other parameters of hot electrons: loss-cone angle, ratio of gyro frequency to plasma frequency, temperature anisotropy ($T_\perp/T_{||}$ = 3).

Thus, it is long ago known that the whistlers can be excited by relativistic beam with loss-cone anisotropy. Formula 13.4 in Breizman (1987), used in Chernov (1989) and as

formula (29) in Chernov 2006) for evaluating the smallest possible relaxation length of beam, has no limitations in the value of energy of fast particles.

Critical comparison of models has been repeated in Zlotnik (2010), only with a new remark concerning the Manley-Rowe relation for the brightness temperature of electromagnetic radiation in result of coupling of Langmuir and whistler waves:

$$T_b = \frac{\omega T_l T_w}{\omega_l T_w + \omega_w T_l}. \tag{10}$$

Zlotnik (2010) states that since $\omega_w << \omega_l$, in the denominator, only the first term remains and T_b depends only on T_l, and $T_b \sim T_l$, i.e. the process does not depend on the level of whistler energy. However, Kuijpers (1975) (formula (32) in page 66) shown that the second term $\omega_w T_l$ should be >> $\omega_l T_w$ due to $T_l >> T_w$. Analogous conclusion was made by Fomichev and Fainshtein (1988) with more exact relation with three wave intensities (then used by Chernov and Fomichev (1989), see also formula (11) in Chernov (2006)). Therefore T_b in the process $l + w \rightarrow t$ depends mainly on T_w.

Thus, our conclusion, that the entire magnetic trap can be divided into intermittent layers of whistler amplification and absorption remains valid for a broad energy range of fast particles.

In Zlotnik (2009) the main matter which is ignored is that the model involves quasilinear interactions of whistlers with fast particles, allowing one to explain all the fine effects of the ZP dynamics, mainly the superfine structure of ZP stripes and the oscillating frequency drift of the stripes which occurs synchronously with the spatial drift of radio sources.

5.2. Models of ZP Formation during Radio Wave Propagation in the Corona

Let us consider the capabilities of alternative models. One of the first such models was proposed in Laptuhov *et al.* (2005) and further developed in Laptuhov and Chernov (2006), where a one-dimensional inhomogeneity was considered in which the plasma and field parameters varied periodically in space along one coordinate x with a period $L_x = L$ (e.g., in the presence of nonlinear thermal structures) and the magnetic field B = (0, 0, B) was perpendicular to the inhomogeneity gradient and directed along the z axis.

The wave equation obtained from Maxwell's equations and hydrodynamic equations for the perturbed velocity of electrons and ions in a cold nonuniform magnetoactive plasma yields a generalized vector equation for the perturbed electric field, which has separate solutions for ordinary and extraordinary waves. The problem is reduced to deriving the corresponding dispersion relations in a spatially inhomogeneous medium in which the profiles of both the plasma density and magnetic field are approximated by stepwise functions. An analysis of the solutions to this problem revealed the existence of transparent regions separated by opaque regions of different width depending on the inhomogeneity scale L.

Thus, the dark ZP stripes observed in the radio emission spectrum can form due to the existence of opaque regions in a spatially periodic medium. The frequency separation between transparent regions increases with frequency (in agreement with observations). The number of harmonics grows with increasing amplitude of the inhomogeneity, but is

independent of the ratio of the plasma frequency to the gyrofrequency in the source. This may help to overcome all the difficulties in explaining the large number of ZP stripes and small values of the magnetic field determined from the frequency separation of stripes (e.g., in the DPR-based model).

At practically the same time, Barta and Karlicky (2006) analyzed a similar problem in which the formation of harmonics during the propagation of a wave through regular inhomogeneities (such as oscillations behind a shock front) was considered in a simplified approach. The wave equation was written for an unmagnetized plasma, the dispersion relations for harmonics were not derived, and solutions for the amplitudes of reflected and transmitted waves were searched. From the conservation laws and boundary conditions admitting the existence of nontrivial solutions, the frequency dependence of the transmission coefficient was found. As a result, multiple narrow harmonics (transmission regions, called interference stripes) separated by opacity (reflection) regions were obtained. In view of analogy with the results of Laptuhov and Chernnov (2006), it is worth comparing the parameters of transmission regions obtained in these two papers.

In Ledenev *et al.* (2006), a similar problem was considered in an even simpler approach in which the interference pattern produced by the incident rays and those reflected from regular inhomogeneities was analyzed. The problem was solved in the geometrical optics approximation by using the eikonal equation (by analogy with the problem of light propagation through a crystal lattice). The size of the radio emission source was assumed to be infinitely small, and the emission spectrum was considered to be sufficiently broad. Evidently, in case of radio wave reflection from smooth inhomogeneities, the interference pattern cannot show as much contrast as that produced by light reflected from a solid body. Moreover, the ordinary and extraordinary waves are reflected from layers with different plasma densities. Therefore, the modulation depth of the total interference pattern produced by many small-sized sources is relatively small.

In Laptuhov and Chernov (2006), the propagation of electromagnetic waves through a spatially periodic plasma was investigated to explain the ZPs observed in solar radio bursts. The possibility of existence of one-dimensional spatially periodic structures in the solar atmosphere was demonstrated in Kovalev (1990); Laptuhov (1991). Laptuhov and Chernov (2006) assumed that the waves propagate in an unbounded collisionless plasma along the x axis perpendicular to the magnetic field $\mathrm{B} = (0, 0, B(x))$.

In Laptuhov and Chernov (2009), a more realistic model in which a spatially periodic plasma occupies a region of thickness NL containing N identical plasma layers of thickness L was considered. For simplicity, each layer is assumed to consist of two piecewise-homogeneous layers with thicknesses $a < L$ and $b = L - a$. In the regions $x < 0$ and $x > NL$, the plasma is uniform.

Let us consider the propagation of broadband radio emission in such a plasma. As a matter of fact, the region occupied by the spatially periodic plasma is a frequency filter with multiple transparency windows separated by opaque regions (see fig. 1 in Laptuhov and Chernov (2006)). If broadband radiation is incident on the filter input ($x = 0$), then, at the output ($x = NL$), the radiation spectrum will only contain the frequencies that correspond to the transparency windows of the filter, while the amplitudes of waves with frequencies corresponding to opaque regions will be practically zero. As a result, after passing through such a filter, a structure similar to the ZP observed in the solar radio spectrum will form. This is the essence of the physical mechanism that was proposed in Laptuhov and Chernov (2006)

to explain the ZP formation in solar radio emission. In this case, the mechanism for the generation of primary broadband radio emission can be arbitrary (e.g., beam – plasma or cyclotron loss-cone instability (Zheleznyakov, 1995).

Let us first analyze the propagation of an ordinary wave, the field of which is described by the following simple formula (see Eq. (8) in Laptuhov and Chernov (2006)):

$$\frac{d^2E}{dx^2}+k^2E=0, \quad k^2=\frac{\omega^2-\omega_p^2}{c^2}, \quad \omega_p^2\equiv\omega_e^2+\omega_i^2 \tag{11}$$

The plasma frequency $\omega_p(x)$ and the corresponding constants k_m in different plasma regions are defined by the formulas

$$\begin{aligned}
&\omega_p(-\infty<x<0)=\omega_0, \quad \omega_p(NL<x<\infty)=\omega_3,\\
&\omega_p((n-1)L<x<a+(n-1)L)=\omega_1, \quad n=1,2...N,\\
&\omega_p(a+(n-1)L<x<nL)=\omega_2, \quad \omega_0\ge\omega_3\ge\omega_1,\\
&k_m\equiv\sqrt{(\omega^2-\omega_m^2)}/c, \quad m=0,1,2,3.
\end{aligned} \tag{12}$$

where all of the four frequencies ω_j, ($j=0,1,2,3$) are constant. In this case it is assumed that in the regions $x < 0$ and $x > NL$ the plasma is uniform, and between them ($0 < x < NL$) is located N of the identical layers, each of which is piecewise-uniform and has thickness L. Let an electromagnetic wave with frequency $\omega > \omega_0$ propagate along the x axis in the region $x < 0$. Then, taking into account wave reflection from the region $0 < x < NL$, a general solution to Eq. (11) in the region $x < 0$ can be written as

$$E(x<0)=E_0\exp(ik_0x)+E_r\exp(-ik_0x), \tag{13}$$

where E_0 is the amplitude of the incident wave, which is assumed to be given, and E_r is the amplitude of the reflected wave.

In the region $x > NL$, there is only the transmitted wave. Therefore, in this region, we have

$$E(x\ge NL)=E_t\exp(ik_3(x-NL)), \tag{14}$$

After simple manipulations, we obtain the transmission and reflection coefficients

$$K_t\equiv\mathrm{mod}\left(\frac{k_3E_t^2}{k_0E_0^2}\right), \; K_r=\mathrm{mod}\left(\frac{E_r^2}{E_0^2}\right)=1-K_t, \tag{15}$$

By definition, the coefficient K_t is equal to the ratio of the intensity $Q = c[E,B]/4\pi$ of the transmitted wave to that of the incident wave. It can easily be shown that the coefficient of reflection from N inhomogeneous plasma layers is $K_r = 1 – K_t$.

Note that the results obtained can also be generalized to the case of extraordinary waves described by Eq. (17) in Laptuhov and Chernov (2006) (cf. Eq. (11)). Below, we will consider some examples of calculating the reflection and transmission coefficients for different parameters of plasma inhomogeneities.

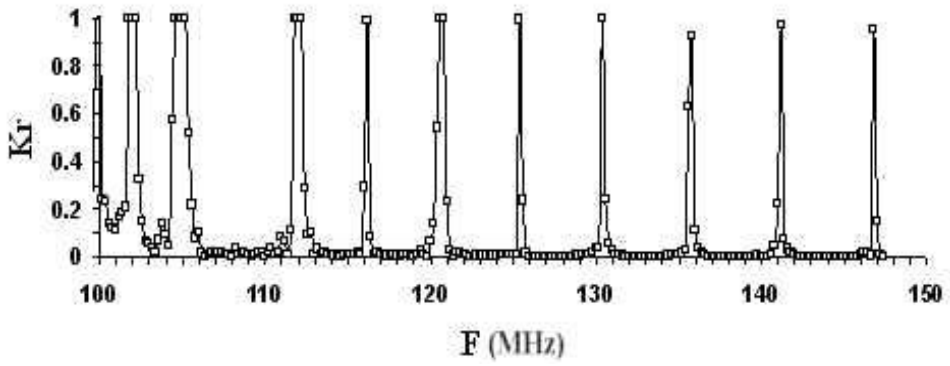

Figure 33. The reflection coefficient Kr of ordinary waves as a function of the frequency F for n1 = n2 · 0.84 = n3, n0 = n2, a = b = 10 m, n2 = 1.2d + 8, and N = 50 (from Laptuhov and Chernov, 2009).

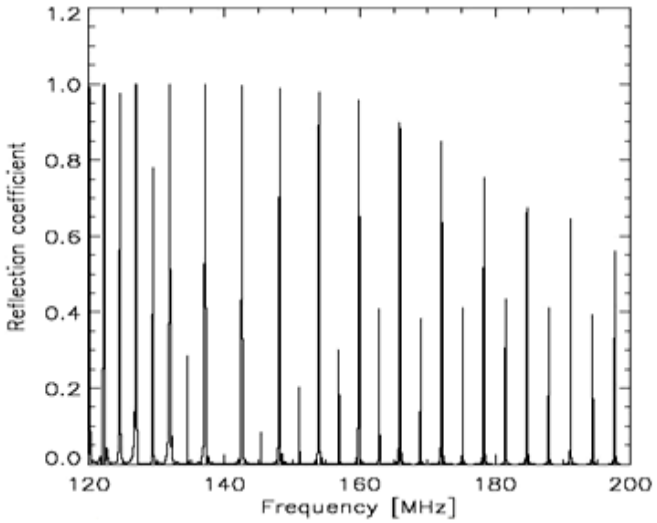

Figure 34. The reflection coefficient R = 1 − T for the series of 50 density wells produced by the density drop as a function of the frequency of an incidentwave (from Barta and Karlicky, 2006).

The number of stripes and their shape depend on the parameters (such as the size and number) of inhomogeneities. The profile of the harmonics of the reflection coefficient in the form of narrow peaks separated by relatively wide frequency intervals (see Figure 33) can be interpreted as radiation stripes similar to those present in the lower spectrum in Figure 1). Thus, in this case, the ZP is probably observed in reflected radiation. Note that the harmonics of the reflection coefficient in Figure 33 agree better with observations than the results of similar calculations in Barta and Karlicky (2006) presented in Figure 34. In our case, this is an even comb of harmonics in which the frequency separation between neighboring

harmonics increases gradually with frequency, whereas in Barta and Karlicky (2006), intense harmonics alternate with weak ones. Presumably, inhomogeneities in the form of density dips, which were considered in Barta and Karlicky (2006), cannot provide the observed widths of the ZP stripes. Moreover, we take into account the fact that the magnetic field and harmonics of an ordinary wave agree better with observations.

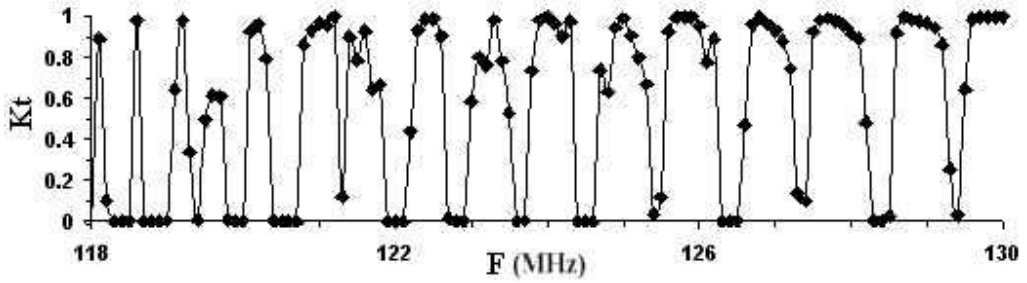

Figure 35. The transmission coefficient Kt of ordinary waves as a function of the frequency F for n0 = n3 = 1d + 8, n2 = 1.5n0, n1 = n2/2, a = 45 m, b = a, N = 10, and B = 5 G (from Laptuhov and Chernov, 2009).

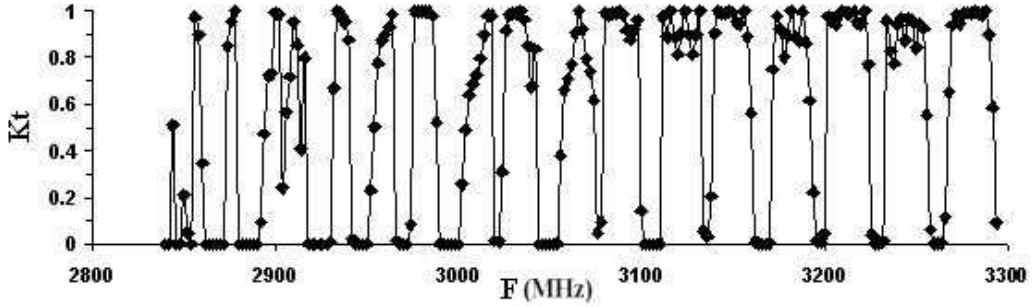

Figure 36. The transmission coefficient Kt of ordinary waves as a function of the frequency F for n1 = n2/α, n0 = 2n2/(1 + α) = n3, b = L/(1 + α), a = αb, L = 3 m, α = 2, n2 = 1.0d + 11, and B = 100 G (from Laptuhov and Chernov, 2009).

For a smaller number of larger inhomogeneities with a = 45 m, the frequency profile of the transmission coefficient (see Figure 35) yields nearly symmetric harmonics, which are most frequently observed (see the upper spectrum in Figure 1).

Figure 36 shows the results of calculations of the transmission coefficient in the microwave range. It is seen that, after passing through inhomogeneities with a thickness of L = 3 m, the spectrum of ordinary waves consists of symmetric harmonics, the frequency separation between which increases gradually with frequency, which agrees with observations. A sufficiently large number of harmonics are produced when the number of inhomogeneities is >10.

Some Concluding Remarks

An analysis of the difficulties arising in different models shows that the improvement of these models necessitates imposing new stringent conditions on the parameters of plasma and

waves in the source. The simplest model is related to the propagation of radio waves through regular inhomogeneities, because inhomogeneities are always present in the solar corona. However, for the cm range the effectiveness of this model requires inhomogeneities over the size of several meters. Such scales can be produced by ion-acoustic waves or the oscillator structure of the density and the magnetic fields behind the shock wave front. Existence of such waves in the flare region with the magnetic reconnection is completely probable. The alternative mechanism of the formation of small-scale heterogeneities could be the tearing-mode instability of the current-carrying loops in the process of magnetic reconnection (Tan, 2010). In this case, the dynamics of ZP stripes (variations in the frequency drift, stripe breaks, etc.) may be associated with the propagation of inhomogeneities, their evolution, and their disappearance.

The observed frequency difference between neighboring ZP stripes increases with frequency. This corresponds to the propagation of ordinary waves, the electric field of which is parallel to the unperturbed magnetic field, through a spatially periodic plasma. The number of discrete harmonics does not depend on the ratio of the plasma frequency to the gyrofrequency in the source. The latter circumstance can eliminate all the difficulties that arise in explaining the large number of ZP stripes and the small magnetic field value determined from the frequency separation of stripes (e.g., in the DPR based model).

The superfine structure observed in the microwave range, when all the continuous emission consists of spikes (Fig. 29), indicates the presence of plasma wave – whistler interaction in the pulsed regime of whistler interaction with ion acoustic waves in the radio emission source generating ordinary waves (this mechanism was considered in Chernov *et al.* (2003)). An alternative source of pulsed radio emission may be associated with plasma density pulsations caused by the propagation of a finite amplitude wave. The generation of electron cyclotron maser radiation, which is considered a possible cause of the observed spikes Fleishmann and Mel'nikov (1998), is dominated by extraordinary waves.

5.3. Other Recent Models

5.3.1. Nonlinear Periodic Space – Charged Waves in Plasma

Kovalev (2009) has investigated periodic nonlinear waves that can arise in plasma due to the excitation of potential oscillations by accelerated electrons with unstable distributions. As was noted in Kovalev and Petviashvili (1994), one- dimensional single-peak distributions of accelerated electrons are most likely to exist in the solar flare plasma. Such electron distributions excite resonant Langmuir oscillations with frequencies $\omega_2 < \min \{\omega_B, \omega_P\}$, due to the anomalous Doppler resonance. Low- and high- frequency modes of Langmuir oscillations can form large-amplitude periodic nonlinear waves. The corresponding spectrum of electromagnetic waves excited resonantly by the current of a potential wave is calculated. It is shown that an equidistant spectrum of electromagnetic radiation in plasma can form in the presence of a periodic potential wave.

Thus, the radio emission harmonics can be generated directly in the source in the form of a nonlinear periodic space charge wave in plasma. In Kovalev (2009), a solution in the form of such a wave propagating in a magnetic field was obtained using the hydrodynamic approach (without taking into account wave dispersion). The spectrum near the breaking point, in the vicinity of which the number of harmonics increases substantially, was

calculated. Due to electron bunching, the periodic wave with the spatial period $l = 2\pi u/\omega_2$ has the form of spatially alternating negatively and positively charged layers with an increased and a decreased electron density. In the presence of a wave electric field, the accelerated particles are subject to additional periodic acceleration and deceleration, due to which an electromagnetic wave is generated.

For a sufficiently large amplitude of density oscillations (a), a large number of harmonics with frequency separation close to the electron-cyclotron frequency can be excited. The number of these harmonics is determined by the parameter $N = \frac{3}{2^{3/2}(1-a)^{3/2}}$, which characterizes the degree of nonlinearity. Thus, for $a \sim 0.9$, we have $N \approx 34$. Since the radio emission can be generated in a relatively small-size source, the key difficulty of the DPR-based model, namely, the excitation of a large number of harmonics in a distributed source, is overcome (Figure 20). The number of harmonics can be fairly large when one of the plasma oscillation modes is dominate. In this case, the amplitudes of harmonics decrease fairly slowly ($\propto s^{-1/3}$) with increasing harmonic number s.

Due to inverse processes, the energy of background electromagnetic waves can transform into the energy of potential oscillations at the resonance frequencies $s\omega_2$. This can lead to the formation of an absorption zebra pattern consisting of stripes with a depressed radiation intensity.

The efficiency of the quite natural mechanism associated with nonlinear space charge waves depends on whether strong nonlinearity is reached; however, conditions for achieving the nonlinear regime were not considered in Kovalev (2009). The nonlinearity should rapidly increase and disappear in the course of wavebreaking (at $a = 1$).

5.3.2. The New Alternative Mechanism of the ZP due to Development of Explosive Instability in the System Beam – Plasma

Observations of ZPs during powerful flares make it possible to assume that the particle acceleration to relativistic velocities and excitation of different wave modes occurs in the radio source. Therefore, probably, other possible interactions of waves and particles should be taken into account. For example, in Fomichev and Fainshtein (1981) was proposed the decay instability of whistlers to the harmonics of the ion sound, which have weak spatial dispersion and small damping at frequencies much less than the ion Langmuir frequency ω_{oi}. In Fomichev *et al.* (2009) an alternative mechanism of ZPs is discussed, due to the development of explosive instability in the system, which is a weakly relativistic beam with nonisothermic plasma. The explosive instability appears in the nonequilibrium system, where there are waves of negative energy (Kadomtsev, *et al.* 1964), moreover, in the resonance triplet the wave of the highest frequency of ω_3 must possess by negative energy, and two lowest waves ($\omega_{1,2}$) have positive energy. Fomichev *et al.* (2009) have shown, that the mechanism of the generation of the ion-acoustic "saw" as a result of the development of explosive instability in the system with weakly-relativistic flow of protons and strongly nonisothermic plasma is more effective in the energy sense.

The number of harmonics of ionic sound *n* is determined by two factors: 1) the dispersion of ion sound must be sufficiently small [†]); 2) $v_{ef} << \omega$ (ω – the angular frequency of sound), i.e., the *n*- harmonic of sound must weakly attenuate.

The quasi-hydrodynamic approximation was utilized for describing the interaction of the particles of the beam and plasma (Fainshtein and Chernova, 1996; Ginzburg, 1967). Linearizing the hydrodynamic equations for the processes of ~ *exp(iωt–ikx)*, a dispersion equation for the system of flow–plasma was obtained:

$$1-\frac{\omega_{0i}^2}{\omega}-\frac{\omega_{0i}^2}{c_s^2k^2}-\frac{\omega_{0s}^2}{(\omega-kV_0)^2\left(1-\frac{\omega-ck}{3ck}\right)}=0, \tag{16}$$

where $\omega_{0s}^2=4\pi e^2 N_{0s} M_0^{-1}$, $\omega_{0i}^2=4\pi e^2 N_0 M^{-1}$; ω is the cyclic frequency, k is the wave number; *e*, M_o, *M* – electron charge, the rest mass of ion beam, the mass of the ion of the plasma respectively; $\bar{\rho}_s = N_{0s} + \rho_s$; $\bar{V}_s = V_0 + V_s$; ρ_s, V_s, ρ_i, V_i – the deviation respectively of ion concentrations of beam, speed of the ions of beam, concentration of the ions of plasma, and velocity of the ions of plasma from their equilibrium values N_{0s}, V_0, N_0 , *0.* With $V_0/c_s >> 1$, $N_{0s}/N_0 << 1$ from (16) the approximate dispersion equations were obtained:

$$\omega_1 \equiv \Omega \approx c_s k_1 \equiv c_s m q; \tag{17}$$

$$\omega_{3,2} - k_{3,2} V_0 \approx \mp \omega_{0s} + \delta; \frac{\delta}{\omega_{0s}} << 1. \tag{18}$$

Equation (17) describes the ion-acoustic wave (energy positive), and (18) - slow (ω_3, negative energy) and rapid (ω_2, positive energy) beam waves. The number $m > 0$- is selected from the escape condition of radio emission from the corona. It is easy to determine that for the slow beam wave (ω_3, k_3), the fast beam wave (ω_2, k_2) and the sound (Ω, q) the conditions of synchronism are satisfied (Tsytovich, 1970). From taking the conditions of synchronism (17), (18) into account we will obtain:

$$mq \approx 2\omega_{0s} V_0^{-1} \tag{19}$$

Since the sound has weak dispersion, the cascade process is possible:

$$mq + mq \to 2mq + mq \to 3mq + mq \ldots mnq.$$

Then, after decomposing nonlinear terms up to the quadratic terms and after using the standard procedure in the weak turbulence (Weiland and Wilhelmsson, 1977; Tsytovich,

[†]) n2 q2 cs2 ω 2oi ; q – wave number of the base ion-sound mode; cs – ion-sound speed (cs2 = œTe M-1), M – ion mass , œ – Boltzmann constant.

1970), the shortened equations for the complex amplitudes of coupling modes are obtained: beam modes $a_j \ (j=1,2)$ and ion sound $b_k \ (k=1,2,...mn)$. The analysis of interaction coefficients showed that the systems of such equations describe the stabilized "explosion" (Fainshtein, 1976).

It is also shown that the increment of the growth of ion sound in this case considerably exceeds the values obtained in Fomichev and Fainshtein (1981). Therefore the mechanism in question occurs much more effectively.

The generable sound is scattered over the fast protons, which move with a speed of $V \sim V_0 \sim 10^{10}$ cm s^{-1} and, according to the mechanism described in Fomichev and Faishtein (1981), the radiation from the source frequency is $\omega^t \approx mqnV$, and frequency separation between the stripes is $\delta\omega^t = mqV$. Taking into account equation (15) and selected parameters ($N_0 \sim 5 \cdot 10^9$ cm^{-3}, $N_s \cdot N_0^{-1} \sim 10^{-3}$, the constant magnetic field ~ 30 G) we obtain for the emission frequency of $\geq$ 634 MHz the value of coefficient $m = 15$, ($7 \cdot 10^2 \leq mn << 15 \cdot 10^3$) and the frequency separation between the adjacent stripes $\delta\omega^t \approx 15$ MHz. The obtained value of $\delta\omega^t$ corresponds to the observed frequency separation in the decimeter wave band (Chernov, 2006). In the given above estimations the wavelength of the ion sound ~ 100 m, the initial frequency ~1.0 kHz and the cyclic frequency of the slow beam wave $\omega_3 \sim 7 \cdot 10^2 \ \omega_{0i}$ (that correspond to ~ 10 GHz).

Discrete emission bands are possible when the width of each emission band will be less than the value of the frequency separation. This condition imposes a restriction on the dispersion of the beam velocities. As shown in such estimations, and implemented in Fomichev and Fainshtein (1981), the beam of protons must be sufficiently quasi-monoenergetic, in the case in question $\Delta V_0 / V_0 < 10^{-3}$.

6. The Most Recent Results

6.1. Zebra Pattern with Superfine Structure in the Short Radio Burst of 29 May 2003

The short radio burst of May 29, 2003 (02:12:30–02:14:30 UT) was connected with the M1.5 flare (in the GOES classification) (02:09–02:24 UT) in AR 10368 has been analyzed. It was observed by the SRBS (NAOC, station Huairou, Beijing) in the 5.2–7.6 GHz range at the temporal resolution of 5 ms in the frequency band of 10 MHz. Positions of radio bursts were obtained by radioheliographs of SSRT (5.7 GHz) and Nobeyama (NoRH) (17 GHz). Positions and sizes of the radio sources were determined from observed data obtained at SSRT, cross-shaped radiointerferometer operating in the 5.67–5.79 GHz frequency range (Smolkov et al., 1986; Grechnev et al., 2003). Two-dimensional solar disk maps are acquired every 2–3 minutes depending on the solar declination and the hour angle of observations. The full temporal resolution of one-dimensional scans is ≈ 14 ms at the spatial resolution of ≈ 15".

Dynamic spectra in Figure 37 showed that all the emission comprised millisecond pulses (spikes) of 5–10 ms duration in the instantaneous band of 70 to 100 MHz, forming the superfine structure of different bursts, essentially in the form of fast or slow-drift filaments and various zebra-structure stripes. Five scales of zebra stripes have been singled out.

The time profiles Figure 37 show simultaneous observations at SSRT (the NS line) and the NAOC spectropolarimeter at 5.68 GHz. The similarity between amplitudes and shapes of

the millisecond pulses (marked by Arabic numerals 1-8) measured independently by two spaced instruments indicates that the observed fine time structure is of solar origin.

It is worth noting that pulses 1, 2 and 4 correspond to the intersection of the SSRT receiving band by bursts which drift to low frequencies in the dynamic spectra; pulses 3 and 5,- to fibers, which drift in the opposite direction and look like fiber bursts. The sixth pulse is the superfine structure of the zebra-stripe low-frequency edge; pulses 7 and 8 are close to the horizontal zebra-structure stripe in episode IV; here, pulse 7 has inverse polarization.

Time-expanded zebra-structure fragments are shown in the lower panels (b) of Figure 37. Separated intervals of ZP are marked with Roman numerals I-V.

Drift ZP stripes of different frequency scales were observed for four seconds in a wide frequency range (5.8 – 7.2 GHz). All the stripes were made up of isolated pulses. The shortest ZP episode I (around 7 GHz) did not contain clear stripes. Such ZS behaviour is known in literature as "braided" ZP (Slottje, 1981). In episode II, the frequency drift of stripes df/dt = 1.3 – 1.5 GHz s^{-1} with a frequency separation between the stripes $\Delta f \approx$ 300–350 MHz. In episode III, df/dt = 3.2–3.6 GHz s^{-1} with $\Delta f \approx$ 170–200 MHz. From approximately 02:13:03.3 UT, two neat almost stationary stripes (IV) with frequency separation of ≈ 450 MHz appeared between 5.8 and 6.4 GHz. Between them fragments of slow-drift stripes are visible. After 02:13:03.8 UT they might have been taken for the frequency splitting of two main stripes.

Nearly 1.5 s after this fragment, in the interval of 02:13:05.4 to 02:13:05.8 UT at 6.6 – 7.6 GHz, there were three more ZP stripes (V) with $df/dt \approx$ 1500 MHz/s and $\Delta f \approx$ 250 MHz. They were weak and diffuse, but held a spike structure and occurred with additional fragments between stripes (frequency splitting). There was also a very short fragment of small-scale ZP at 02:13:03.3 UT at ~7.150 GHz: the frequency separation was ~40 MHz; the width of these two stripes in the emission at the limit of the instrument resolution, ~ 20 MHz.

The combination of all the data on the positions of radio sources is presented in Figure 38.

The flare configuration may be expected to be based on two loop systems R-L_S (long) and R-L_N (short). The presence of a shorter loop with bases in R and L_S polarized emission centers is confirmed by the location of emission intensity center at 17 GHz between them. Between the bases of the second, longer and higher loop system, there is a flare emission region at 5.7 GHz, extended along the photospheric field neutral line.

The background in Figure 38 is the MDI magnetogram taken for the later period in order to show the evolution of the field delta configuration. The thin black lines (dashed lines are the S-polarity, solid lines, the N-polarity) indicate magnetic islands; the wide ribbon is the neutral line. Yellow crosses 1–8 mark approximate positions of the spike source centers, coordinates of which were obtained using the projection method by comparing one-dimensional SN and EW scans with the maximum accuracy of 5" to 10".

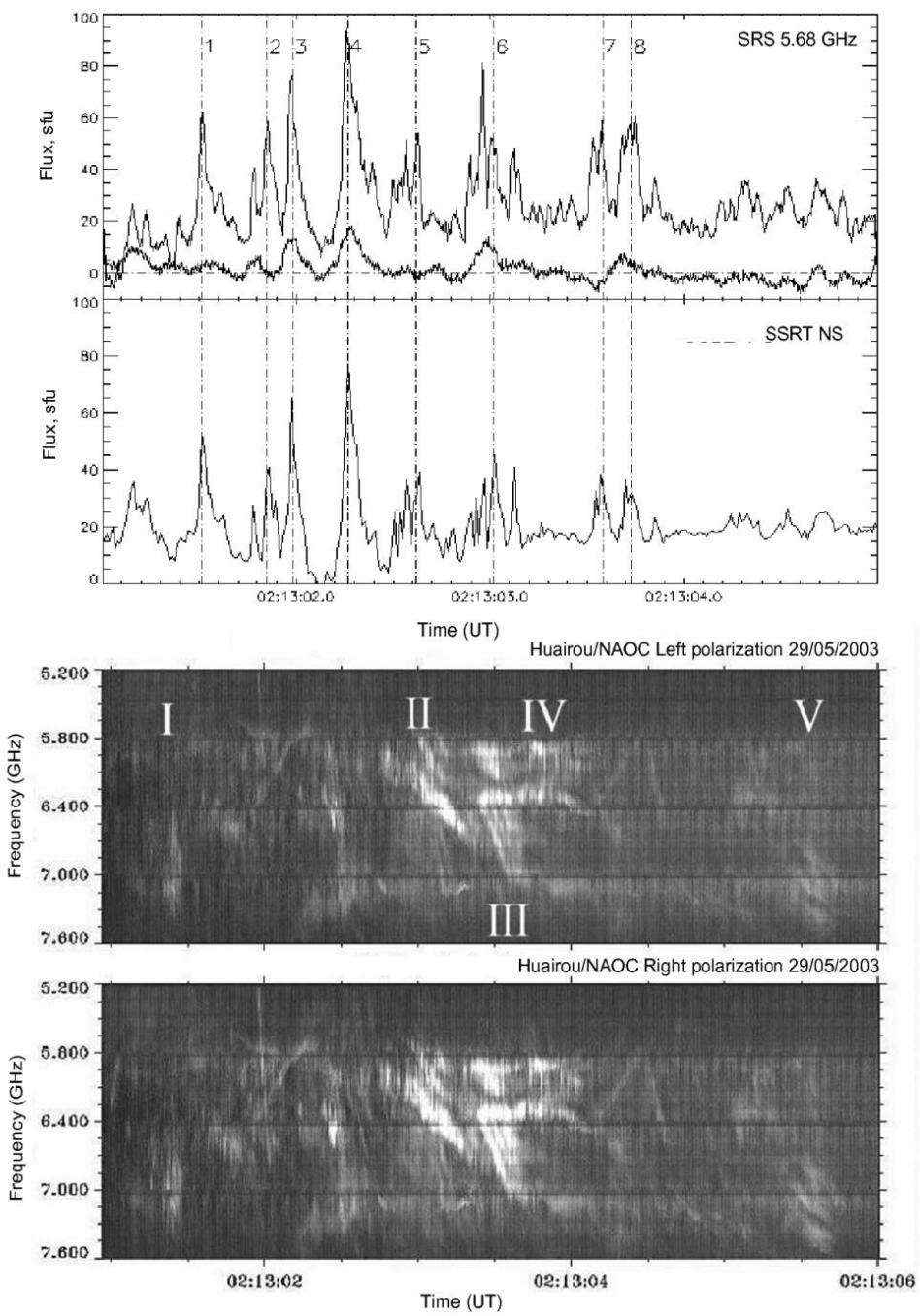

Figure 37. The comparison of the time profiles recorded at SSRT and NAOC (a) and the dynamic spectrum (b) registered by the NAOC spectropolarimeter (from Chernov et al., 2011).

The spikes were weakly polarized for the most part, and therefore there is no point in determining the wave type. Even for spikes 3 and 4 with moderate polarization (20–30 %) the wave type determination encounters difficulties in accurate assessment of magnetic field polarity.

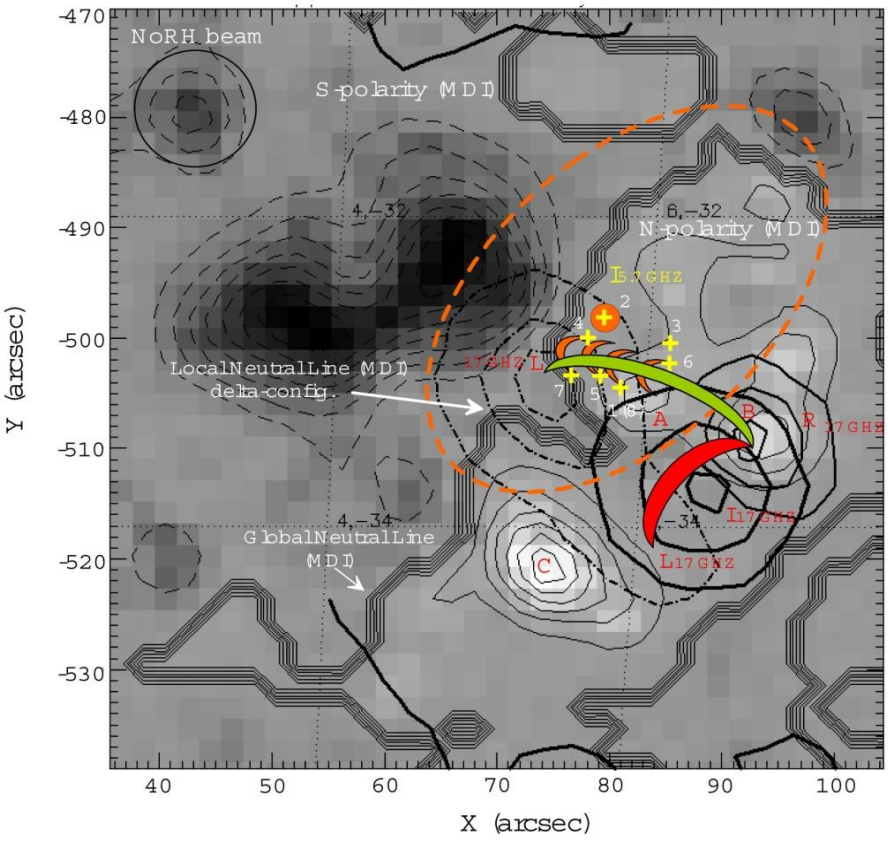

Figure 38. The positions of radio sources at 5.7 GHz (SSRT) and 17 GHz (NoRH) superimposed on the MDI magnetogram. The orange dashed line indicates the position of the left polarized local source at 5.7 GHz at 02:17:54.8 UT. The thick dash-and-dot line shows the position of the left polarized background source of the burst at 17 GHz (extended southwestward) at 02:13:00 UT. The straight crosses are the positions of spike sources 1–8 (from Chernov et al., 2011).

The analysis has revealed that there were three emerging magnetic islands during the field delta-configuration evolution. They are lettered A, B and C. Just in the place where the island A emerged, positions of SSRT spikes group together. It is the island B where all fast bursts are located at 17 GHz. The large ribbons (green and red) denote possible flare loops. In their common base, the highest magnetic field intensity near the photosphere was ~800 G.

The main process associated with the occurrence of R-polarized pulses at 17 GHz is the appearance of a new R source.

The positions of the spike source centers at the SSRT receiving frequency were estimated from the projection profiles (scans) of sources. The SSRT diagram did not exhibit broadening of the spike sources, therefore their sizes might be assessed as <15”. The significant difference between parameters of each zebra-structure patterns suggests that their sources resided in different magnetic loops (different feet or tops of the loops).

6.1.2. Generation Mechanisms

The emission of fine structures in dynamic spectra is associated with coherent mechanisms.

The mazer mechanism (ECME, Fleishman, Melnikov, 1998) drops out because of the low-intensity magnetic field under the region of the sources (< 200 G). In this case, the cyclotron harmonics above the tenth one become ineffective.

The interaction between plasma waves and whistlers in a pulse regime and the interaction between whistlers and ion-sonic waves are a distinct possibility (Chernov et al., 2003; Chernov et al., 2001a). The presence of whistlers in flare loops is confirmed by the appearance of fibers and zebra-structure stripes. This mechanism may be even preferable because it can explain the observable chaotic distribution of structures in the wide frequency range (all the emission consisted of spikes).

In this case, one can naturally explain the appearance of fibers and zebra structure with the same superfine structure in the form of millisecond pulses (Chernov, 2006). The whistlers were gradually captured into the flare loops; different loops gave stripes of different scales. The instantaneous emission band of an isolated pulse is determined from linear sizes of particle beams with small velocity dispersion (beam instability) or from sizes of whistler wave packets (in a model with whistlers).

DPR Model for ZP

The widespread mechanism of zebra structure under double plasma resonance (DPR) conditions (Zheleznyakov, Zlotnik, 1975a, b; Winglee, Dulk, 1986) is engaged when at discrete levels in the magnetic trap the upper hybrid frequency equals to an integer of electron cyclotron harmonics. The phenomenon discussed may be used as an example to demonstrate possible difficulties the mechanism at DPR faces in order to explain the zebra structure with sporadic stripes. Originally it was developed on the condition that there are always DPR levels in the source and only the presence of fast particles with loss-cone or ring (DGH) velocity distribution provides the excitation of the regular zebra structure of different modulation depth (depending on the particle energy spectrum) (Kuznetsov and Tsap, 2008). The presence of such particles may be considered obvious, and therefore the absence of zebra-structure at the beginning of the burst suggests the absence of DPR levels. DPR levels can not quickly appear and disappear in the corona. Processes of emergence of new magnetic fluxes and formation of new loops are very slow. Changes in height scales of density and magnetic field may be associated only with flare ejections and shocks. With the ejection velocity taken as Alfvén velocity (≈ 1000 km s^{-1}), the DPR levels (in view of the magnetic field line freezing-in) may shift by half the flare loop (green in Figure 38) with sizes of ~ 10” for approximately 7 s. This time exceeds the lifetime of zebra-structure stripes by an order of magnitude. The sporadic nature of ZS stripes itself, the wave-like drift of two stripes, their splitting, and the presence of isolated fibers with forward and reverse drift rule out the existence of any regular DPR levels. Moreover, the validity of the DPR conditions in fine flare loops along which density and magnetic field strength vary only slightly is in doubt (Aschwanden, 2004).

At the same time, all the effects can be naturally explained in the joint model of zebra structure and fibers when plasma waves interact with whistlers (Chernov, 2006).

The Model with Whistlers

All papers discussing the DPR mechanism (and its upgrading) omit a very important feature of the fast particle distribution function with loss-cone: the particles excite whistlers simultaneously, and the entire dynamics of the distribution function and emissions depends on the interaction of fast particles with whistlers (Chernov, 1996). Let us note first of all that whistler excitation growth rates in the microwave range exceed their value in the meter range (Yasnov et al. 2002).

According to the model described in (Chernov, 2006) (Section 3.6), zebra-structure stripes are associated with the whistler excitation by the anomalous Doppler effect at the top of the magnetic particle trap. Whistler wave packets fill the magnetic trap and propagate downward (at a significant angle to the magnetic field) at a group velocity of ~ 10^9 cm s^{-1}.

The wave packet size in the corona is determined by the linear size of relaxation of the whistler-exciting fast particle beam (Formula (13.4) in Breizman (1987), see also the discussion of Formula (29) in (Chernov, 2006) and (Chernov, 2010).

For the central ZP frequency of 6.4 GHz, the ratio of the gyrofrequency to the plasma frequency $\frac{\omega_B}{\omega_p}$ ~0.1 and the ratio of the cold plasma concentration to the hot particle one $\frac{n^c}{n^h}$ ~ 10^6 we obtain the linear size of relaxation of ~ $2.8 \cdot 10^6$ cm. In the Avrett table model (Avrett, 1981), this size corresponds to the change in the plasma frequency of ~350 MHz. This very frequency separation between ZP stripes was observed in Episode II (Figure 37).

The large flare loop (green in Figure 38) extends for about 20''. Whistlers should go from its top to base at a group velocity of ~10^9 cm s^{-1} for ~ 0.7 s. It is the longest duration of stripes in ZP fragments II and IV. The shorter ZP episodes must have emanated from a smaller flare loop (red in Figure 38). The Allen concentration model gives much the same plasma frequency gradient (for example, see Fig, IV.1 in Kruger (1979). It corresponds to the density height scale at these heights about 10^7 cm.

We can determine the magnetic field strength from the frequency separation between stripes Δf ~ 350 MHz. The whistler group velocity peaks at the whistler frequency f^w ~ 0.25 f_B. With the value of separation between emission and absorption taken as ~ 0.5 Δf and set equal to the whistler frequency it is easy to obtain the electron gyrofrequency f_B ~ 700 MHz (the magnetic field strength B ~ 250~G) which warrants our choice of the ratio $\frac{\omega_B}{\omega_p}$ ~0.1.

Let us consider ZP pattern IV: two stripes with slightly wave-like frequency drift (in zero value) and large frequency separation, ~450 MHz. They are not identical: the low-frequency stripe started 0.4 second early; their intensity and frequency drift were not similar, and besides the low-frequency stripe bifurcated two times, exhibiting the frequency splitting at 02:13:03.4 and 02:13:03.9 UT. The sources must have been located at tops of different flare loops. Spike 6 (Figure 37) is in the spectrum at the beginning of the low-frequency stripe, and according to the two-dimensional map its source was at the top of the large flare loop (green in Figure 38).

The absence of the frequency drift is likely to be tied to propagation of whistler packets almost along the level of equal density at the top of the loop. In this case, whistlers may be excited by the normal Doppler effect or more precisely the scattering of fast particles by whistlers sets the distribution function into the oscillation regime when excitation by normal

or anomalous Doppler effects is dominant. In a borderline case, both the effects work simultaneously, and at these moments we can see the frequency splitting of ZP stripe because the excitation by different effects occurs with a frequency shift. This excitation may be referred to as the analogue of the "fan" instability (see section 4.) In the meter range, this effect has been discussed two times to explain the frequency separation of ZS stripes and the wave-like frequency drift (Chernov et al. 1998; Chernov, 2005).

The change in the frequency drift of stripes at the "fan" instability is associated with the smooth change in the whistler group velocity direction. Episode III and the low-frequency ZP stripe from IV might be tied to the small flare loop (red in Figure 38).

ZP episode V at higher frequencies (6.7--7.6 GHz) with a frequency separation of ~300 MHz and the explicit stripe splitting the very short episode of the small-scale ZP at 02:13:03.3 UT at ~7.150 GHz: the frequency separation is ~40 MHz

The sporadic nature of the fine structure suggests multiple pulsating acceleration of fast particles. However, the superfine spike structure is not necessarily determined by such a pulsating acceleration as in (Kuznetsov, 2007). It is much more probable that the spike nature of the entire emission is formed by the pulsating mechanism of emission. ZP is generated by periodic whistler packets filling a magnetic trap. But whistlers should occupy the entire radio source and propagate in different directions. Spikes might therefore be related to the pulsating interaction of whistlers with ion-sound waves and subsequent coalescence with plasma waves. This mechanism is discussed in Chernov et al. (2001). In the microwave range therewith, it may be more effective because near the reconnection region the presence of nonisothermic plasma ($T_e >> T_i$) as a condition for ion sound excitation is much more likely. ZP did not appear at lower frequencies (2.6--3.8 GHz), and there was no spike structure of the entire emission there. That is why we can say that the spike structure appeared only in regions of the source where whistlers existed.

However, at 5.2--7.6 GHz we could see many weak diffuse bursts with different frequency drifts, which did not exhibit the spike structure. Their polarization properties were similar to ZP ones. It can even be said that they were the extension of ZP. They may therefore have been excited by the plasma mechanism at the upper hybrid frequency, when there were no conditions for DPR.

Kuznetsov (2008) proposed a new mechanism of superfine structure in which the emission modulation is associated with top-down propagation of MHD oscillations. But this mechanism gives the superfine structure only for ZP stripes, not for the whole emission; hence the pulsating regime of whistlers remains preferable in our case.

All recent models (LaBelle et al., 2003; Laptukhov and Chernov, 2006; Ledenev et al., 2006; Fomichev et al. (2009); Kovalev ,2009) must be realized only in specific conditions. Their role in the ZS model hierarchy is still ill-defined.

7. Conclusion

We have considered several of the most recent events with new peculiar elements of zebra patterns. Important new results are obtained by simultaneous studies of the positions of radio sources, using Nançay Radio Heliograph at 164 and 236 MHz. In particular, correlation between the direction (sign) of the frequency drift of stripes on the spectrum and the direction of the drift of source in space is discovered. In most events the polarization corresponds to the

O- radio mode. All new properties are considered in light of both what was known earlier and new theoretical models. All the main properties of the emission and absorption stripes can be explained in a model involving interactions between electrostatic plasma waves and whistlers, taking into account the quasi-linear diffusion of fast particles with the loss-cone distribution on whistlers. Within the framework of this mechanism alone not simply the stripes in the emission and the absorption are explained, but also the entire dynamics of the stripes on the spectrum and of their radio sources (splitting of stripes, movements of the sources, superfine spiky structure).

In two events (2004 July 24 and 2004 November 3) the large-scale ZP consisted of small-scale fiber bursts. The appearance of such an uncommon fine structure is connected with the following special features of the plasma wave excitation in the radio source: both whistler and plasma wave instabilities are too weak at the very beginning of the events (the continuum was absent), and the fine structure is almost invisible. Then, whistlers generated directly at DPR levels "highlight" the radio emission only from these levels due to their interaction with plasma waves.

A unique fine structure was observed in the event 2006 December 13: spikes in absorption formed darks ZP stripes against the absorptive type III-like bursts. The spikes in absorption can appear in accordance with the well known mechanism of absorptive bursts. The additional injection of fast particles filled the loss-cone (breaking the loss-cone distribution), and the generation of the continuum was quenched at these moments, which was evidenced by the formation of bursts in absorption. The maximum absorptive effect occurred at the DPR levels. The parameters of millisecond spikes are determined by small dimensions of the particle beams and local scale heights in the radio source.

Thus, in each new event the new special features of the fine structure are revealed. However, they are usually related with the varied conditions in the source. In such a case, one ought not to find the special emission mechanism for each event, which was repeatedly done before. The DPR model helped to understand several aspects of unusual elements of ZPs. In this connection, the calculations of growth rates of upper hybrid waves with a different distribution function of fast electrons inside of the loss-cone is very important (Kuznetsov and Tsap, 2007). However, discussions concerning the validity of taking into account of one or several harmonics in a hybrid band continue. At the same time, Laptuhov and Chernov (2009) showed that the simultaneous existence of several tens of the DPD levels in the corona is impossible for any realistic profile of the plasma density and magnetic field (if we do not assume the order of magnitude of the local density and magnetic field scale heights to be smaller).

Since all known models still have deficiencies, the attempts to create new theories continue. We examined three new theories. The formation of transparency and opacity bands during the propagation of radio waves through regular coronal inhomogeneities is the most natural and promising mechanism. It explains all main parameters of regular ZP. The dynamics of ZP stripes (variations in the frequency drift, stripe breaks, etc.) can be associated with the propagation of inhomogeneities, their evolution, and disappearance. Inhomogeneities are always present in the solar corona, however direct evidences of the existence of inhomogeneities with the scales of several meters in the corona are absent, although ion-sound waves could serve this purpose.

The model of a nonlinear periodic space, charge waves in plasma (Kovalev, 2009) is also a very natural mechanism in the solar flare plasma. However, in the case of intrinsic plasma emission it gives a constant frequency separation between stripes of $\approx \omega_B$, while the

observations verify the increase of the frequency separation with frequency. In eddition, the condition of achieving strong nonlinearity remains uncertain.

The mechanism of scattering of fast protons on ion-sound harmonics in explosive instability looks as very uncommon, and it requires a number of strict conditions. Although the fast protons always exist in large flares, and the presence of nonisothermic plasma is completely feasible in the shock wave fronts.

The last two models could be useful in describing large radio bursts. All three models are related to a compact radio source. The number of discrete harmonics does not depend on the ratio of the plasma frequency to the gyrofrequency in the development of all three models. The latter circumstance can eliminate all the difficulties that arise in the DPR model.

The short event 29 May 2003 provided a wealth of data for studying the superfine structure with millisecond resolution. All the emission in the spectrum in the 5.2 – 7.6 GHz frequency range consisted of spikes of 5-10 ms duration in the instantaneous frequency band of 70 to 100 MHz. These spikes make up the superfine structure of different drift bursts, fiber bursts and zebra pattern stripes. The coalescence of plasma waves with whistlers in pulse regime of the interaction between whistlers and ion-sound waves ensures the best explanation for generating spikes (as initial emission).

Acknowledgments

We are grateful to the Nobeyama, TRACE, RHESSI and SOHO (LASCO/EIT) teams for operating the instruments and performing the basic data reduction, and especially, for their open data policies. G.P.Chernov appreciates the support of the Chinese Academy of Sciences and NSF of China, with Prof. Yan Yihua, which enabled this work with NAOC colleagues, as well as the Russian Foundation of Basic Research (RFBR), grant No. 11-02-00757.

References

Abada-Simon, M., Lecacheux, A., Louran, P., Dulk, G.A., Belkora, L., Bookbinder J.A., Rosolen, C.: 1995, *Proceeding of IAU Coll.* **151**, *Flares and Flashes*, Monograph, Eds. J.Grenier *et al.* v. 454, p. 32.

Aschwanden, M.J.: 2004, *Physics of the Solar Corona*, Pruxis Publishing.

Ashour-Abbdalla, M.: 1972, *Planet. And Space Sci*. **20**, 639.

Avrett, E.N.: 1981, In *The Physics of Sunspots*, Ed. By L.E. Cram and J.N. Thomas, Sacramento Peak Obs. P. 235.

Bárta, M. and Karlický, M.: 2001, *Astron. Astrophys.* **379**, 1045.

Bárta, M. and Karlický, M.: 2006, *Astron. Astrophys.* **450**, 359.

Benz, A.O., and Kuijpers, J.: 1976, *Solar Phys.* **46**, 275.

Bespalov, P.A. and Traxtenherz, V.Iu.: 1986, *Alvenic Mazers*, IPFAN, Gorkii (in Russian). *Rev. Plasma Phys.*, **10**, 155.

Breizman, B.N.: 1987, in *Problems in Plasma Theory*, Kadomtsev, B.B. Eds., Energoizdat, Moscow (in Russian), **15**, p.55.

Chen, B., Yan, Y.: 2008, *Astrophys J.* **689**, 1412.

Chernov, G.P.: 1976a, *Sov. Astron.* **20**, 582.

Chernov, G.P.: 1976b, *Sov. Astron.* **20**, 449.
Chernov, G.P.: 1990, *Sol. Phys*. **130**, 75.
Chernov, G.P.: 1996, *Astron. Reports* **40**, 561
Chernov, G.P.: 1997, *Astron. Lett* **23**, 827.
Chernov, G.P.: 2005, *Plasma Phys. Rep.* **31**, 314.
Chernov, G.P.: 2006, *Space Sci. Rev*. **127**, 195.
Chernov, G. P., Klein, K.-L., Zlobec, P., Aurass, H.: 1994, *Solar Phys.* **155**, 373.
Chernov, G. P., Markeev, A. K., Poquerusse, M., Bougeret, J.L., et al.: 1998, *Astron. Astrophys*. **334**, 314.
Chernov, G.P., Fu, Q., Lao, D.B. and Hanaoka, J.: 2001a, *Solar Phys.* **201**, 153.
Chernov, G. P., Yasnov, L. V., Yan, Yi-Hua, Fu, Qi-Jun: 2001b, *Chin. J. Astron. Astrophys*. **1**, 525.
Chernov, G.P., Yan, Y.H., and Fu, Q.J.: 2003, *Astron. Astrophys*. **406**, 1071.
Chernov, G.P., Yan, Y.H., Fu, Q.J., and Tan, Ch.M.: 2005, *Astron. Astrophys*. **437**, 1047.
Chernov, G.P., Sych, R.A., Yan, Y.H., Fu, Q.J., Tan, Ch.M., Huang, G.L.,Wang, D.Y. and Wu, H.G.: 2006, *Solar Phys.* **237**, 397.
Chernov, G.P.,Yan, Y.H., Fu, Q.J., Tan, Ch.M. and Wang Sh.J.: 2008, *Solar Phys.* **250**,115.
Chernov, G.P., Yan, Y.H., Tan, Ch.M., Chen, B. and Fu, Q.J.: 2010. *Solar Phys.* **262**, 149.
Chernov, G.P., Sych, R. A.., Meshalkina, N. S., Yan, Y.H., Tan, Ch.M.: 2011, *Astron. Astrophys*. (accepted).
Dabrowski, B.P., P. Rudawy, R. Falewicz, M. Siarkowski, and A. J. Kus,: 2005, *Astron. Astrophys.* **434**, 1139.
Dory, R., Guest, G., and Harris, E.: 1965, *Phys. Rev. Lett.* **14**, 131.
Dulk G.A., McLeen D.J.: 1978, *Solar Phys*.**57**, 279.
Elgarøy, Ø.: 1982, *Intermediate drift bursts*, Report N 53, ITA, Univ. Oslo.
Fainstein, S.M.: 1976, *Zh. Eksp. Teor. Fiz.* **71**, 1021 [*Sov. Phys. JETP* **44**, 534].
Fainstein, S.M. and Chernova, E.A.: 1996, *Zh. Eksp. Teor. Fiz.* **109**, 821 (1996) [*JETP* 82, 442].
Fleishman, G.D., Stepanov, A.V., Yurovsky, Yu. F.: 1994, *Solar Phys.* **153**, 403.
Fleishman, G. D.and Mel'nikov, V. F.: 1998, *Usp. Fiz. Nauk* **168**, 1265 [*Soviet Physics Uspekhi*. **41**, 1157].
Fomichev V. V. and Fainshtein S. M.: 1981, *Solar Phys*. **71**, 385.
Fomichev, V.V. and Fainshtein, S.M.: 1988, *Sov. Astron.* **32**, 552.
Fomichev, V.V., Fainshtein, S.M. and Chernov, G.P.: 2009, *Plasma Phys. Rep.* **35**, 1032.
Fu, Q.J., Qin, Z.H., Ji, H.R., Pen, L.B.: 1995, *Solar Phys.* **160**, 97.
Fu, Q.J., Ji, H.R., Qin, Z.H., Xu, Z.C., Xia, Z.G., Wu, H.A. *et al*.: 2004, *Solar Phys.* **222**, 167.
Gendrin, R.: 1981, *Geophys. and Space Phys.* **19**, 171.
Ginzburg, V.L.: 1967, *Propagation of Electromagnetic Waves in Plasma*, Moscow, Nauka.
Ginzburg, V.L. and Rukhadze, A. A.: 1975, *Waves in Magnetoactive Plasma* (Nauka, Moscow,) [in Russian].
Gladd, N.T.: 1983, *Phys. Fluids*, **26**, 974.
Grechnev, V. V., Lesovoi, S.V., and Smolkov, G.Ya. et al.: 2003, Solar Phys. **216**, 239.
Guo, Y., Ding, M.D., Wiegelmann, T., Li, H.: 2008, *Astrophys. J*. **679**, 1629.
Huang, Guang-Li: 2003, *New Astronomy*, **8**, 313.
Huang, Guang-Li: 2004, Proceedings of the IAU Symposium 226, Beijing, Eds K. Dere, J. Wang, and Y. Yan, Cambridge University Press, p.95.
Huang Jing, Yan Yihua, Liu Yuying: 2007, *Adv. Space Res*. **39**, 1439.

Kadomtsev, B.B., Mihailovsky, A.B. and Timifeev, A.V.: 1964, *Zh. Eksp. Teor. Fiz.* **47**, 2266 [Sov. Phys. JETP 20, 1517].
Karlicky, M. and Barta, M.: 2007, *Adv. Space Res.*, **39**, 1415.
Karlicky, M., Barta, M., Jiricka, K. et al.: 2001, *Astron. Astrophys.* **375**, 638.
Klassen, A.: 1996, *Sol. Phys*. **167**, 449.
Kovalev, V. A.: 1990, *Kinemat. Fiz. Nebesn. Tel* **6**, 38.
Kovalev, V. A.: 2009, *Plasma Phys. Rep.* **35**, 394.
Kovalev, V. A. &. Petviashvili, V. I: 1994, *Russian Phys. J*. **37**, 699 [Russ. *Izv. Vyssh. Uchebn. Zaved., Fiz.*, No. 7, 118].
Krishan, V., Fernandes, F. C. R., Cecatto, J. R., and Sawant, H. S.: 2003, *Sol. Phys.*, **215**, 147.
Krüger, A.: 1979, *Introduction to Solar Radio Astronomy and Radio Physics*, Reidel, Dordrecht.
Kuijpers, J.: 1975a, *Collective wave-particle interactions in solar type IV radio source*, Ph.D Thesis, Utrecht University.
Kuijpers, J.: 1975b, *Solar. Phys.* **44**, 173.
Kuijpers, J.: 1980, in M.R.Kundu and T.E.Gergely (eds), *Theory of type IV dm Bursts*, Radio Physics of the Sun, p. 341.
Kuznetsov, A.A.: 2007, *Astron. Lett.* **33**, 319.
Kuznetsov, A.A.: 2008, *Solar Phys.* **253**, 103.
Kuznetsov, A.A., and Tsap, Yu.T.: 2007, *Solar Phys.* **241**, 127.
LaBelle J., Treumann R.A., Yoon P.H., Karlicky M.*:* 2003, *Astrophys. J*. **593**, 1195.
Laptukhov, A. I.: 1991, in *Interplanetary Medium and Magnetospheric Processes*, Nauka, Moscow [in Russian].
Laptuhov, A.I. and Chernov, G.P.: 2006, *Plasma Phys. Rep.* **32**, 866.
Laptuhov, A.I. and Chernov, G.P.: 2009, *Plasma Phys. Rep.* **35**, 160.
Laptuhov, A.I., Chernov, G.P. and Kovalev, V.A.: 2005, in *International Symposium "Astronomy-2005: Current State and Prospects,"* Moscow, 2005, Book of Abstracts, Paper P2.31; *Tr. GAISh* **78**, 31.
Ledenev, V. G., Karlický, M., Yan, Y., and Fu, Q.: 2001, *Sol. Phys.*, **202**, 71.
Ledenev, V. G., Yan, Y., and Fu, Q.: 2006, *Sol. Phys.*, **233**, 129.
Lin, J., and Forbes, T. G.: 2000, *JGR*, **105**, 2375.
Ning, Zongjun, Fu, Qijun, Lu, Quankang: 2000, *Astron. Astrophys*. **364**, 853.
Magdalenic´, J., Vršnak, B., Zlobec, P., Hillaris, A., Messerotti, M.: 2006, *Astrophys. J.* **642**, L77.
Mészárosová, H., Karlický, M, Sawant, H. S, Fernandes, F. C. R., Cecatto, J. R., and de Andrade, M. C.: 2008, *Astron. Astrophys*. **491**, 555.
Mollwo, L.: 1983, *Solar Phys.* **83**, 305.
Mollwo, L.: 1988, *Solar Phys.* **116**, 323.
Ossakov, S.L., Ott, E., and Haber, I.: 1972, *J.G.R.*, **15**, 2314.
Osten, R.A., and Bastian, T.S.: 2006, *Astrophys. J*. **637**, 1016.
Parail, V.V. and Pogutse, O.P.: 1981, *Problems in Plasma Theory*, Kadomtsev B.B. Eds., Atomizdat, Moscow, no.11. p.5.
Pick, M., De´moulin, P., Krucker, S., Malandraki, O. and Maia, D.: 2005, *Astrophys. J*. **625**, 1019.
Priest, E. and Forbes, T.: 2000, *Magnetic reconnection*, Cambridge Univ. Press.
Roussev, I.I., Forbes, T. G., Gombosi, T.I. *et al.* : 2003, *Astrophys. J*. **588**, L45.

Sazhin, S.S..: 1987, *Planet.Space Sci.*, **35**, 753.
Sawant, H. S., Fernandes, F. C. R., Cecatto, J. R., et al.: 2002, *Adv. Space Res.*, **29**, 3, 349.
Schwenn, R., Raymond, J. C., Alexander, D. *et al*.: 2006, *Space Sci. Rev.* **123**, 127.Slottje, C.: 1972, *Sol. Phys.* **25**, 210.
Shapiro, V.D., Shevchenko, V.I.: 1987, *Plasma turbulence in Space*, Itogi Nauki i Tekh., Ser. Astronomiya, Moscow, VINITI, p.235.
Slottje, C.: 1981, *Atlas of fine Structures of Dynamic Spectra of Solar Type IV-dm and Some Type II Bursts*, Utrecht Observatory.
Smolkov, G.Ya. Pistolkors, A. A., Treskov, T.A. et al., *Astrophys. Space Sci.* **119**, 986.
Stepanov, A.V.: 1974, *Soviet Astron.* **17**, 781.
Stepanov, A.V., and Tsap, Y.T.: 1999, *Astron. Reports* **43**, 838.
Stepanov, A.V. and Tsap Y.T.: 2002, *Solar Phys.* **211**, 135.
Strong, K.T. Bruner, M. Tarbell, T. Title, A.and Wolfson, C.J.: 1994, *Space Sci. Rev.* **70**, 119.
Sych, R.A., Sawant, H.S., Karlický, M., Mészárosová, H.: 2006, *Adv. Space Res.* **38**, 979.
Tan, B.L,: 2010, *Astrophys. Space Sci.* **325**, 251.
Tan, B.L., Yan, Y. H., Tan, C. M., and Liu, Y. Y.: 2007, *Astrophys. J*. **671**, 964.
Tsang, K.T.: 1984, *Phys. Fluids*, **27**, 1659.
Tsuneta, S.: 1996, *Astrophys. J*. **456**, 840.
Tsytovich, V.N.: 1970, *Nonlinear Effects in Plasma*, Plenum Press, New York.
Wang, S.J. Yan, Y.H., Liu, Y.Y., Fu, Q.J. Tan, B.L., Zhang Y.: 2008, *Sol. Phys.* **253**, 133.
Weiland, J. and Wilhelmsson, H.: 1977, *Coherent Non-linear Interaction of Waves in Plasma*, Pergamon Press.
Winglee, R.M. and Dulk G.A.: 1986, *Astrophys. J*. **307**, 808.
Wu, D.J., Huang, J., Tang, J.F., Yan, Y.H.: 2007, *Astrophys. J*. **665**, L171.
Yan, Y., Huang, J., Chen, B., Sakurai, T.: 2007, *PASJ*, **59**, S815.
Young, C.W., Spenser, C.L., Moreton, G.E., and Roberts, J.A.: 1961, *Astrophys. J*. **133**, 243.
Zaitsev, V.V., and Stepanov, A.V.: 1975, *Astron. Astrophys*. **45**, 135.
Zheleznyakov, V. V.: 1995, *Radiation in Astrophysical Plasmas*, engl. transl. Kluwer Academic Publisher, Dordrecht (in Russ., Izdat. Nauka, Moscow, 1977).
Zheleznykov, V.V., and Zlotnik, E.Ya.: 1975a, *Solar. Phys.* **44**, 447.
Zheleznykov, V.V., and Zlotnik, E.Ya.: 1975b, *Solar. Phys.* **44**, 461.
Zlobec, P., Karlický, M.: 2007, *Solar Phys.* **246**, 419.
Zlotnik, E.Ya.: 2009, *Cent. Eur. Astrophys. Bull*. **33**, 281.
Zlotnik, E.Ya., Zaitsev, V.V., Aurass, H., Mann, G., Hofmann, A.: 2003, *Astron. Astrophys.* **410**, 1011.
Zlotnik, E.Ya., and Sher, E.M.: 2009, *Izv. VUZov Radiofizika*, **52**, 95 *(Rus)*, *Radiophysics and Quantum Electronics* **52**, 88.
Zlotnik, E.Ya., Zaitsev, V.V., Aurass, H., Mann, G.: 2009, *Solar. Phys.* **255**, 273.
Zlotnik, E.Ya.: 2010, *Solar-Terrestrial Physics, Collected articles*, Sibirian Depatement of Russian Academy of Sciences Eds, (in Russian), **16**, 49.